The Dissertation Committee for Eric Fitts Certifies that this is the approved version of the following dissertation:

Novel Virulence Factors in the Pathogenesis of *Yersinia pestis* Infection, the Causative Agent of Plague

Committee:

Ashok Chopra, PhD, CSc, Mentor, Chair

Johnny Peterson, PhD

Vladimir Motin, PhD

Wyndham Lathem, PhD

Heather Stevenson-Lerner, MD, PhD

Dean, Graduate School

Novel Virulence Factors in the Pathogenesis of *Yersinia pestis* Infection, the Causative Agent of Plague

by

Eric Charles Fitts, B.A.

Dissertation

Presented to the Faculty of the Graduate School of

The University of Texas Medical Branch

in Partial Fulfillment

of the Requirements

for the Degree of

Doctor of Philosophy

The University of Texas Medical Branch

August, 2016

Dedication

I dedicate this work to: all the people who have supported me through my childhood and education that provided the foundation to reach this milestone. I would have never entered science without the passion for science taught by Ms. Norton in high school biology. Her dedication to her students went well beyond what was required. All the professors in chemistry and biology during my undergraduate career were phenomenal and further reinforced my desire for a career in science, especially Drs. Bur and Lammert, who despite teaching in different fields of organic chemistry and immunology, respectively, had in common a love of teaching and took joy in the complexity and wonder they found in science. Lastly, but certainly not least, my partner in crime, Rose Langsjoen, has been instrumental in making me a better person, both in and outside of science. Without her I would never have come to the University of Texas and would never have live up to my potential. I love her and thank her for putting up with me on a daily basis.

Acknowledgements

Thank you to all the people who had a hand in ensuring this dissertation was complete. I especially want to thank my lab mates Jourdan Andersson and Michelle Kirtley for both help in the lab for making work, much less onerous through their humor and comradery. I'd also like to thank everyone else in the Chopra lab group both past and present including: Dr. Christina van Lier, Dr. Jian Sha, Dr. Tatiana Erova, Dr. Elena Kozlova, Dr. Duraisamy Ponnusamy, and Dr. Chopra. I'd also like to thank everyone in the next gen sequencing lab at UTMB for their help and advice in undertaking the transcriptomics work in this project. I would also like to acknowledge the funding that made this work possible. I was supported by the MD/PhD program at UTMB for the first two years of the program and during my graduate work in Dr. Chopra's laboratory I was supported by the Biodefense T32 (AI060549) and my project was funded through an NIH/NIAID R01 grant under Dr. Chopra (AI064389).

Novel Virulence Factors in the Pathogenesis of *Yersinia pestis* Infection, the Causative Agent of Plague

Publication No._____

Eric Charles Fitts, PhD

The University of Texas Medical Branch, 2016

Supervisor: Ashok K. Chopra

Identification of new virulence factors in *Yersinia pestis*, the causative agent of plague, and understanding their molecular mechanisms during an infection process are necessary in designing a better vaccine or to formulate an appropriate therapeutic intervention. By using a high-throughput, signature-tagged mutagenic approach, we screened 5,088 mutants of *Y. pestis* CO92. From this screen, 118 clones showing impairment in disseminating to spleen were obtained. In a subsequent screen, 20/118 mutants exhibited attenuation when tested individually in a mouse model of bubonic plague, with 10/20 aforementioned mutants providing 40% or higher survival rates at an infectious dose of 40 LD_{50}. Upon sequencing, six of the attenuated mutants carried interruptions in genes encoding hypothetical proteins or proteins with putative functions. In-frame deletion mutation of two of the genes identified from the screen were also found to exhibit some attenuation at 11-12 LD_{50} in a mouse model of pneumonic plague. Likewise, among the remaining 18 signature-tagged mutants, 9 were also attenuated (40-100%) at 12 LD_{50} in a pneumonic plague mouse model. Combinatorial deletions including the newly identified genes, *rbsA* and *vasK*, were significantly attenuated in

pneumonic plague models. Interestingly, *rbsA* gene products have been associated with a highly conserved inter-bacterial signaling system mediated by autoinducer-2 (AI-2) quorum-sensing molecule. Deletion of the gene encoding the synthetic enzyme for AI-2 substrate, *luxS*, leads to either no change or, paradoxically, an increase in *in vivo* bacterial virulence. Deletion of *rbsA* and *lsrA* genes, ABC transport components interacting with AI-2, synergistically disrupted AI-2 signaling patterns and resulted in an over 50-fold decrease in *Y. pestis* CO92 virulence in a mouse model. Deletion of *luxS* from the Δ*rbsA*Δ*lsrA* strain reverted the virulence phenotype similar to wild-type CO92. Administration of AI-2 in mice infected with the Δ*rbsA*Δ*lsrA*Δ*luxS* mutant strain attenuated this triple mutant. Role of AI-2 signaling genes that modulated bacterial virulence was determined by RNAseq. Characterization of AI-2 signaling in *Y. pestis* should lead to re-examination of AI-2 systems in other pathogens and may represent a broad-spectrum therapeutic target to combat antibiotic-resistant bacteria.

TABLE OF CONTENTS

List of Tables

List of Figures

List of Abbreviations

World Health Organization	WHO	Signature tagged mutagenesis	STM
Centers for Disease Control and Prevention	CDC	Luria-Bertani	LB
Disseminated intravascular coagulopathy	DIC	Heart infusion broth	HIB
Pigmentation locus	Pgm	Galveston National Laboratory	GNL
Yersiniabactin	Ybt	University of Texas Medical Branch	UTMB
High pathogenicity island	HPI	Tetracycline	Tc
Hemin storage locus	hms	Ampicillin	Ap
Insertion element	IS	Flippase	FLP
Fraction 1 capsular antigen	F1	Flippase recognition target	FRT
Braun lipoprotein	Lpp	Phosphate buffered saline	PBS
Plasminogen-activator protease	Pla	Intranasal	i.n.
Adhesion invasion locus	Ail	Subcutaneous	s.c.
Type III secretion system	T3SS	Institutional Animal Care and Use Committee	IACUC
Lipopolysaccharide	LPS	Animal biosafety laboratory level	ABSL
Toll-like receptor	TLR	Digoxigenin	DIG
Gloabal stress response protein	GsrA	Room temperature	RT
Yersinia outer proteins	Yops	Sodium dodecyl sulfate	SDS
Yop secretion system	Ysc	50 percent lethal dose	LD_{50}
Low calcium response	Lcr	Kanamycin	Km
Type VI secretion system	T6SS	Tris buffered saline	TBS
Hemolysin-coregulated protein	Hcp	Quorum sensing	QS
Valine glycine rich G protein	VgrG	Autoinducer-2	AI-2
Virulence-associated secretion protein K	VasK	Interleukin	IL
Interferon gamma	IFN-γ	luxS regulated	luxS
Tumor necrosis factor	TNF-α	ATP binding cassette	ABC
Yersinia adhesin C	YadC	Small regulatory RNA	sRNA
Wild type	WT	Phosphotransferase system	PTS
pH 6 antigen	Psa	Raltive luminescence unit	RLU
Intracellular survival	ICS	Multiplicity of infection	MOI

Chapter 1: Introduction to Plague

One of the most loaded words in the English language, the word “plague,” describes not only disastrous events but is the descriptor for a specific disease of bacterial etiology. The bacterium *Yersinia pestis* has been identified as the causative agent of the Black Death, from which it derives its moniker “plague,” as well as in epidemics from ancient history up to modern times. Contracting the disease caused by this bacterium resulted in the deaths of millions during ancient times and is still deadly in modern times despite an age of antibacterial therapies.

CLINICAL DISEASE

The disease caused by *Y. pestis* can be differentiated into several different subcategories based upon the presentation and route of infection. The most common disease course of plague, bubonic plague, results from the intradermal inoculation of bacteria delivered by the bite of a rodent flea (1). The bacteria deposited into the skin migrate into the regional lymph node independent of neutrophil or dendritic cell movement, contrary to long held thought, and start to multiply (2). Infection of the lymph nodes and the subsequent inflammatory reaction to the infection result in formation of the characteristic bubo associated with bubonic plague (3). Massive inflammation and hemorrhagic necrosis have been observed in histological analyses of patient buboes, along with dense extracellular bacterial aggregates (4). Bacterial dissemination occurs following bubo development upon rise of bacteremia, and then infection of spleen, liver, bone marrow, and other major organs occurs, followed by death due to septic shock or organ failure 3-6 days after onset of symptoms (5). In approximately one third of cases in the United States, the second most common form of plague, septicemic plague, is observed (5, 6). Septicemic plague is held to follow infection by flea bite in which the

bacteria bypass the regional lymph node and develop a bacteremia directly. Bubonic plague has a case fatality rate between 21-58% in untreated individuals, while septicemic plague is almost uniformly fatal when untreated. In the United States, the overall case fatality rate for all forms of plague is approximately 11% (World Health Organization [WHO] FAQ page) with prompt antibiotic treatment.

The third most common form is pneumonic plague. Pneumonic plague can develop secondary to bubonic or septicemic plague, or can be a primary manifestation (7). Secondary pneumonic plague develops when bacteremic patients disseminate bacteria from the blood into their lungs, resulting in the development of bacterial pneumonia. Aerosols from patients with secondary pneumonic plague, or alternately from pets or other mammals infected with plague that generate aerosols, can cause a primary *Y. pestis* infection of the lungs culminating in primary pneumonic plague (6, 8). Pneumonic plague presents as a febrile illness and can include dyspnea, coughing, and hemoptysis with rapid progression of disease, and, typically, death ensues approximately 3 days following appearance of initial symptoms. Pneumonic plague is almost universally fatal without treatment, and antimicrobials are required very early in the course of disease to prevent fatalities (9). Late treatment due to misdiagnosis can prevent therapy from being successful.

There are two other major species of *Yersinia* that can cause human disease. Both *Y. pseudotuberculosis* and *Y. enterocolitica* can infect the gastrointestinal tract resulting in a generally self-limiting disease (10). While disease caused by these alternate species can have significant impact on human health, they are outside of the scope of this study. However, it is important to emphasize that *Y. pestis* has evolved from *Y. pseudotuberculosis* and that *Y. enterocolitica* can lead to severe abdominal pain, sometimes misdiagnosed as appendicitis (11). The ability of the latter pathogen to grow in the blood at the refrigeration temperatures is a significant concern related to induction of septic shock in patients transfused with the infected blood (12).

HISTORICAL SIGNIFICANCE

Three Plague Pandemics

Y. pestis has been identified as the primary etiological agent in three widespread pandemics spanning history (13-16). Human samples from the first great pandemic, the 6th century Justinian plague, which is hypothesized to have initiated in Central Africa before spreading north towards Egypt and later into Europe through the Mediterranean countries, has provided genetic evidence identifying *Y. pestis* as the causative agent of plague (13). The Justinian plague lasted for decades and was estimated to have killed 100 million people. The second well-documented pandemic is known as the Black Death and occurred primarily in Europe through the 14th century with an intermittent reemergence for the following several hundred years (14, 15, 17). Through the course of the Black Death, it has been estimated that a quarter of Europe's population was killed. The final pandemic stretches into modern times, beginning in China and then rapidly spreading worldwide in the late 19th century (13, 16). This pandemic resulted in new endemicities globally, including much of the western United States (Fig. 1) (18). The number of casualties in the third pandemic was much more limited than the previous two pandemics; however, there has been a recent reemergence of disease in Asian and African countries with thousands of cases each year globally for the past two decades (19, 20). There are suggestions of plague disease further into ancient times predating Christianity, however, inconsistent records and lack of genomic studies have not resulted in a plurality of evidence (13).

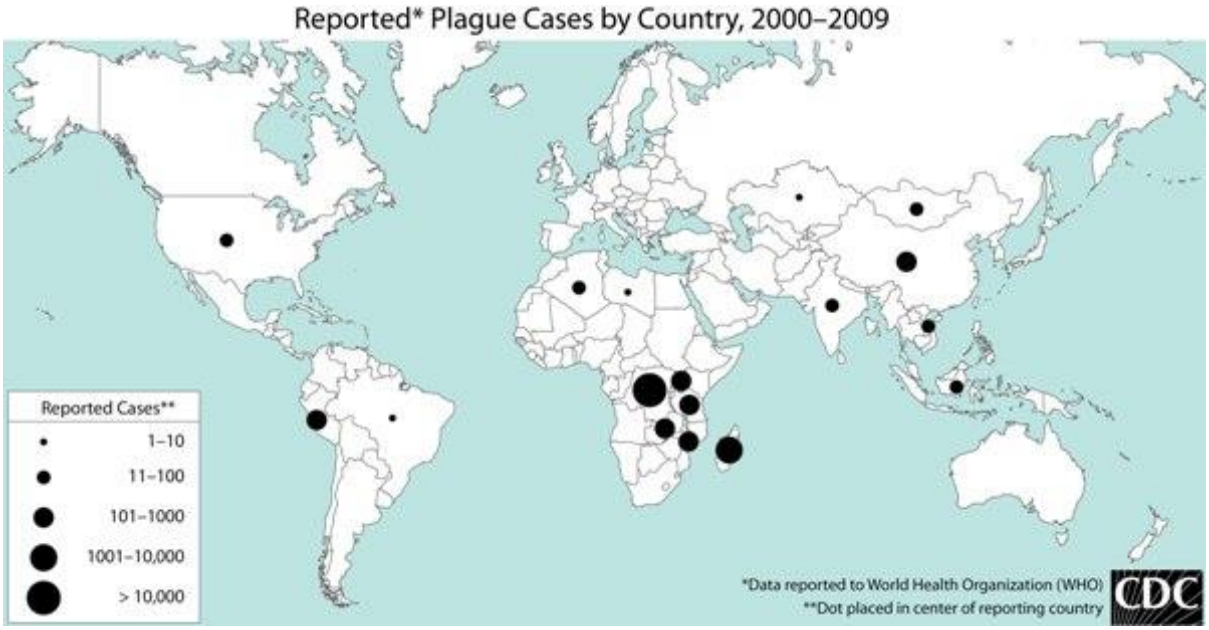

Figure 1. Plague cases reported to WHO globally.

The distribution of cases of human plague as reported to the WHO for the first decade of the 21st century. Figure adapted from the Centers for Disease Control and Prevention (CDC) (7).

Plague in the United States

Plague is a reportable disease in the United States with all laboratory confirmed cases tracked by the CDC. In the summer of 2015, there were 11 confirmed cases of *Y. pestis* infection in six different states including cases in Georgia and California that were linked to exposures at Yosemite state park (21). The median annual number of reported cases is approximately 3, with no known cause for the higher than typical case numbers in 2015 (21, 22). Of the 11 cases, three patients succumbed to infection with a case fatality rate ~27 percent, just above the average of 16 percent case fatality with antibiotic treatment (23). The most significant risk factor for contracting *Y. pestis* infection is outdoor activity in plague endemic areas (18, 23). Significant recent cases of pneumonic plague in the United States were traced to a pet dog that had died in 2014 after a disease course including hemoptysis that was later confirmed to be a *Y. pestis* infection (6, 24, 25). A total of 4 cases were linked to exposure to the dog or potentially with the first

patient, which would represent alarmingly the first human-to-human transmission of pneumonic plague since 1924 (23, 26). While all four cases later recovered from *Y. pestis* infection, the first patient was hospitalized for over 18 days and required six months of convalescence to fully recover from all sequelae (25). Overall, the number of plague cases reported worldwide was approximately 650 between 2010 and 2015 with an increasing trend (20). However, this remains only the number of cases reported and is expected to dramatically underestimate true incidence of disease.

Biodefense

In addition to a long history of naturally-occurring human pandemics, plague has also been subverted for use as a bioweapon numerous times throughout history. As early as the 14th century, *Y. pestis* was utilized in warfare. There is historical evidence of attacking armies besieging cities and introducing plague through catapulting of infected cadavers (27). This is most famously described in the siege of Caffa on the Black Sea coast in 1346 (28, 29). However, the lack of microbiological techniques limited the effectiveness and potential damage of biological warfare agents. Following innovations by Louis Pasteur and Robert Koch, among others, biological warfare could be approached in a systematic fashion and led to the research and development of biological agents in countries spanning the developed world. The most prominent example of large scale use of *Y. pestis* as a specific and microbiologically controlled bioweapon was by Unit 731 of the Japanese army. During World War II, the Japanese forces used a variety of delivery methods to deliberately infect regions of China with plague (27). Research and development of *Y. pestis* as a bioweapon continued through the Cold War era until the United States, United Kingdoms, and Soviet governments signed a declaration prohibiting further research into offensive biological programs. While this declaration limited the research on offensive programs for the signatories, the declaration is considered unenforceable for non-state-sponsored individuals or groups (30). The wide

prevalence of *Y. pestis* endemicities provides an easily obtainable source, and this along with the high case fatality rates and prior history of use as a bioweapon have led to the classification of *Y. pestis* as a category A priority (now Tier-1) select agent for Biodefense research by the National Institute of Allergy and Infectious Disease and the CDC.

BACTERIAL CHARACTERISTICS

Bacterial Basics and Ecology

Y. pestis is a gram-negative bacillus that is a facultative anaerobe with a genome of approximately 4.65 Mb and 3 plasmids that encode several pathogenicity islands (31). The bacterium has a diverse lifestyle and can survive in several different environments, including the soil as well as vertebrate and arthropod hosts (10). *Y. pestis* replicates both at 30°C and at 37°C, promoting growth in both primary lifestyles in arthropods and mammals. A definitive host reservoir has not been identified yet, although a wide array of animals susceptible to infection range from small rodent populations to camels, the latter of which was the suspected host causing an outbreak of rare pharyngeal plague due to consumption of contaminated camel meat (32).

The endemic cycles of several host mammals were tracked in the United States along with environmental variables that were linked to either epizootic outbreaks or human epidemics. There were significant contributions from altitude, precipitation, and distance from artificial surfaces along with presence of one of the primary enzootic species in the region, *Peromyscus maniculatus* (18). Through this analysis, Walsh et al. (18) identified areas of high risk of plague transmission in the United States (Fig. 2). Further regions of enzootic transmission cycles have been identified on five continents, only excluding Australia, from the habitable continents (7). Enzootic cycles have been linked to foci of disease in several rodent species, such as the deer mouse (*Peromyscus maniculatus*), prairie dogs (*Cynomys* spp.), and ground squirrels (*Spermophilus* spp.)

(33). Periodic die-offs in rodent populations have been linked to transmission cycles of *Y. pestis*, and the colonies associated with later die offs were actively transmitting *Y. pestis* weeks to months before the first observed die offs (34). The fleas feeding on the prairie dogs were also positive for *Y. pestis* infection, suggesting that transmission outside of the original rodent colony was possible prior to die-offs and outward signs disease in the colony.

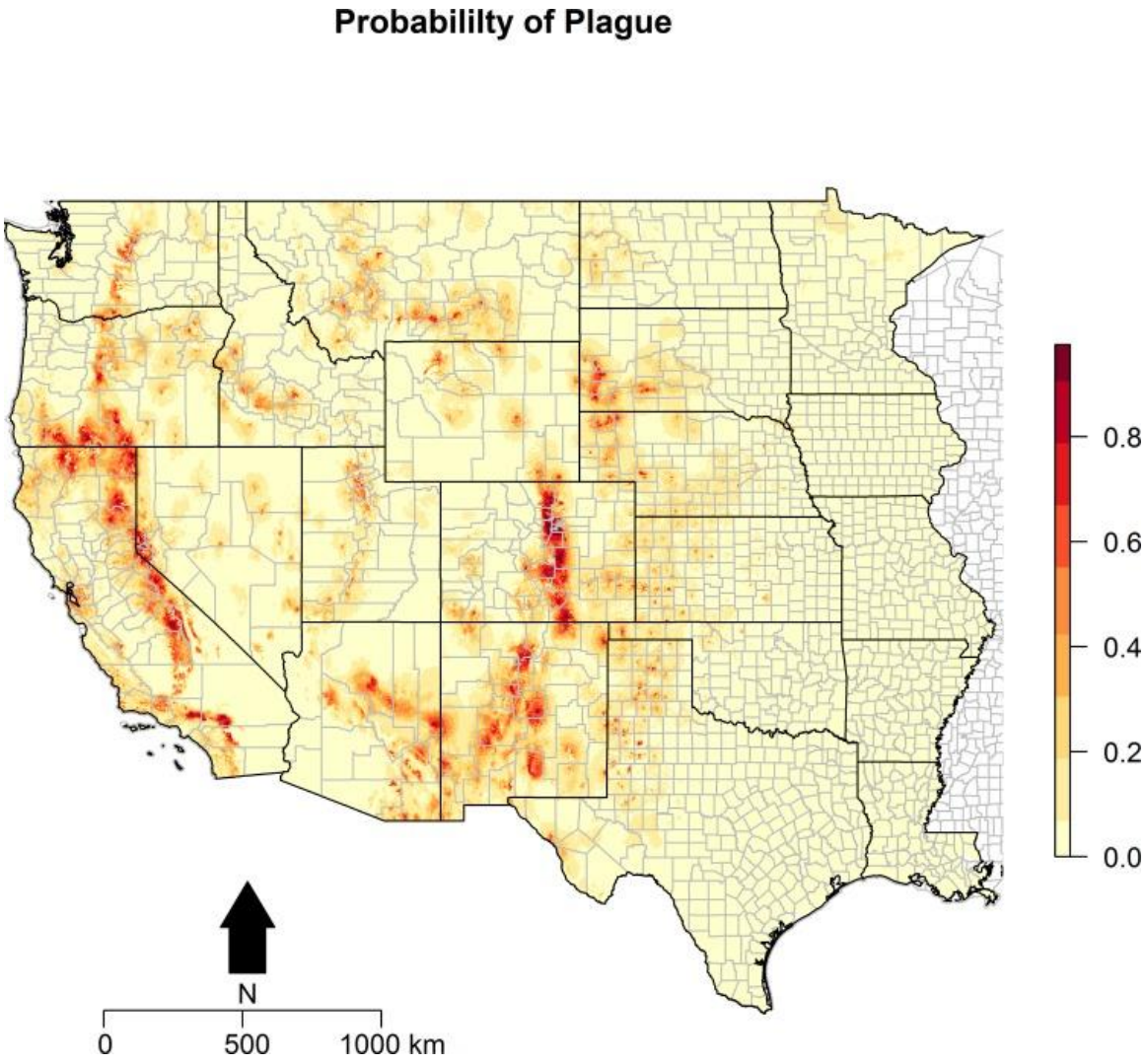

Figure 2. Probability map of epizootic plague outbreaks.

A risk map was determined based on multiple variables showing the likelihood of areas developing an epizootic plague outbreak. Adapted with permission from Walsh et al. (18).

Yersinia pestis lifestyle in flea and mammals

Due to the loss of a single gene, *ureD* (encoding urease), in the evolution of *Y. pestis* from *Y. pseudotuberculosis*, *Y. pestis* is competent to infect fleas without causing rapid morbidity or mortality to the infected flea, allowing for a protracted window for transmission (35-37). Following an infected blood meal, the bacteria remain isolated in the digestive tract of the flea unlike most arthropod borne infectious diseases (38). The bacteria start to form biofilms in the digestive tract until blood flow is blocked in the proventriculus and results in efficient regurgitative transmission of the bacteria (36). Biofilm formation was enhanced by a series of gene losses from *Y. pseudotuberculosis* related to inhibitory regulation of biofilm synthesis, increasing biofilm formation of *Y. pestis* under flea environmental conditions and resulting in an ascending infection of the flea into the foregut (39). Foregut infection of the flea allows for regurgitative transmission and infection into the dermal or subcutaneous skins layers of the mammalian flea host (40).

In the mammalian host, *Y. pestis* is much more aggressive and tends to cause severe morbidity and mortality. In experimental mouse models, bacteria are introduced subcutaneously and then they migrate to the lymph nodes. Migration to the lymph nodes had been thought to be the result of bacterial uptake by leukocytes; however, recent studies have suggested that it is likely due to lymphatic flow into the regional lymph node, although uptake and intracellular dissemination may occur at later stages (41). Early neutrophil infiltration into site of inoculation can effectively control bacterial numbers; however, macrophages have been shown to be particularly vulnerable to intracellular bacterial infection (2). Following lymph node infection, bacterial growth leads to destruction of lymph node architecture with associated tissue necrosis and massive neutrophil influx (4). At this stage, bacteria are presented with a barrier to dissemination into the blood stream; approximately 50% of the time after a low dose

infection with flea bite vector, mice will develop a high grade bacteremia while remaining mice that don't develop bacteremia can resolve infection (41). Dissemination out of the regional lymph node and bacteremia lead to infection of most other major tissues, most notably the liver and spleen. Disseminated intravascular coagulopathy (DIC) can be observed in the later stages of the disease, presenting as black, gangrenous extremities from which the Black Death derived its name (5, 6). However, necrosis and gangrene of the extremities are not features of the rodent models of disease and appears in the late stage of human disease.

PATHOGENESIS/VIRULENCE FACTORS

Identification of virulence factors is critical to understanding the pathogenesis of a disease causing organism as well as to the rational design of attenuated vaccines. A number of potent virulence factors have been described in *Y. pestis.* However, with a large genome encoding approximately 4000 genes, there remains many uncharacterized genes or genes with unknown function that may relate to virulence of the organism. Well characterized virulence factors have been described as follow:

Pigmentation locus

The pigmentation locus is a 102 kb unstable chromosomal region that contains many genes encoding proteins with functions critical for virulence (42). It was first described in 1992 by Fetherston et al. and was termed "pigmentation locus (Pgm)" due to the loss of pigment uptake when grown on Congo red media (42). It was later determined that the large 102 kb locus could be subdivided into two loci based on phenotypic effects on virulence and pigmentation (43-45). The yersiniabactin (*ybt*) locus was identified as a high pathogenicity island (HPI) and is responsible for changes in virulence in mammalian models while the hemin storage locus (*hms*) was identified as essential for disease transmission in the flea host (43, 44, 46). Other phenotypic characteristics include

sensitivity to bacteriocin and pesticin that are encoded across the 102 kb locus (47). This 102 kb region is flanked by insertion element (IS) IS*100* copies that are postulated to increase frequency of homologous recombination, resulting in the instability of the region (42). The entire 102-kb region is spontaneously deleted at a frequency of ~10^{-5}, leading to the observed phenotypic changes. Interestingly and consistent with the findings following the death of a researcher utilizing a *pgm*$^{-}$ strain, an excess of iron in human body (hemochromatosis) allowed *pgm*$^{-}$ mutant to be highly virulent (48, 49). Loss of the *pgm* locus has been the primary defining factor for the attenuated vaccine, EV76, currently in use in countries outside of the United States (50). There are several other iron transport loci annotated in the *Y. pestis* genome, including a *tonB* locus that may be responsible for inorganic iron uptake and scavenging in the absence of adequate uptake through the siderophore system encoded by the *ybt* locus (51, 52).

F1 capsule

Fraction 1 (F1) capsular antigen is encoded on a large ~100-kb plasmid, pMT1, which also encodes several associated proteins (53, 54). *caf1*, the gene that encodes the capsular antigen, is part of an operon of which the other members include an anchor protein, as well as accessory proteins involved in appropriate expression and secretion of F1. Antibodies from hyperimmune serum generated in mice against whole cell killed *Y. pestis* as well as convalescent sera from human patients following plague infection is directed in large part against F1 antigen (55, 56). Further, passive transfer of antibodies to F1 have been shown to be effective at protecting mice against low dose plague challenge (57). Beyond its contribution as a primary immunogen, F1 plays an important role in the pathogenesis of *Y. pestis* infection. Expression of the structural component is strictly regulated, primarily via temperature, with strong expression only at temperatures (37°C) corresponding to mammalian hosts (57, 58). As with capsules present in other pathogens, F1 has antiphagocytic properties, protecting the bacterium from uptake into macrophages

and other phagocytic leukocytes (59). F1 appears to act at the level of receptor interaction, blocking potential binding and lowering the adhesion of bacteria to phagocytic cells. Interestingly, while reducing the anti-phagocytic properties by deletion of other virulence factors leads to avirulence, F1 deletion has a highly variable phenotype ranging from highly attenuated to fully virulent and is route dependent (60, 61). Thus, while the effectiveness of F1 as an immunogen against F1 positive *Y. pestis* strains is attractive, virulent strains have been identified circulating in nature that are capsule negative (62). Similarly, if many vaccines are based, at least partially, upon an F1 antigen, then it stands to reason that a *Y. pestis* strain developed as a bioweapon would be constructed capsule negative to bypass immunity.

Plasminogen-activator protease

Another virulence factor is encoded on the pPCP1 plasmid (~10 kb). The gene *pla* encodes a protease that is implicated in dissemination of the bacteria through proteolytically cleaving clotting factors and altering the host environment (63, 64). The Plasminogen-activator protease (Pla) protein has been shown to act as a protease on plasminogen resulting in its activation into plasmin which degrades fibrin clots (65, 66). While the Pla protein is required for dissemination out of the lymph node after a subcutaneous infection or via flea bite, it is not necessary for the dissemination out of the lungs in a primary pneumonic infection (64). It has been suggested that the highly vascularized tissue of the lung allows ample opportunity for the bacterium to develop a systemic infection without progressing through lymph tissue.

While Pla may not be necessary for the dissemination of *Y. pestis* from the lungs, it does effectively curtail dissemination out of the lymph nodes resulting in a drastically increased LD_{50} in the absence of Pla for bubonic plague models (67, 68). Interestingly, it also plays a significant role in the severity of disease and severity of tissue damage in the lungs in a pneumonic model. When *pla* is deleted, there is a significant reduction in the

tissue damage observed in the lung fields as well as a reduction in the edema associated with plague pneumonia (64). Interestingly, attenuation due to deletion of *pla* synergistically increases with deletion of selected other modestly attenuating virulence factors. In combination with deletion of *lpp*, encoding Braun lipoprotein, a double deletion strain Δ*lpp*Δ*pla* was highly attenuated in both bubonic and pneumonic plague models and provided protection against rechallenge with a fully virulent strain CO92 of *Y. pestis* (69). Therefore, Pla plays significant roles in both pneumonic and bubonic plague disease progression and is a critical virulence factor in the pathogenesis of plague regardless of route. Finally, our group showed the role of Pla in intracellular survival of *Y. pestis* in macrophages (70).

Adhesion & Invasion locus

A chromosomally encoded locus produces a 17 kDa membrane-associated protein that acts as a virulence factor as well as a weak immunogen (71-73). This protein encoding gene was named the adhesion invasion locus (*ail*) due to the functionality of the Ail protein. Ail binds several targets including laminin and fibronectin, and vitronectin is actively recruited to the bacterial surface through Ail activity (74, 75). Ail mediates a close attachment with host cells and has been implicated in efficient translocation of type III secretion system (T3SS) effectors (76-78). Deletion of *ail* from the chromosome results in a diminished adherence to macrophages and lung epithelial cells as well as decreases the invasion into the host cells (76, 79). Additional functions of Ail have also been described, including serum resistance (80). Similar to *pla*, deletion of *ail* results in a modest reduction in virulence in mice in a pneumonic model; however, this reduced virulence can be synergistically increased with additional deletions of virulence factors such as Lpp and MsbB, an acyltransferase, that modifies lipopolysaccharide (LPS) acylation (81). A triple deletion strain, Δ*lpp*Δ*msbB*Δ*ail*, was recently shown to be significantly reduced in virulence to the point where “avirulent” may be an appropriate

descriptor, and that doses of this strain can act as an attenuated vaccine candidate providing protection against fully virulent *Y. pestis* in both bubonic and pneumonic plague models (76, 82). Consequently, this Δ*lpp*Δ*msbB*Δ*ail* mutant was recently excluded from the CDC select agent list (May 26, 2016). As previously stated, Ail is immunogenic and antibodies against Ail are present in mouse convalescent sera; however, recombinant Ail immunization failed to fully protect mice/rats against virulent *Y. pestis* challenge, and reintroduction of mutated Ail (with diminished virulence) into the triple deletion strain of Δ*lpp*Δ*msbB*Δ*ail* had negligible effects on the efficacy of the attenuated vaccine candidate strain (71, 82). Therefore, despite being an immunogen, Ail remains a valid target for deletion in connection with live-attenuated vaccine development.

Braun Lipoprotein and Acyltransferase

As previously mentioned, in connection with several combinatorial deletion mutants, the proteins encoded by *lpp* and *msbB*, Braun lipoprotein and an acyltransferase, respectively, have been characterized as virulence factors in *Y. pestis*. Deletion of *lpp* results in a decreased inflammatory profile mediated through Toll-like receptor (TLR)-2, while deletion of *msbB* results in a similarly decreased inflammatory burden mediated through TLR-4. Lpp is an abundant component of the outer membrane along with LPS (83, 84). The MsbB acts to modify bacterial LPS and results in a pentaacylated LPS rather than the typical hexaacylated LPS that typifies most gram-negative bacterial cell envelopes. Interestingly, *Yersinia spp.* normally display a tetraacylated LPS at mammalian host temperatures (37°C), which may be an adaptation to avoid early inflammation to prevent bacterial killing (85, 86). The deletion of *msbB* reverts LPS modification to pentaacylation that induces a much milder inflammatory profile than the fully acylated version (87). The moderate immune profile resulting from deletions of both *lpp* and *msbB* provides a less immunopathogenic environment within a mouse/rat model

but allows clearing of the bacterium (81). Our studies have also shown that Lpp plays an important role in the intracellular survival of *Y. pestis* in macrophages by modulating production of a global stress response protein, GsrA (70).

Type III Secretion System (T3SS)

The T3SS of *Y. pestis* is perhaps the best characterized virulence mechanism of the bacterium with a diverse array of effectors as well as structural components that have pathogenic functions. The T3SS locus is encoded on a virulence plasmid, pCD1 (~70 kb), and its expression is tightly regulated (31). Regulation of the T3SS occurs in response to two main environmental variables, temperature and calcium levels (88, 89). At mammalian host temperature (37°C) and low calcium levels, as would be encountered in the mammalian host, the T3SS cluster is expressed and effectors can be secreted out in the culture supernatants or translocated into co-cultured mammalian tissue culture cells. The T3SS functions as a molecular needle, forming a bridging structure between the bacterium and the host cell target, and introducing pore forming proteins following translocation of effectors (Fig. 3).

The primary effectors of the *Y. pestis* T3SS are called *Yersinia* outer proteins (Yops). Upon host cell contact with the bacterium, these effectors are translocated into the host cell where they function on a variety of cellular processes that result in a less hostile environment for *Y. pestis* (88). For an exhaustive review of all individual Yop functions and T3SS regulation, please see the review by Plano et al. (88). In brief, Yops translocated into the target cell can be divided into two categories based on the target of interaction. YopE, YopH, YopT, and YpkA interact directly with host cell cytoskeleton components, while YopJ participates in host signaling pathways (88). A sixth Yop, YopM, also has interactions with host signaling pathways by an incompletely understood mechanism. Two Yops, YopB and YopD, function to form a hydrophobic pore structure in the target host cell to effect translocation of the remaining effectors (90). YopJ and

YopM have been found to interact with caspases, though in non-complementary manners that sum towards a diminished IL-1β/IL-18 response (91). Neither YopJ nor YopM when deleted alone were essential for full virulence of the bacterium; however, combinatorial deletion of both YopJ and YopM resulted in a significant attenuation in a mouse model of bubonic plague (91).

The cytoskeletal interacting Yops have several functions that are critical to the virulence of the bacterium. YopE acts as a GTPase-activating protein directed at the RhoA family of GTPases which coordinate the dynamics of actin (92). Actin dynamics are especially critical during the process of phagocytosis, and, as such, YopE functions to reduce phagocytic activity and can cause a dramatic collapse of the cytoskeleton. YopH has a similar anti-phagocytic role but functions through a protein tyrosine phosphatase activity (93, 94). Its cellular targets are typically involved in the targeting of membrane sections that sense bacterial adhesion for phagosome development.

Interestingly, the proteins that make up the structural portion of the T3SS also can influence the host response. The Yop secretion system (Ysc) proteins encompass at least 19 gene products required to form the secretion system, as well as several of the low calcium response (Lcr) proteins (95, 96). Notably, LcrV forms the tip complex of the T3SS needle (97). As will be discussed further, LcrV is also one of the primary immunogens recognized by the mammalian host and antibodies directed against LcrV are protective against *Y. pestis* challenge (71, 98).

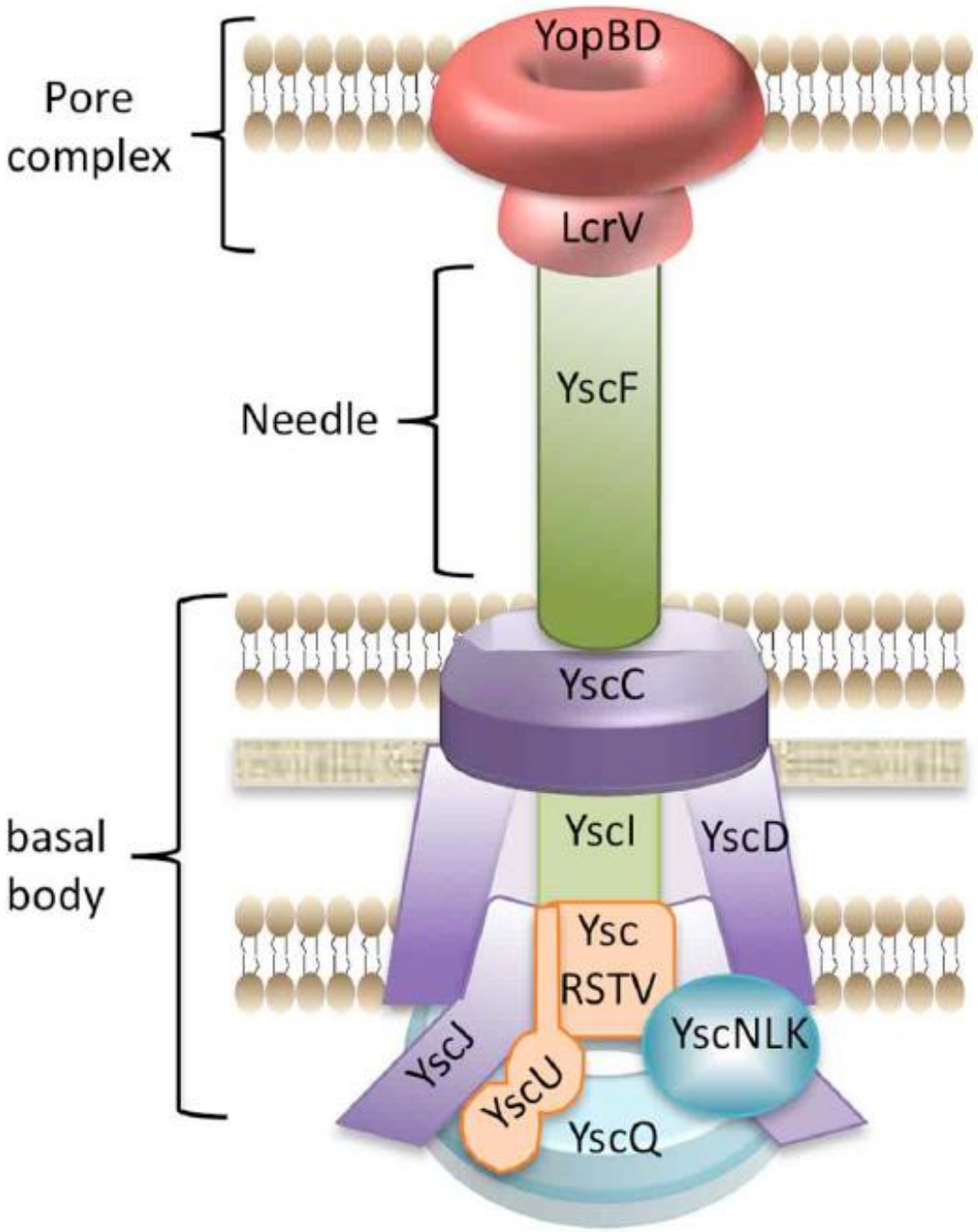

Figure 3. Type III secretion system injectisome structure.

The components of the *Y. pestis* T3SS are shown in diagram representing the layout and general formation that the apparatus takes on to result in translocation of effector Yops. Figure adapted from Dewoody et al. with permission (99).

Type VI Secretion System (T6SS)

Type VI secretion systems (T6SS) in *Y. pestis* have been neglected relative to other secretion mechanisms and little is known about their functionality or role in the bacterial lifestyle or in pathogenesis. There have been six loci that have been identified as containing genes that encode proteins with domains associated with T6SS structural or effector functions (100). In general, T6SSs' are composed of several essential proteins including Hcp (Hemolysin-coregulated protein), VgrG (Valine glycine rich G protein family members), and VasK (virulence-associated secretion protein K), each of which have homologs represented in the *Y. pestis* genome (**Fig. 4**) (101, 102). One of the loci identified in the bioinformatics study by Yen et al. (100) was characterized in both flea and mammalian hosts. Deletion of the locus led to divergent phenotypes due to differential thermoregulation. In macrophages, bacteria cultured at 26°C reproduced more prolifically after deletion of the locus, while bacteria cultured at 37°C had reduced macrophage uptake, suggesting that the T6SS encoded at that locus modulated the interaction between host cells and bacteria (103). Interestingly, T6SS members at different loci were identified as potential virulence factors in a genome wide screen (104). One of the identified genes encoded a protein with domain homology to Hcp, a well characterized effector of T6SSs' in other gram-negative bacteria. Deletion of this specific gene encoding Hcp led to a decrease in virulence *in vivo* mouse models of plague infection (104). This suggests that T6SS(s) are functional in *Y. pestis* but the exact role and the significance of that role in mammalian disease is as yet unknown and is a subject of future studies in our laboratory.

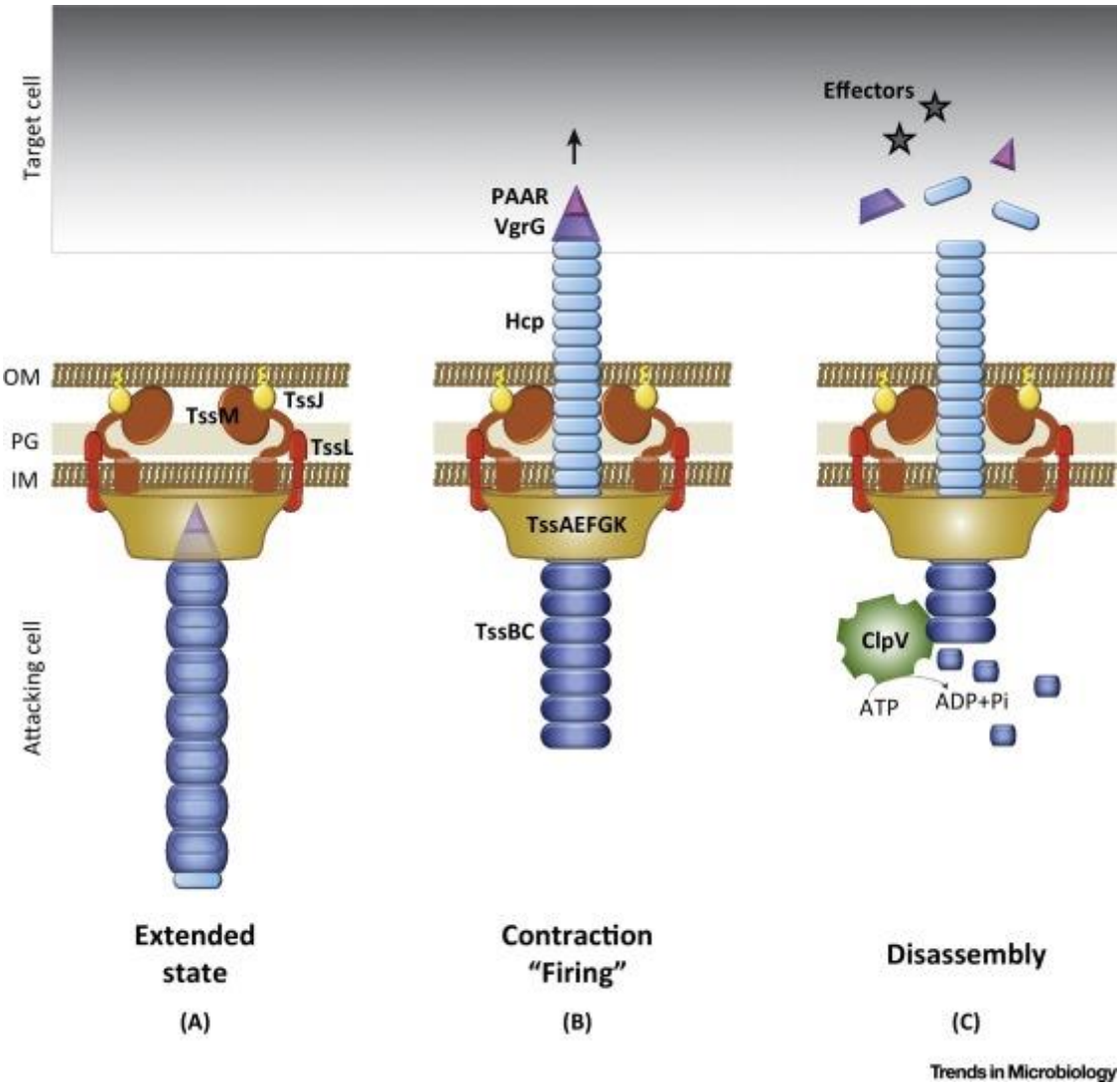

Figure 4. Structural diagram of T6SS apparatus.

A representation of type VI secretion system injectisome with key components indicated. The secretion system goes through distinct conformations with a primed state (A), a firing state (B), and finally disassembly (C) that allows effectors to interact with the targeted cell. Figure was adapted from Cianfanelli et al. with permission (105).

VACCINES

There has been significant interest in developing effective vaccines against plague, given the extreme historical burden of disease as well as for biodefense efforts (106, 107). However, despite the interest and decades of development, no vaccine against plague has been approved in the United States. To develop an efficacious vaccine, appropriate *in vitro* correlates of immunity are essential. Typically, correlates of immunity are divided by type of immunity, either humoral or cell mediated. Studies have demonstrated that passive antibody transfer protects against *Y. pestis* challenge in rodent models (108); however, studies in non-human primate models have shown that variability in protective responses does not correlate well with antibody titers (109). This strongly suggests that antibody titers alone are not sufficient for protection against *Y. pestis* challenge. Interestingly, cell mediated immunity in the absence of or with low antibody titers has been observed to protect animals against *Y. pestis* infection (110, 111). Research has correlated host production of interferon gamma (IFN-γ), tumor necrosis factor alpha (TNF-α), and inducible nitric oxide synthase with protective responses (112). Thus, a live-attenuated vaccine platform would ideally deliver a balanced response composed of both cellular and humoral components.

Historical Vaccine Development

Considered to be too reactogenic to be licensed in the United States, a live-attenuated vaccine called EV76 has been used in China and Russia to prevent both pneumonic and bubonic plague (53). EV76 is an empirically derived vaccine that was isolated from a human patient in Madagascar by Girard and Robic in 1926. Following 76 passages on culture media, they found that the isolate was spontaneously attenuated and provided protection against plague in multiple animal models. Vaccination by EV76 was initiated in 1934 in Africa while subcultures were delivered to the former USSR and

China, as well as other endemic areas (53). The genetic determinants of attenuation in EV76 were of great interest and a disruption in a large chromosomal region, the pigmentation (*pgm*) locus, was identified as a major contributor to loss of virulence (43, 44, 50). A laboratory strain with a similar loss of the *pgm* locus recently was involved in a laboratory exposure resulting in the death of a researcher (48). The infection exposed an underlying iron transport disorder, hemochromatosis, in the researcher allowing a virulent phenotype to emerge from the previously highly attenuated strain. The abnormally high levels of iron available in his body provided an alternate source that overrode the loss of the efficient iron transport system in the *pgm* locus, demonstrating the potential for high virulence and the general unsuitability for widespread vaccination using *pgm* locus deletion attenuated strains.

Attempts to develop an effective and safe vaccine to prevent plague resulted in both heat-killed and formalin inactivated whole-cell vaccines. However, both iterations of killed vaccines had very low tolerability and severe adverse reactions. The heat-killed vaccine was given at a dosage designed to cause the recipient to develop a fever of 102°F and as such would not be approved in the current climate of regulation (113). Further, while the vaccine showed efficacy against bubonic forms of disease, the vaccine generally failed to protect against pneumonic disease (114). Similarly, the formalin inactivated whole-cell vaccine that was licensed in the US in the mid-1900s was efficacious against bubonic plague but caused significant adverse reactions including severe injection site reactions as well as flu-like symptoms, particularly following the booster injections required to maintain protection (107). The formalin inactivated whole-cell vaccine also failed to adequately protect against the pneumonic plague and was not deemed suitable as a biodefense measure against aerosolized plague (115).

Modern Vaccine Development

RECOMBINANT VACCINES

Following identification of surface antigens and major immunogens of *Y. pestis*, development turned towards subunit vaccines. A recombinant vaccine utilizing F1 capsular antigen and LcrV provide protection against both bubonic and pneumonic forms of disease in animal models at moderate challenge doses (98). A subunit vaccine consisting of F1 capsular antigen and LcrV has also demonstrated safety in a phase 1 clinical trial and shown immunogenicity with a 2 dose vaccine regimen in a phase 2a trial conducted in China (116). Interestingly, it was shown that recombinant subunit vaccines including LcrV protein are effective at inducing a partial T-cell response through interaction with dendritic cells, unlike most recombinant subunit vaccines (117). Worryingly, in two different non-human primate models used to determine efficacy, the two models behaved divergently. In cynomolgus macaques, the subunit vaccine provided between 80-100% protection against aerosol challenge, while in African green monkeys, it was either ineffective or partially protective (0-75%) (109). In both models, similar antibody titers were observed suggesting that the observed differences in protection may be related to cell-mediated immunity. While the subunit vaccine has shown reasonable protection and an excellent safety profile, the multiple dosing requirement and the general expense of recombinant protein vaccines provide much room for improvement.

In addition to the well characterized F1 and LcrV antigens, several other antigens have also been developed as potential subunit vaccine candidates. In particular, pH 6 antigen (Psa) and *Yersinia* adhesin C (YadC) have also been investigated in animal models. Psa has been shown to influence macrophage phagocytosis by *in vitro* modeling but has a negligible impact on virulence *in vivo* when deleted from wild type (WT) background (118). Given as a recombinant vaccination, Psa afforded partial protection against a WT *Y. pestis* strain suggesting that it might, in combination with other antigens,

be a useful addition to a subunit vaccinating strategy (119). Using a *Salmonella enterica* platform to express Psa and vaccinate mice to protect against *Y. pestis* challenge has also been investigated and found that the mice generated antibody titers against Psa but that vaccination was insufficient to protect against virulent *Y. pestis* challenge (120). Similarly, YadC, an outer-membrane protein of *Y. pestis* found to modulate invasion of eukaryotic cells, has been investigated for immunogenic properties (121). Mice vaccinated with recombinant portions of the YadC protein were partially protected against challenges modeling either bubonic or pneumonic plague (121). A *S. enterica* strain expressing YadC also elicited partially protective responses in mice (122).

Other platforms for plague vaccines have also been investigated with mixed successes. An adenovirus based platform was recently shown to protect non-human primates against aerosolized *Y. pestis* CO92 at extremely high challenge doses, over 10,000 times the 50 percent lethal dose (LD_{50}) (123). Similarly, a T4 bacteriophage platform has been demonstrated to provide effective protection against pneumonic plague in mice and rats, as well as inducing balanced TH1 and TH2 responses (124). However, the existence of F1-negative, fully virulent strains of *Y. pestis* as well as multiple variants of LcrV may limit the cross-protective capacity of subunit or recombinant vaccines solely based on F1 and LcrV.

LIVE ATTENUATED VACCINES

The most attractive platform for efficacious and affordable vaccines remains a live-attenuated vaccine. Live-attenuated vaccines can provide a much more diverse range of antigens than subunit or other recombinant type platforms, in addition to typically inducing a much more robust immunity in fewer doses than killed vaccines. Of course, the drawback being that attenuated vaccines can be associated with greater safety risks or adverse events (45). To minimize the potential for reversion or adverse events, development of attenuated vaccines should progress rationally with combinatorial gene

deletions to appropriately attenuate but maintain adequate immunogenicity (125). Deletions in several genes have been characterized as vaccine candidates including deletions in *yopH*, *ail*, *pla*, and combinations of several deletions of virulence factor encoding genes such as Δ*lpp*Δ*msbB* or Δ*lpp*Δ*msbB*Δ*ail* (69, 70, 76, 82, 126). The key to development of a successful vaccine candidate will be a repertoire of virulence factors that can be deleted in combination to generate a safe but immunogenic candidate that has deletions spread through the genome to provide insurance against reversion. However, we are limited by the characterized virulence factors. Several, such as F1 capsular antigen, Ail and most of the T3SS effectors, are important immunogens which may compromise immunogenicity should they be deleted for attenuation. Others, such as the *pgm* locus, have a history of high virulence despite attenuation or are poorly defined. As such, identification of novel virulence factors or virulence regulatory mechanisms is a priority for future vaccine development.

PURPOSE OF THE PROJECT

Major gaps in knowledge necessary to develop safe and efficacious vaccines or effective therapeutic countermeasures have become apparent. Despite the current knowledge of virulence factors and some encouraging data from animal models and small clinical trials, no vaccines are available to protect against *Y. pestis* infection in the United States from either endemic, natural infections or from purposefully released attacks applying *Y. pestis*. Further, the therapeutic options available to treat infections are limited to short therapeutic windows and could be countered by antibiotic resistance. Development of new therapeutic targets as well as the rational development of live-attenuated vaccines requires knowledge of virulence factors and the mechanisms by which they function. Therefore, the goals set forth by this research are as follow:

1. Identify novel virulence factors in the pathogenesis of plague, particularly as they relate to pneumonic plague;
2. Characterize novel virulence factors in terms of function and mechanism to identify targets for vaccine and therapeutic development.

Together, these results will contribute to the pool of knowledge required to protect the population from *Y. pestis* infections. Further, identification of novel virulence factors may result in the recognition of orthologous virulence factors in other pathogenic bacteria expanding the utility of any therapeutic targets described herein.

Chapter 2: High-throughput signature-tagged mutagenic approach to identify novel virulence factors of *Yersinia pestis* CO92 in a mouse model of infection

INTRODUCTION

Identification and characterization of novel virulence factors of *Y. pestis* to rationally design a better live-attenuated vaccine and also to formulate effective new therapeutics are of significant importance. Various virulence factors of *Y. pestis* have been identified and are primarily of plasmid origin, e.g., the T3SS is carried by the pCD1 plasmid, plasminogen-activator (Pla) protease and pesticin genes are harbored on the pPCP1 plasmid, and the F1 capsular antigen-encoding gene is located on the pMT1 plasmid (127-131). Apart from these well-known virulence factors of *Y. pestis*, very limited information is available on other virulence factors/mechanisms that contribute to the extreme virulent phenotype of the plague bacterium. More recently, Braun lipoprotein (Lpp) and an acyltransferase (MsbB) that modifies lipid A moiety of lipopolysaccharide (LPS), were shown to contribute to *Y. pestis* virulence during both bubonic and pneumonic plague, and currently, mutants devoid of these genes are being exploited for developing live-attenuated plague vaccines (131-133). Similarly, an outer membrane protein Ail which provides serum resistance to *Y. pestis* plays an important role during septicemic plague, allowing the plague bacterium to resist host complement-mediated killing (134). Since *Y. pestis* is a facultative intracellular pathogen, during its intracellular life cycle, the bacterium up-regulates the expression of various virulence genes, including those that code for F1 capsular antigen and pH 6-antigen (Psa), the latter of which is an adherence factor (59, 135).

Recently, a number of genome-wide functional studies have been performed, mainly utilizing array-based approaches to identify other possible virulence factors of *Y. pestis*. During mammalian host infection, *Y. pestis* increases expression of genes associated with insecticidal-toxin synthesis, iron acquisition and storage, metabolite transportation, amino acid biosynthesis, and proteins that provide *Y. pestis* a survival advantage against neutrophil generated reactive nitrogen species (136-139). Although efforts have been made to further explore these targets to comprehend their underlying pathophysiological mechanisms in the disease process, the knowledge accumulated in this area is still limited (63, 140). In the same vein, we performed these studies to identify novel virulence factors that are critical during infection and dissemination of *Y. pestis* in a mouse model. We employed a high-throughput signature-tagged mutagenesis (STM) approach, and subsequently screened the mutants for attenuation *in vivo* models of bubonic and pneumonic plague.

STM is a powerful genome manipulation technique in both prokaryotes and eukaryotes and has been successfully used to identify virulence factors of many pathogens, such as *Salmonella* Typhimurium, *Mycobacterium tuberculosis, Vibrio cholerae,* and *Yersinia enterocolitica* (141). In this approach, multiple mutants can be combined together and subjected to a screening process to determine competitive value of each of the mutants. A recent study by Palace et al., focusing on factors essential for deep tissue growth, revealed that various amino acid and sugar transporters are necessary during the deep tissue survival of *Y. pestis* (142). Notably, a branched-chain amino acid importer gene (*brnQ*) was identified as essential in evoking bubonic plague in a mouse model (142). The use of this approach in other *Yersinia* species helped in identifying genes related to the biosynthesis of LPS, T3SS, and other metabolic pathways as necessary virulence factors during infection of the host (143-145).

In this study, by using STM approach with 53 unique signature tags, 5,088 mutants of *Y. pestis* CO92 were created and screened for impairment in disseminating to

the spleen in a mouse model of pneumonic plague. Among 118 clones that failed to disseminate to the spleen, 15 mutants were either attenuated in a mouse model of bubonic plague at a higher infectious dose and/or in a pneumonic mouse model with an infectious dose equivalent to 12 LD_{50} of WT CO92. Subsequently, the role of *rbsA* that codes for a putative sugar transport system ATP-binding protein; *vasK*, a component of the type VI secretion system; and *ypo0498* (a gene within another T6SS cluster with a putative function) in the pathogenesis of *Y. pestis* infection was studied by in-frame deletion of these genes from WT- or the Δ*lpp* single and Δ*lpp* Δ*msbB* double mutant background strains of CO92.

MATERIALS AND METHODS

Bacterial strains, plasmids, and culture conditions.

Bacterial strains and plasmids used in this study are provided in **Table 1**. *E. coli* cultures were grown overnight at 37°C with 180 rpm shaking in Luria-Bertani (LB) broth or grown on LB agar plates for 18-20 h. *Y. pestis* strains were cultured overnight at 28°C, unless specifically noted, with shaking at 180 rpm in heart infusion broth (HIB) (Difco, Voigt Global Distribution Inc., Lawrence, KS) or grown for 48 h on 5% sheep blood agar (SBA) (Teknova, Hollister, CA) or HIB agar plates. As appropriate, the organisms were cultivated in the presence of antibiotics such as ampicillin, kanamycin, and polymyxin B at concentrations of 100, 50, and 35μg/ml, respectively. All of the experiments with *Y. pestis* were performed in the Centers for Disease Control and Prevention (CDC)-approved select agent laboratory in the Galveston National Laboratory (GNL), UTMB.

Table 1. Bacterial strains and plasmids used in this study

Strain or Plasmid	Genotype and/or relevant characteristics	Reference or Source
***Y. pestis* CO92**		
WT CO92	Virulent *Y. pestis* biovar Orientalis strain isolated in 1992 from a fatal human pneumonic plague case and naturally resistant to polymyxin B	CDC
WT CO92 pBR322	WT *Y. pestis* CO92 transformed with pBR322 (Tc^s)	18
WT CO92 *luc2*	WT *Y. pestis* CO92 integrated with the luciferase gene (*luc*), used as a reporter strain	39
miniTn*5*Km2STM mutants	Random transposon insertion mutants of *Y. pestis* CO92	This study
WT CO92 pKD46	WT *Y. pestis* CO92 transformed with plasmid encoding λ-phage recombination system	This study
Δ*ypo0498*	*ypo0498* gene deletion mutant of *Y. pestis* CO92	This study
Δ*rbsA*	*rbsA* gene deletion mutant of *Y. pestis* CO92	This study
Δ*rbsA* pBR322	Δ*rbsA* transformed with pBR322 (Tc^s)	This study
Δ*rbsA* pBR322-*rbsA*	Δ*rbsA* complemented with pBR322-*rbsA* (Tc^s)	This study
Δ*vasK*	*vasK* gene deletion mutant of *Y. pestis* CO92	This study
Δ*vasK* pBR322	Δ*vasK* transformed with pBR322 (Tc^s)	This study
Δ*vasK* pBR322-*vasK*	Δ*vasK* complemented with pBR322-*vasK* (Tc^s)	This study
Δ*lpp*	*lpp* gene deletion mutant of *Y. pestis* CO92	20
Δ*lpp* pKD46	Δ*lpp* transformed with plasmid encoding λ-phage recombination system	This study
Δ*lpp* pBR322	Δ*lpp* transformed with pBR322 (Tc^s)	This study
Δ*lpp* Δ*rbsA*	*lpp* and *rbsA* double gene deletion mutant of *Y. pestis* CO92	This study
Δ*lpp* Δ*rbsA* pBR322	Δ*lpp* Δ*rbsA* double mutant transformed with pBR322 (Tc^s)	This study
Δ*lpp* Δ*rbsA* pBR322-*rbsA*	Δ*lpp* Δ*rbsA* double mutant complemented with pBR322-*rbsA* (Tc^s)	This study
Δ*lpp* Δ*msbB*	*lpp* and *msbB* double gene deletion mutant of *Y. pestis* CO92	19

Δlpp ΔmsbB pKD46	Δ*lpp* Δ*rbsA* double mutant transformed with plasmid encoding λ-phage recombination system	This study
Δ*lpp* Δ*msbB* Δ*rbsA*	*lpp*, *msbB*, and *rbsA* triple gene deletion mutant of *Y. pestis* CO92	This study
Δ*lpp* Δ*msbB* Δ*rbsA* pBR322	Δ*lpp* Δ*msbB* Δ*rbsA* triple mutant transformed with pBR322 (Tc^s)	This study
Δ*lpp* Δ*vasK*	*lpp* and *vasK* double gene deletion mutant of *Y. pestis* CO92	This study
Δ*lpp* Δ*vasK* pBR322	Δ*lpp* Δ*vasK* double mutant transformed with pBR322 (Tc^s)	This study
A. hydrophila*		
SSU	*Aeromonas hydrophila** human diarrheal isolate	43
Δ*vasK*	*vasK* gene deletion mutant of *A. hydrophila** SSU	43
E. coli		
S17-1-pUTminiTn*5*Km2STM	*E. coli* strain S17-1, *recA* pro *hsdR* RP4-2-Tc::Mu-Km::Tn*7* integrated into the chromosome, carries plasmid pUTminiTn5Km2STM	35
Plasmids		
pUTminiTn*5*Km2STM	Mini-transposon plasmids each carrying one of 53 unique STM tags	35
pKD46	Plasmid for λ-phage recombination system under arabinose inducible promoter	37
pKD13	Template plasmid for PCR amplification of the Km^r gene cassette flanked by FLP recombinase target sites	37
pFlp2	Plasmid for FLP enzyme under constitutively expressing *lac* promoter (Ap^r)	38
pBR322	A variant of pBR322 (Tc^s)	70
pBR322-*rbsA*	Plasmid containing the *rbsA* gene-coding region and its putative promoter inserted in the Tc^r cassette of vector pBR322	This study
pBR322-*vasK*	Plasmid containing the *vasK* gene-coding region and its putative promoter inserted in the Tc^r cassette of vector pBR322	This study

CDC=Centers for Disease Control and prevention; Tc^r=Tetracycline resistance; Tc^s=tetracycline sensitive; Ap^r=Ampicillin resistance; FLP=flippase; FRT=flippase recognition target; **A. hydrophila* SSU has now been reclassified as *A. dhakensis* SSU (146).

Construction of *Y. pestis* CO92 signature-tagged transposon mutant library.

A total of 5,088 transposon mutants of WT CO92 were created, which included 96 mutants for each of the 53 unique 40 bp long signature tags (147). As a source of the tags, 53 *E. coli* S-17 strains, each harboring the plasmid pUTminiTn*5*Km2STM with a unique tag, were used as donor strains and conjugated with WT CO92 (148). Initially, 56 tags were chosen as previously described (148) and were tested for their cross-hybridization. Three out of the 56 tags showed cross-reaction under our tested conditions, and, therefore, were excluded from the study. For each of the 53 signature tags, the following procedures were carried out. The *E. coli* S17-1 strain **(Table 1)** carrying the transposon with a unique signature tag was grown overnight, sub-cultured, and then further grown for 4 h (OD_{600}~0.6). Separately, WT CO92 was grown overnight and mixed in a 4 to 1 ratio with the above-mentioned donor *E. coli* strains. An aliquot of the mixture was spread on LB agar plates and incubated at 30°C for 24 h. Subsequently, the cultures from the LB plates were collected in sterile phosphate-buffered saline (PBS), and a portion of the mixture was spread on HIB agar plates containing polymyxin B and kanamycin for 48 h at 28°C. Following the incubation period, separate trans-conjugant colonies were tested for resistance to polymyxin B (WT CO92 is naturally resistant to this antibiotic) **(Table 1)** and kanamycin, but sensitive to ampicillin. Finally, 96 trans-conjugants, which did not show any obvious growth defects, with each tag were randomly picked and individually inoculated in the wells of a 96-well microtiter plate. After 24 h of growth, the plates were stored at -80°C after the addition of glycerol to a final concentration of 15% **(Fig. 5)**. From the fifty three 96-well plate stocks, 96 mutant pools were prepared by combining 20 µl of stock cultures from the same respective positions of 96-well microtiter plates **(Fig. 5)**. Thus, each mutant pool represented a collection of 53 transposon mutants, each with a unique signature tag.

Preparation of input mutant pools of *Y. pestis* CO92 and collection of corresponding output mutant pools from the spleen in a mouse model of pneumonic plague.

Each of the 96 mutant pools prepared above was individually tested in female Swiss-Webster mice (Taconic Biosciences, Inc., Hudson, NY) after infecting them via the intranasal (i.n.) route. The animal experiments were conducted in accordance with the Institutional Animal Care and Use Committee (IACUC)-approved protocol in the Animal Biosafety Level (ABSL)-3 facility located in the GNL. **Figure 4** shows the schematic used for screening the mutants. For each of the mutant pools with 53 unique DNA tags, three animals were infected. Before infection of the mice, a portion of the bacterial inoculum was subjected to genomic DNA isolation using DNeasy Blood & Tissue Kit® (Qiagen, Inc., Valencia, CA) and was referred to as input DNA pool or input pool. The remaining inoculum was used to infect mice at a dose of 2,500 colony forming units (CFU), representing 5 LD_{50} (1 LD_{50}=500 CFU) equivalent of WT CO92 (131). Three days post infection (p.i.), the spleens were excised to recover the output mutants. Briefly, the spleens were homogenized in sterile PBS and an aliquot of the homogenates was spread on LB agar plates containing kanamycin. After 24 h of incubation, the bacterial colonies were collected for genomic DNA isolation, which was referred to as output DNA pool or output pool.

DNA hybridization-based screening of input and output mutant pools of *Y. pestis* CO92.

The DNA hybridizations were performed for each of the input and output pools separately, as previously described (148). Briefly, 53 signature tags were polymerase chain reaction (PCR) amplified (Phusion® High-Fidelity PCR Kit, New England Biolabs, Inc., Ipswich, MA) using primers P2 and P4 from the respective transposon plasmids pUTminiTn*5*Km2STM (**Fig. 5 and Tables 1&2**). The PCR products were digested with the *Hin*dIII restriction enzyme (New England Biolabs, Inc.) to remove primer sequences,

gel purified using QIAquick® Gel Extraction Kit (Qiagen, Inc.), and then 15 ng of the tag DNA was spotted individually on a positively charged nylon membrane (Amersham Hybond-N+, GE Healthcare Life Sciences, Pittsburgh, PA). The DNA probes on the membranes were sequentially subjected to denaturation in 1.5 M NaCl and 0.5 M NaOH solution for 3 min, neutralization in 1.5 M NaCl and 0.5 M Tris-HCl [pH 7.4] solution for 5 min and again 1 min in the same but fresh solution, and washing in 2x SSC (0.3 M NaCl and 0.03 M sodium citrate [7.0]) for 2 min. Finally, DNA was UV-cross linked to the membranes.

With P2 and P4 primers (**Table 2**), the tag sequences from each of the input and the corresponding output DNA pools were PCR amplified and gel purified as described above, and digoxigenin (DIG) (Roche Applied Science, Indianapolis, IN) labeled by PCR using P2 and P4 primers as described previously (148). The labeled tags were digested with the *Hin*dIII restriction enzyme to remove the primer sequences, and denatured at 95°C for 5 min before proceeding to hybridization. The membranes prepared as mentioned above were pre-hybridized with the DIG hybridization solution (Roche Applied Science), and finally, the labeled tags were added to the membrane in a fresh-hybridization solution and incubated overnight at 42°C.

Following hybridization, the membranes were subjected to washing, blocking, and developing at room temperature (RT), unless otherwise stated, as follow: i) twice for 5 min each in 2x SSC plus 0.1% sodium dodecyl sulfate (SDS), ii) twice for 5 min each in 0.1x SSC plus 0.1% SDS at 65°C, and once for 5 min in 0.1 M maleic acid, 0.15 M NaCl [pH 7.5], 0.3% [wt/vol] Tween 20 (MNT) buffer. Then, the membranes were placed in 1x blocking solution (Roche Applied Science) for 30 min and were probed with monoclonal anti-DIG antibody in 1x blocking solution for 30 min. The membranes were washed twice for 5 min each in MNT solution, and equilibrated for 5 min in 0.1 M Tris-HCl, 0.1 M NaCl [pH 9.5] solution. Finally, CDP-Star ready-to-use solution (Roche Applied Science) was applied to each membrane, incubated for 5 min, and the positive

hybridization signals were visualized on luminescent image analyzer (Imagequant LAS4000, GE Healthcare Life Sciences). All of the hybridization steps were performed in a hybridization oven.

Testing individual signature-tagged transposon mutants of *Y. pestis* CO92 in bubonic and pneumonic plague mouse models.

Mutant clones that exhibited either complete or partial loss in virulence in terms of their ability to disseminate to the spleen, as determined by the hybridization reactions, were selected for further study. Each of the mutants was individually used to infect a group of five Swiss-Webster mice via the subcutaneous (s.c.) route at a dose equivalent to 8 LD_{50} of WT CO92 (1 LD_{50} by the s.c. route is 50 CFU) (131). The attenuated mutants after the first screen by bubonic infection were subjected to a stringent second screen in mice (n=10 to 20) at a higher infectious dose of 40 LD_{50}. The animals were observed for mortality over a period of 21-28 days. The mutant clones that were attenuated to show at least 40% animal survival, were selected for genomic characterization of the transposon insertion sites.

Transposon mutants that showed promising results during the first s.c. screening were further tested for their level of attenuation in a pneumonic plague mouse model. Each selected mutant was used to infect a group of five Swiss-Webster mice at an infection dose equivalent to 12 LD_{50} of WT CO92. The animals were observed for mortality over a period of 14 days.

Genomic characterization of transposon insertion sites in the signature-tagged mutants of *Y. pestis* CO92.

Inverse PCR was used to amplify DNA fragment flanking the mini-Tn*5* insertion as described previously (148, 149). Briefly, genomic DNA from the above selected signature-tagged transposon mutants was extracted by using a DNeasy blood and tissue kit (Qiagen, Inc.). An aliquot (2 µg) of the genomic DNA was digested with the

restriction enzymes *Bam*HI, *Mlu*I, *Pst*I, *Sal*I or *Xba*I (New England Biolabs), and the resulting fragments were ligated using T4 DNA ligase (Promega, Madison, WI). Inverse PCR was performed using outward-facing primers P1 and P3 annealing to mini-Tn*5* sequence **(Table 2)**. Subsequently, a nested PCR amplification was carried out on each of the inverse PCR products using primers P5 and P6 **(Table 2)**. The primers P5 and P6 annealed downstream to the primer pair P1 and P3. Then, the resulting PCR products were gel purified and sequenced using the primer P6 **(Table 2)**. Based on the sequence information, transposon insertion sites were identified in the genome of *Y. pestis* CO92 (128).

Table 2. Sequences of primers used in this study

Primers or primer pairs	Primer sequences (5′–3′) (Forward, Reverse)	Purpose
P2-P4	TACCTACAACCTCAAGCT, TACCCATTCTAACCAAGC	PCR amplification of STM tags
P1-P3	GCGCAACGGAACATTCATC, GCAAGCTTCGGCCGCCTAGG	Identification of Mini-Tn*5* insertion sites
P5-P6	AGGGTCAGCCTGAATACGCG, CTGACTCTTATACACAAGTGC	Identification of Mini-Tn*5* insertion sites
Kmypo2500	TTAGCTGGTAAGCGTGTCAATTCTCGCTCTGCTCA GGCAGAGCGATAACCGTGTAGGCTGGAGCTGCTTC (FRT sequence), TAATGCACTCCCTGTTGCGTGAAGCATGATGTTAT TAGATTCAATTTCATATTCCGGGGATCCGTCGACC (FRT sequence)	Construction of a DNA fragment with Km^r gene cassette and FRT sequence for the *rbsA* gene mutation
*ypo2500*V	CGTATTGCACTGGGTATCGCGTTGG, GTCATTTAACCCGCTCATTAAGACA	PCR verification of the *rbsA* gene deletion
*ypo2500*C	CGGGATCCGGTTAGCGTAGACGGCCAACCA (*BamH*I), ACGCGTCGACTCATAATGCACTCCCTGTTG (*Sal*I)	Cloning of the *rbsA* gene in plasmid pBR322
Km*ypo3603*	GACAACTCAAACCATGATCGCCATGGAATGCCACA GGAGCGTTAGCGCATGTGTAGGCTGGAGCTGCTTC (FRT sequence), TGCGATCTGTCTCAATACAATCGTGTGTCTCAATA CAGAGTGTCTGGCAGATTCCGGGGATCCGTCGACC (FRT sequence)	Construction of a DNA fragment with Km^r gene cassette and FRT sequence for the *vasK* gene mutation
*ypo3603*V	TAAACCGGCAACCACAGCAATCCGA, TTGACCTCTGGCCGTGCCGGGTGGT	PCR verification of the *vasK* gene deletion
*ypo3603*C	CTAGCTAGCCTACAGATGATAAACCGGCAA (*Nhe*I), ACGCGTCGACTCAATACAGAGTGTCTGGCA (*Sal*I)	Cloning of gene *vasK* into plasmid pBR322
Km*ypo0498*	ACCATTAGCACGATGACGTGGATGAATAGCCA AAATAAGAGGACATAGATGTGTAGGCTGGAGC TGCTTC (FRT sequence), TACCTCTTAATCTCCAGAGATTTTAGATCCTTT GCGTGTCAGATAGGACAATTCCGGGGATCCGT CGACC (FRT sequence)	Construction of a DNA fragment with Km^r gene cassette and FRT sequence for the *ypo0498* gene mutation
*ypo0498*V	GCTATTCGCTGGTTGAGGCT, AACGCTGGCAGAGAGATGAG	PCR verification of the *ypo0498* gene deletion

Construction of in-frame deletion mutants and testing in mouse models of bubonic and pneumonic plague.

To construct in-frame deletion mutants of *Y. pestis* CO92, λ-phage recombination system was used (150). Initially, the WT CO92 strain was transformed with plasmid pKD46 **(Table 1)** and grown in the presence of 1 mM L-arabinose to induce the expression of λ-phage recombination system. The above-mentioned *Y. pestis* culture was processed for the preparation of electroporation competent cells (150, 151). The latter were then transformed with 0.5 to 1.0 µg of the linear dsDNA constructs carrying the kanamycin resistance (Km^r) gene cassette that was immediately flanked by bacterial FRT (flippase recognition target) sequence followed by on either side by 50 bp of DNA sequences homologous to the 5' and 3'ends of the gene to be deleted from WT CO92. The plasmid pKD46 from the mutants that had successful Km^r gene cassette integration at the correct location was cured by growing the bacteria at 37°C. The latter mutants were transformed with plasmid pFlp2 **(Table 1)** to excise the Km^r gene cassette (38). Eventually, the plasmid pFlp2 was also cured from the kanamycin sensitive (Km^s) clones by growing them in a medium containing 5% sucrose (38). To confirm the in-frame deletion, mutants showing sensitivity to kanamycin and ampicillin were tested by PCR using appropriate primer pairs **(Table 2)** and sequencing of the PCR products.

To construct double or triple in-frame deletion mutants of CO92, a similar procedure was followed using selected single (Δ*lpp*) or double (Δ*lpp* Δ*msbB*) in-frame deletion mutants that existed in the laboratory **(Table 1)**. To construct a recombinant plasmid for complementation studies, complete open reading frame of the gene of interest along with 200 bp upstream DNA sequence corresponding to the promoter region of that gene from WT CO92 was PCR amplified using Phusion® High-Fidelity PCR Kit (New England Bioloabs). Then, the DNA construct was cloned in plasmid pBR322 in place of the tetracycline resistance (Tc^r) conferring gene cassette **(Table 1)**.

Single, double, and triple isogenic mutants, and their complemented strains, were then tested in both bubonic and pneumonic plague mouse models along with the WT CO92 strain as a control. For re-challenge experiments, after 28 days post infection (p.i.) with the selected mutants, the bioluminescent WT CO92 carrying luciferase gene operon, *luxCDABE* **(Table 1)**, was used to infect mice as described previously (152). Also *in vivo* imaging was performed on re-challenged animals using IVIS 200 bioluminescent and fluorescence whole-body imaging workstation (Caliper Corp. Alameda, CA).

Western blot analysis for detecting a T6SS effector, Hemolysin-coregulated protein (Hcp), in the isogenic mutants of *Y. pestis* CO92

Overnight grown cultures of various *Y. pestis* and *Aeromonas hydrophila* strains (the latter was reclassified as *A. dhakensis* (153) were harvested and the supernatants mixed with 20% trichloroacetic acid (v/v). The resulting precipitates were dissolved in the SDS-PAGE buffer by boiling and subjected to SDS 4-15% gradient polyacrylamide gel electrophoresis. The proteins from the gel were then transferred to a Hybond™-ECL™ nitrocellulose membrane (GE Healthcare) by following the standard procedure (154). The membrane was blocked with 1% bovine serum albumin [BSA] or 5% skim milk, and, subsequently, incubated with anti-Hcp antibodies specific for *Y. pestis* (1:1000) followed by incubation with the secondary antibodies (Goat anti-mouse IgG [1:10000]) (Southern Biotechnology Associates, Inc., Birmingham, AL). The membrane was washed with TBS (Tris Buffered Saline: 20 mM Tris-base, 136 mM NaCl [pH 7.4])/0.05% Tween 20, and the blot was developed using SuperSignal® West Dura Extended Duration Substrate (Pierce, Rockford, IL). Finally, the positive signal was detected by using ImageQuant LAS4000 platform (GE Healthcare). Polyclonal antibodies raised in mice against Hcp of *Y. pestis* were used for immunoblot analysis. The *hcp* gene (*YPO3708*) of *Y. pestis* CO92 was over-expressed in *E. coli* using the pET30a vector system as a His-tag recombinant protein and purified by using Ni^{2+} chromatography (41). As a loading control for

immunoblot analysis, we used monoclonal antibodies against DnaK (Enzo, Farmingdale, NY), a member of conserved Hsp70 chaperone family.

Growth kinetics of WT *Y. pestis* CO92, its Δ*rbsA* mutant, and the complemented strain.

Overnight cultures of various *Y. pestis* strains were washed in PBS and normalized to the same absorbance by measuring optical density at 600 nm (OD_{600}). These bacterial cultures were then inoculated separately (with approximately 1 x 10^7 CFU) in 20 mL of the modified M9 medium (1 x M9 salts [22 mM KH_2PO_4, 33.7 mM Na_2HPO_4, 8.55 mM NaCl, 9.35 mM NH_4Cl], 1 mM $MgSO_4$, 2.5 mM $CaCl_2$, 0.001 mg/mL $FeSO_4$, 0.0001% thiamine, 0.1% casamino acids) (all chemicals were obtained from Sigma-Aldrich, St. Louis, MO) contained in 125 mL polycarbonate Erlenmeyer flasks with HEPA-filtered tops. The medium either did not contain any sugar or supplemented with 0.4% glucose or 0.4% ribose, and the cultures were incubated at 28°C with shaking at 180 rpm. Samples were taken by removing 100 µL of the culture from each of the flasks at the indicated time points. Each of the samples was serially diluted, plated on SBA agar plates, and incubated at 28°C for 48 h to determine CFU/mL.

Statistical procedures.

Animal survival rate was statistically analyzed using Kaplan-Meier survival estimates with Bonferroni *post-hoc* test. *In vitro* growth of WT CO92, its Δ*rbsA* mutant or the complemented strain, under different nutritional conditions was analyzed by one-way ANOVA followed by Tukey *post-hoc* test. Wherever applicable, the *p*-values were reported, and a p value of ≤ 0.05 was considered significant.

RESULTS

Y. pestis CO92 signature-tagged transposon mutant library and its primary screen in a mouse model of pneumonic plague.

We generated a library of mutants with 53 unique DNA tags from WT CO92 by using a transposon Tn*5*-based system **(Fig. 5)**. For each signature tag, 96 mutants potentially representing Tn*5* hits at different locations on the chromosome or the plasmids of WT CO92 were randomly picked from the HIB agar plates, thus resulting in a library consisting of 5,088 mutants. During this selection process, any mutant clones that exhibited visual growth defects, such as a smaller colony size, were not included as they would be out-competed in a mixed culture infection resulting in false positives. We observed a transfer efficiency of 1.5×10^{-4} transposon mutants per donor colony when the Tn*5* harboring *E. coli* strains were mixed with the recipient WT CO92 strain at a ratio of 4:1 for the conjugation process. Finally, 96 input mutant pools, each containing a collection of 53 mutants (one clone for each one of the signature tags), were generated for screening in a mouse model of pneumonic plague for their attenuation in terms of dissemination to the internal organs, i.e., the spleen **(Fig. 5)**.

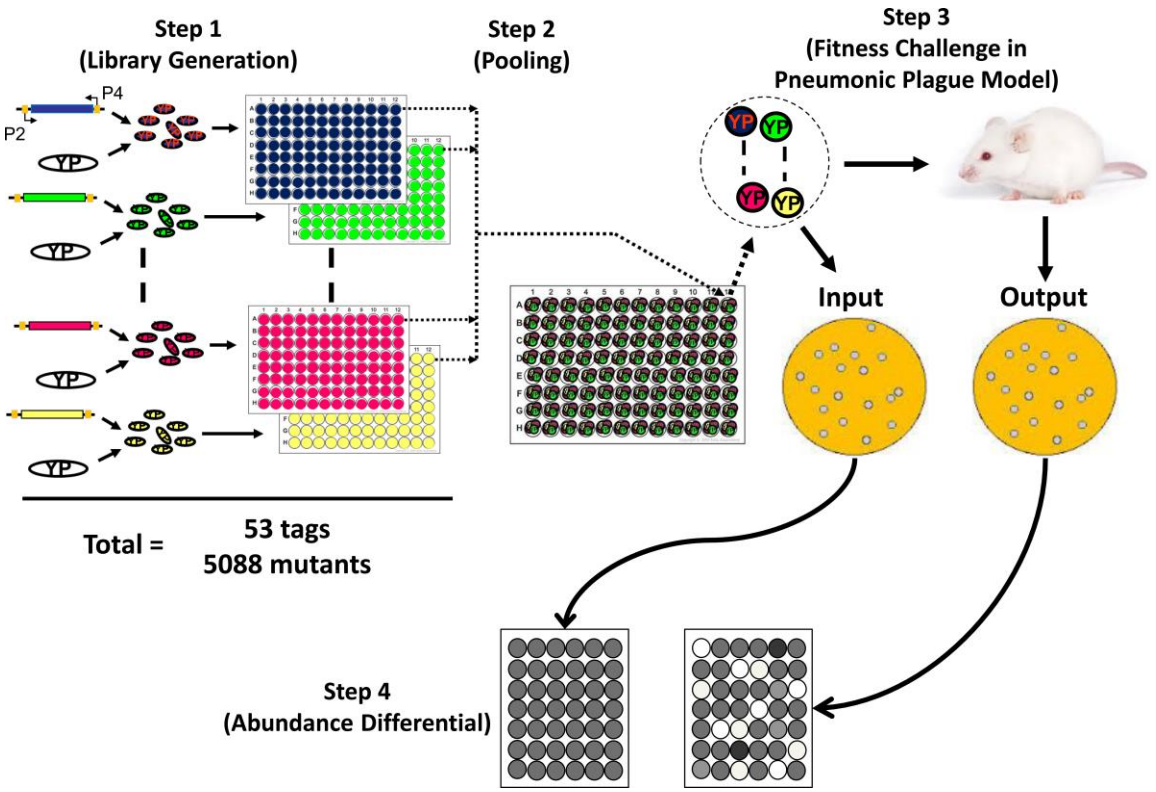

Figure 5. Schematic illustration of the signature-tagged mutagenesis approach (STM).

(Step 1)- Transposon mutants were generated through a mini-Tn*5* transposon system with 53 unique signature tags to create a library of representative 96 *Y. pestis* (YP) mutants for each tag, totaling 5,088 mutants. **(Step 2)**- One mutant for each tag was combined to generate 96 pools of 53 uniquely tagged clones. **(Step 3)-** Each pool was used to generate an input pool of bacterial DNA and to infect mice by the i.n. route (5 LD_{50}). At 3 days p.i., disseminated mutant bacteria were isolated from the spleens and DNA extracted, providing the output pool of bacterial DNA. **(Step 4)-** Signature tag probes were generated by PCR with primer pair P2-P4 common sequences adjacent to the signature tags for input and output pools of bacterial DNA. Then, each pool of the DNA (input and out) was separately hybridized to membranes spotted with an array of the 53 unique signature tags. After hybridization, the membranes were developed and the input and output pool membranes compared for changes in corresponding signature abundance.

The infectious dose of input 96 mutant pools in mice given by the i.n. route was 5 LD_{50} equivalent of the WT CO92 (131). Three days p.i., ~60% of the animals died due to developing pneumonic plague and the remaining animals had clinical symptoms of plague, such as lethargy and ruffled fur. The excised spleens from these mice, irrespective of their survival status, had high bacterial counts in the range of 1 x 10^7 to 1 x 10^8 CFU per organ. Under the conditions of hybridization and washing optimized for the study, the nylon membranes harboring purified 53 unique signature tags hybridized with the 96 input pool DNA probes (obtained from each transposon mutant pool with 53 signature tags), and showed a clear pattern of positive reactions without any background (a representative blot is shown in **Fig. 6**).

By this hybridization approach, we identified a total of 118 potential mutant candidates; among these 108 had no detectable signal on the output DNA pool membranes, and the remaining had very weak signals when compared to the corresponding input DNA pool membranes (a representative blot is shown in **Fig. 6**).

Second screen of selected signature-tagged transposon mutants of *Y. pestis* CO92 in a mouse model of bubonic plague.

We performed a second screen with the above-generated 118 mutant clones by injecting mice with individual mutants via the s.c. route at an aimed 8 LD_{50} equivalent of WT CO92 (131). Of 118 mutant clones tested, 20 of them (~17%) showed attenuation to the level of at least 20% or more animal survival (up to 100%) when compared to the WT CO92 on day 21 p.i. **(Table 3)**. One of our long term goals is to identify candidate genes that could be deleted from the WT CO92 to develop a novel live-attenuated plague vaccine. Therefore, we also tested some of the surviving animal groups after infection with representative transposon mutants to withstand re-challenge with the WT CO92. The

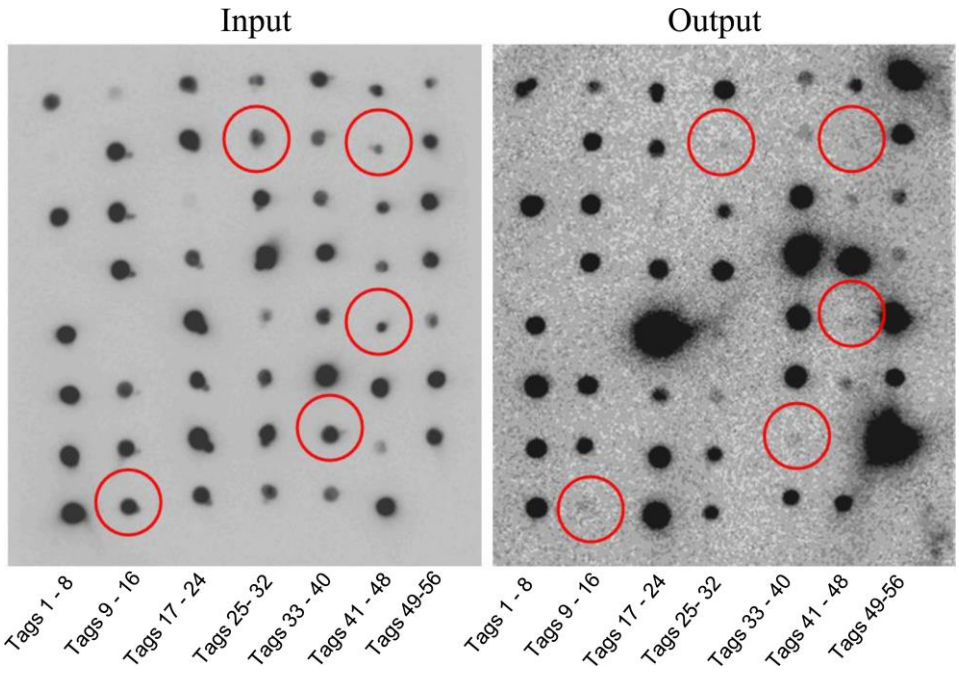

Figure 6. Representative STM hybridization reactions.

Bacterial DNA was isolated from input and output mutant pools, signature tags amplified, labeled with DIG, and then were used to hybridize membranes spotted with a signature tag array. Out of 56 initial signature tags, 3 were found to be cross-reactive (4, 13 and 56) and were subsequently excluded. Each array was composed of 53 signature tags that were shown to be specific. The circles highlight those mutants that show a reduction in abundance between the input and the output pools. The tag numbers (1-56) are indicated.

Table 3. Survival patterns for selected transposon mutants in mouse models of bubonic and pneumonic plague

Clone ID	Gene Locus ID	% Survival Post ~8 LD_{50} Infection (s.c.)			% Survival Post 12 LD_{50} Infection (i.n.)	
		Day 7	Day 14	Day 21	Day 3	Day 9
WT CO92	--	40	0	0	0	0
15-F2	YPPCP1.07	100	100	80	60	0
19-F7	unconfirmed	100	80	80	80	0
29-F7	YPO2468	60	60	60	80	40
2-H3	YPO1717	80	60	60	20	0
39-A7	YPO3319	60	60	60	80	0
39-G4	YPMT1.80c	100	40	40	20	0
42-B8	YPO2500	100	100	100	NT*	NT*
44-B5	YPO0498	80	60	60	100	40
44-F11	YPO3603	80	60	60	NT*	NT*
45-B9	YPO2884	100	80	60	100	100
47-F10	unconfirmed	80	80	80	60	0
47-G5	YPO3164	100	80	80	20	0
48-G1	PMT1 Caf1R	100	100	100	100	20
49-B1	YPO1484	80	60	60	100	100
52-B1	YPO3248	80	60	60	100	80
52-B5	Intergenic YPO0093-0094	60	60	20	100	80
53-C3	YPO1616	80	80	80	100	100
53-F10	YPO1995	100	100	100	100	0
53-G5	YPO0815	100	60	60	100	100
54-F6	Intergenic YPO1119-1120	100	100	100	100	60

Note: Clone ID represents the signature tag number and alphanumeric of individual mutants containing that signature. s.c.=subcutaneous; i.n=intranasal; NT=not tested; *prepared isogenic mutants and tested.

re-challenge occurred by a more stringent i.n. route, which evokes pneumonic plague, to gauge immunogenicity of the transposon mutant clones. As noted in **Fig. 7**, 100% of the animals that were initially infected with the transposon mutants (15-F2, 42-B8, 44-B5, 52-B1 and 53-C3) **(Table 3)** followed by re-challenge with WT CO92 strain (10 LD_{50}) were protected over a period of 21 days. All of the control naïve mice died by day 4. These second screen mutant candidates were then subjected to a higher stringency screen in a bubonic plague mouse model by increasing the challenge dose to 40 LD_{50} **(Table 4)**. As noted from this table, 10 out of 20 mutants showed 40% or more survival rate on day 21 p.i. Following this final high stringency screen, we identified the insertion sites within the disrupted genes for each of the mutant candidate strains.

Genetic characteristics of signature-tagged transposon mutants of *Y. pestis* CO92 that are attenuated in a mouse model of bubonic plague

Identification of the disrupted genes or genetic regions in the transposon mutants was accomplished using inverse PCR followed by confirmation of the mutation location by sequencing of the PCR products. Genomic characterization of 18 out of 20 attenuated mutants identified during the first screen by s.c. challenge was listed in **Table 3**, while genomic locations of transposon integration for mutant clones 19-F7 and 47-F10 were not confirmed. Of these confirmed 10 mutants showing attenuation under high stringency in a mouse model of bubonic plague, transposon insertion was identified in one of six uncharacterized genes **(Table 4)**. For example, clones 52-B1 and 2-H3 encode putative surface-exposed and membrane protein, respectively. Clones 44-B5, 53-C3, 54-F6, and 39-G4 code for hypothetical or proteins with putative functions. In clone 47-G5, the transposon interruption occurred in the cytochrome o ubiquinol oxidase subunit II **(Table 4)**. Two of the genes encoded previously characterized virulence factors and included the *pla* protease gene located on the pCP1 plasmid of *Y. pestis* (64, 131). The *pla* protease gene was interrupted in the mutant clone (15-F2) **(Table 4)**, adding credibility to our

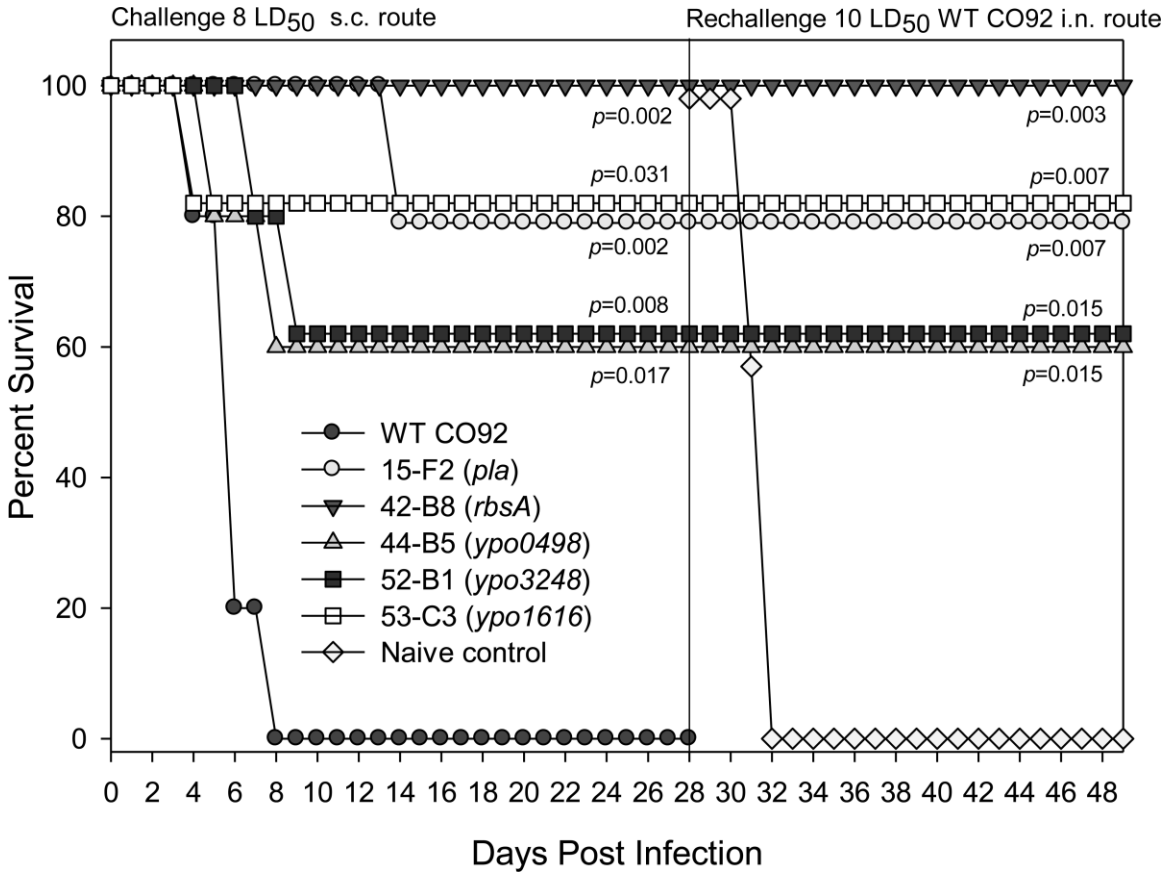

Figure 7. Survival of mice after initial infection with *Y. pestis* CO92 mutants in a bubonic plague model and subsequent re-challenge to evoke pneumonic plague with WT CO92.

Five adult Swiss-Webster mice were challenged with an infectious dose of 8 LD_{50} by the s.c. route with the mutants and the WT CO92 strain. Surviving mice from the initial challenge with the selected mutant groups were followed for 28 days p.i. and then re-challenged with 10 LD_{50} of WT CO92. Survival data were analyzed for significance by Kaplan-Meier survival estimates with Bonferroni *post-hoc* test. The *p* values are for each of the strains compared to WT CO92 or naïve control for the re-challenge study.

screening process. This mutant was highly attenuated, as 85% of the animals survived the challenge in a bubonic plague model on day 21 p.i. **(Table 4)**.

Mutant clone 44-F11, with 60% of the mice surviving the challenge, was identified as having a disruption in a gene whose product has homology to VasK of *A. dhakensis* SSU, a key component of the T6SS (155) **(Table 4)**. Clone number 42-B8 was identified as having a transposon insertion within the gene referred to as *rbsA,* and 85, 70, and 60% of the animals survived after challenge on days 7, 14, and 21 p.i., respectively, in a mouse model of bubonic plague **(Table 4)**. This gene is part of the *rbs* operon that codes for a putative ribose transport system and has been described in orthologous systems (156, 157). Likewise, the clone 44-B5 in which the transposition occurred in a hypothetical gene was highly attenuated, with 100, 85, and 85% survival of animals on days 7, 14, and 21 p.i., respectively **(Table 4)**.

Table 4. Survival patterns for selected transposon mutants over a 21 day period in a mouse model of bubonic plague at an infectious dose of 40 LD_{50}

Clone ID	Gene Interrupted	% Survival Post ~40 LD_{50} Infection (s.c.)			Gene or protein description / Protein homology
		Day 7	Day 14	Day 21	
WT CO92	--	15	0	0	--
15-F2	***pla***	**85**	**85**	**85**	**Plasminogen activator**
2-H3	*ypo1717*	80	60	60	Putative membrane protein
39-G4	*ypmt1.80c*	100	40	40	Putative transposase
42-B8	*rbsA* (*ypo2500*)	85	70	60	Putative sugar transport system, ATP-binding protein
44-B5	*ypo0498*	100	85	85	Hypothetical protein, associated with a type 6 secretion system locus
44-F11	***vasK* (*ypo3603*)**	**60**	**60**	**60**	**Type-6 secretion system component-VasK**
47-G5	*ypo3164*	100	80	40	Cytochrome o ubiquinol oxidase subunit II
52-B1	*hxuB* (*ypo3248*)	100	60	60	HxuB (hemolysin secretion protein) / putative surface-exposed protein
53-C3	*ypo1616*	85	60	60	Hypothetical protein
54-F6	*ypo1119-ypo1120*	100	100	100	Insertion in intergenic region between two conserved hypothetical protein

Note: Bolded mutants represent those that had transposon disruption in genes previously identified as virulence factor-encoding genes in *Y. pestis*, i.e., *pla*, or in *A. dhakensis* SSU, i.e., *vasK*. The number of animals used per group ranged from 10 to 20.

Pathodynamics of bubonic plague infection for the isogenic mutants of *Y. pestis* CO92 deleted for genes *rbsA, vasK* or *ypo0498* in a mouse model.

Transposon mutagenesis does not always provide a true estimate of bacterial attenuation during infection due partly to possible polar effects, and, therefore, we created isogenic mutants for three of the genes *rbsA, vasK,* and *ypo0498* **(Table 4)**. Gene *rbsA* was targeted as it had the most functional information available from orthologs in other bacterial species (156, 157). Similarly, the gene *ypo3603* (*vasK*) was targeted due to the virulence attributes associated with orthologous genes (155). Another candidate gene, *ypo0498,* which encodes a hypothetical protein and is part of another T6SS locus, was also selected. These mutants were then used to challenge mice by the s.c. route to replicate data obtained during the transposon mutant screening.

Animals infected with the Δ*rbsA* or the Δ*vasK* isogenic mutant by the s.c. route showed a statistically significant attenuation, as 40% (p=0.042) and 70% (p=0.002), respectively, of the mice survived when challenged with 10 LD_{50} equivalent of WT CO92 **(Fig. 8)**. The control animals infected with the WT CO92 showed a survival of less than 5% in three combined independent experiments by day 14 p.i. When the Δ*ypo0498* isogenic mutant was used to challenge mice by the s.c. route, an increase in mean time to death was noted at a much higher 35 $LD_{50,}$ although the data did not reach statistical significance **(Fig. 8)**.

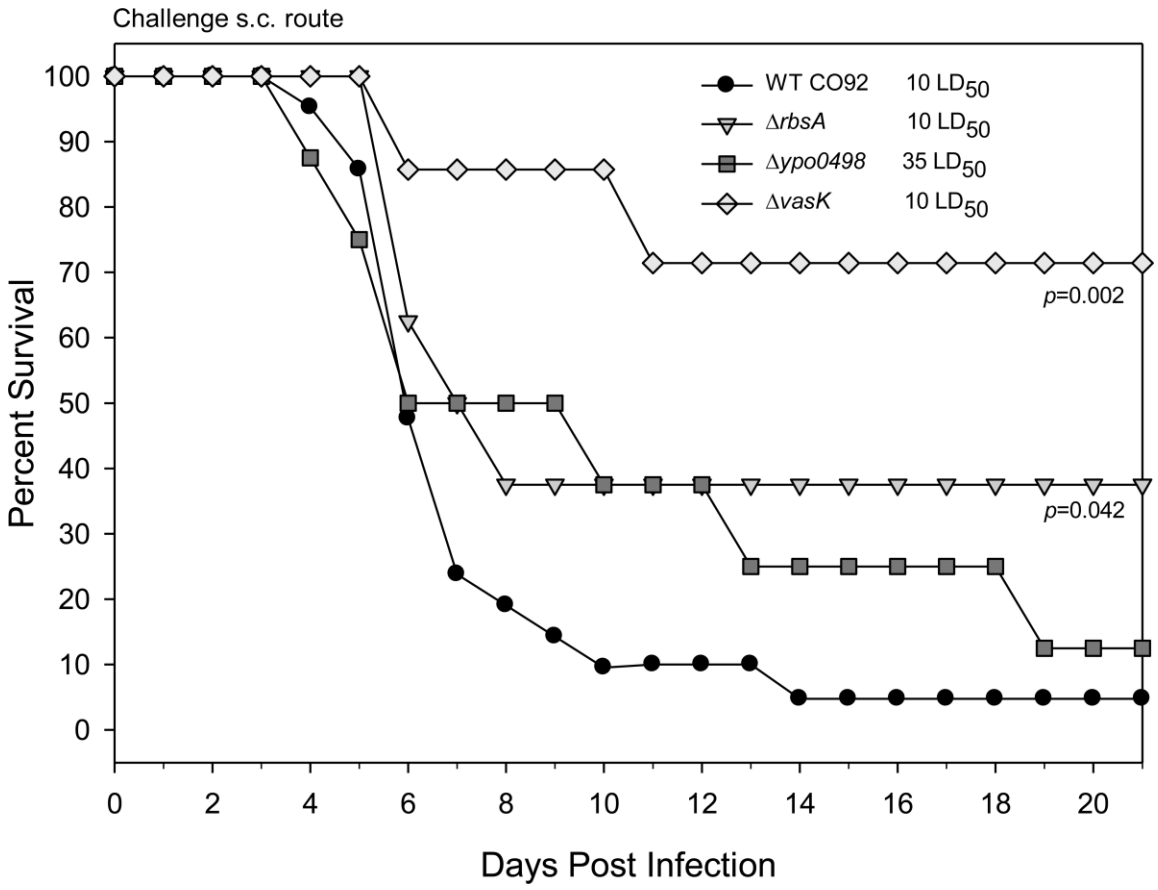

Figure 8. Survival of mice after challenging with the indicated isogenic mutants of *Y. pestis* CO92 in a bubonic plague model.

After generation of the isogenic mutants for *rbsA*, *vasK*, and *ypo0498*, each strain was used to challenge 10 adult Swiss-Webster mice by the s.c. route at the indicated LD_{50}s. The animals challenged with WT CO92 represented pool from three independent experiments, with a total number of 22 mice. Survival data were analyzed for significance by the Kaplan-Meier survival estimates with Bonferroni *post-hoc* test. The *p* values are for each of the mutant strains compared to pooled WT CO92.

Characterization of the Δ*vasK* mutant of *Y. pestis* CO92 in a mouse model of pneumonic plague.

Following evaluation by the s.c. route of the disease (bubonic plague), the Δ*vasK* mutant was then assessed for attenuation in a mouse model of pneumonic plague. At a dose equivalent to 12 LD_{50} of WT CO92, the mice exhibited a 20 percent survival rate (p=0.031) by day 21 p.i., with no survival of animals challenged with a similar dose of WT CO92 (**Fig. 9A**). To further confirm that deletion of the *vasK* gene resulted in this attenuated phenotype, mice challenged with the complemented strain (Δ*vasK* pBR322-*vasK*) **(Table 1)** recapitulated the WT phenotype with no survival at an equivalent dose of the isogenic mutant. Although the attenuation of the Δ*vasK* mutant was not high in a stringent pneumonic plague mouse model, we obtained the first mutant which was attenuated in developing both bubonic and pneumonic plague.

In addition to generating a Δ*vasK* single mutant, we also deleted the *vasK* gene from the Δ*lpp* background strain of CO92. Braun lipoprotein (Lpp) has previously been shown in our laboratory to provide attenuation in mouse models of pneumonic and bubonic plague through decreased intracellular survival in macrophages (132, 133, 158). The rationale for deleting the Δ*vasK* gene from the Δ*lpp* background strain of CO92 was to delineate whether additive or synergistic attenuation could be achieved with the Δ*lpp* Δ*vasK* double mutant in a mouse model of pneumonic plague.

Infection by the i.n. route with the Δ*lpp* Δ*vasK* double mutant resulted in 90% survival (p<0.001) of mice at a dose equivalent to 12 LD_{50} when compared to only 5% survival rate of animals after challenge with the Δ*lpp* single mutant by day 21 p.i. at a comparable challenge dose **(Fig. 9A)**. These data indicated synergistic attenuation of the Δ*lpp* Δ*vasK* double mutant in a mouse model of pneumonic plague.

To determine if the attenuating effect of the *vasK* gene deletion from WT CO92 or its Δ*lpp* mutant in mice was related to the inhibition of secretion of a T6SS effector,

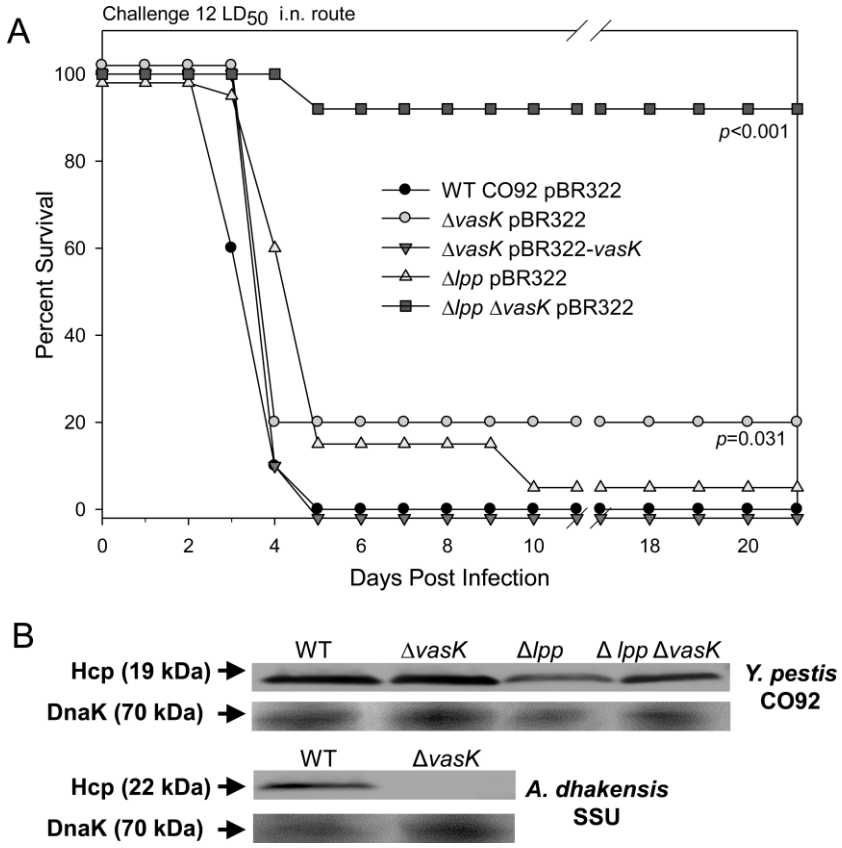

Figure 9. Survival of mice challenged with the Δ*vasK* isogenic mutants of *Y. pestis* CO92 in a pneumonic plague model and secretion of Hcp through the T6SS.

(A) Adult Swiss-Webster mice were challenged by i.n. route with 12 LD_{50} of WT CO92 pBR322 (n=10), Δ*vasK* pBR322 (n=10), Δ*vasK* pBR322-*vasK* (n=10), Δ*lpp* pBR322 (n=20), and Δ*lpp* Δ*vasK* pBR322 (n=10). Mice were followed for survival up to 21 days and data analyzed for significance by the Kaplan-Meier survival estimates with Bonferroni *post-hoc* test. The *p* values are for each of the mutant strains compared to WT CO92. **(B)** Western blot analysis was performed to detect Hcp in the supernatants of various bacterial cultures using specific anti-Hcp antibodies and the level of DnaK in bacterial pellets was examined as a loading control for samples used during Western blot analysis. The molecular weight of Hcp and DnaK are indicated.

Hcp, a Western blot analysis was performed on the culture supernatants of WT CO92 and its Δ*lpp* single, Δ*vasK* single, and Δ*lpp* Δ*vasK* double mutants. We have shown earlier that the secretion of Hcp was blocked when the *vasK* gene was deleted from a diarrheal isolate SSU of *A. dhakensis* (155). As seen in **Fig. 9B**, no differences in the secretion of Hcp were observed between the WT CO92 strain and the Δ*vasK* mutants, irrespective of whether the bacterial cultures were grown at either 28 or 37°C. As expected, while the correct size Hcp was detected in the supernatant of WT *A. dhakensis* SSU, the protein band was absent from its corresponding Δ*vasK* mutant. Since Hcp of *Y. pestis* and *A. dhakensis* exhibits high homology (81%), the same antibodies detected Hcp in both the pathogens. A higher molecular size of Hcp detected in *A. dhakensis* (22 kDa) when compared to that in *Y. pestis* (19 kDa) is likely due to post-translational modification as was also observed in the Hcp from *Vibrio cholerae* (159).

The gene *rbsA* is required for the full virulence of *Y. pestis* CO92 in a pneumonic plague mouse model and in the utilization of ribose.

In a pneumonic plague model, the Δ*rbsA* mutant was attenuated with 30% of the mice (p=0.0098) having survived the challenge, while the animals infected with the WT CO92 or those infected with the *rbsA* complemented strain died by day 6 at a similar infectious dose of 11 LD_{50} **(Fig. 10A)**.

Earlier studies suggested that domains with sequence homology to the RbsA protein function as a ribose transport system (156, 157). To explore the role of ribose utilization, the Δ*rbsA* mutant was grown in a modified minimal medium that was restricted for the carbon source. In a minimal medium supplemented with 0.4% ribose, the Δ*rbsA* mutant displayed a delayed growth pattern similar to when no ribose was added to the medium **(Fig. 10B)**. However, the WT CO92 and the Δ*rbsA* pBR322-*rbsA* complemented strain exhibited normal and similar growth kinetics in a ribose-containing medium **(Fig. 10B)**.

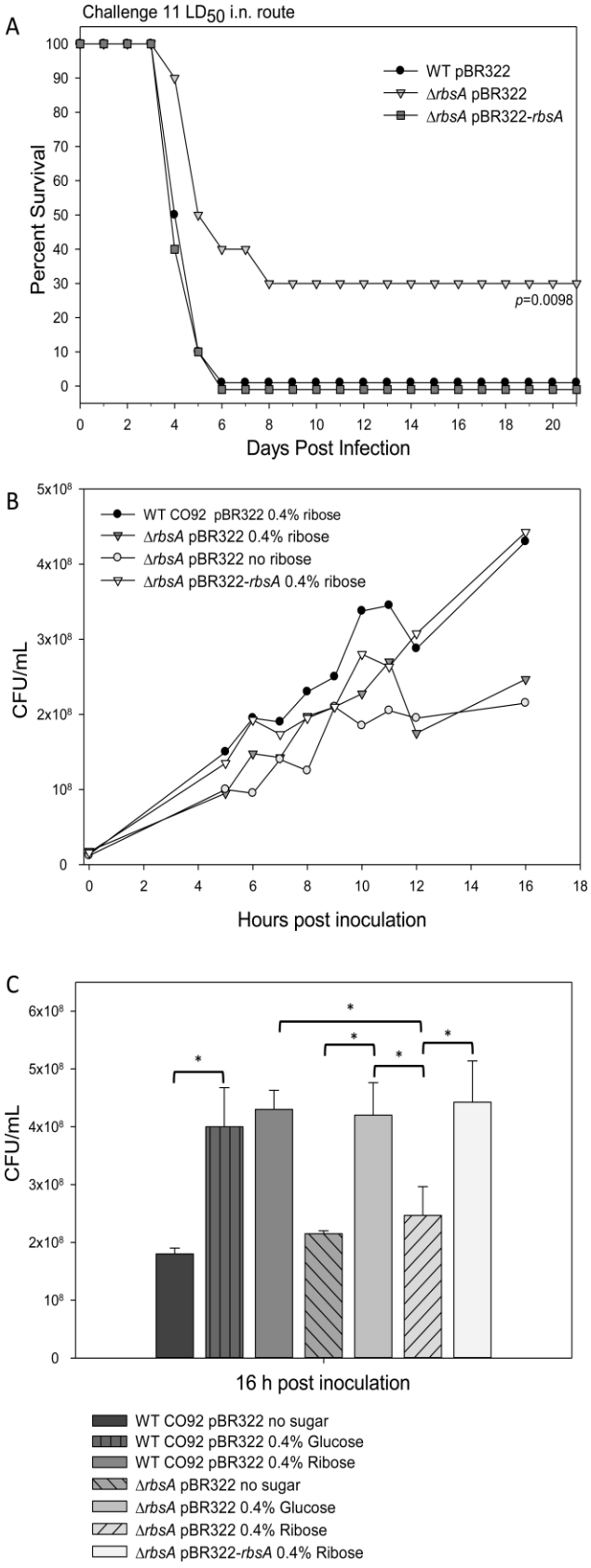

Figure 10. Survival of mice challenged with the Δ*rbsA* isogenic mutant of *Y. pestis* CO92 in a pneumonic plague model and ribose utilization.

(A) Ten adult Swiss-Webster mice were challenged by the i.n. route with 11 LD_{50} for each of the tested strains followed by observing mortality for 21 days. Survival data were analyzed for significance by the Kaplan-Meier survival estimates with Bonferroni *post-hoc* test. The *p* values are for each of the strains compared to WT CO92. **(B)** Growth of mutants and WT CO92 in a modified M9 minimal medium with or without the supplementation of 0.4% ribose. Samples were taken at time points indicated and plated for CFU. **(C)** At 16 h post inoculation, culture titrations were determined for the WT CO92 pBR322, Δ*rbsA* pBR322, and Δ*rbsA* pBR322-*rbsA* grown in a modified M9 minimal medium with or without the supplementation of 0.4% glucose or 0.4% ribose. Statistical significance was analyzed by one-way ANOVA with Tukey *post-hoc* test. Significant comparisons are between groups indicated with (*) and brackets at a $p<0.001$.

In a minimal medium, WT CO92 without any carbon source grew poorly after 16 h of incubation; however, the addition of either 0.4% glucose or ribose resulted in luxuriant bacterial mass ($p<0.001$) **(Fig. 10C)**. As mentioned in **Fig. 10B**, the Δ*rbsA* mutant grew poorly in the minimal medium supplemented with ribose after 16 h of incubation and had a bacterial mass similar to when no carbon source was added to the medium **(Fig. 10C)**. However, the Δ*rbsA* mutant exhibited similar growth as noted for the WT CO92 when the medium was supplemented with glucose **(Fig. 10C)**. The complemented Δ*rbsA* mutant strain restored the ability to utilize ribose and allowed the bacteria to grow to a density twice that of the non-complemented strain ($p<0.001$) **(Fig. 10C)** and similar to the WT CO92 strain when grown in the ribose or glucose supplemented medium.

To assess the potential of *rbsA* deletion as a component of the live attenuated vaccine and to further characterize its attenuating characteristics, we constructed double and triple isogenic mutants in which the *rbsA* gene was deleted from the Δ*lpp* and Δ*lpp* Δ*msbB* background strains of CO92. The *msbB* gene encodes an acylytansferase that attaches lauric acid to the lipid A moiety to increase biological potency of LPS (160). The Δ*lpp* Δ*msbB* double mutant exhibited increased attenuation compared to respective single mutants alone (132). The resulting double (Δ*lpp* Δ*rbsA*) or the triple (Δ*lpp* Δ*msbB* Δ*rbsA*) isogenic mutant showed a synergistic reduction in virulence (**Fig. 11A**).

While none of the Δ*lpp* Δ*msbB* double mutant-infected mice survived day 5 p.i. at 20 LD_{50}, 90% of the mice challenged with 15 LD_{50} of the WT CO92 died (**Fig. 11A**). Animals infected with the Δ*lpp* Δ*rbsA* double mutant showed 75% survival ($p<0.001$) at a dose of 20 LD_{50}. Challenge with 20-50 LD_{50} of the Δ*lpp* Δ*msbB* Δ*rbsA* triple mutant in mice by the i.n. route provided 100% survival over 28 days p.i. ($p<0.001$) **(Fig. 11A)**. As was observed with the Δ*rbsA* single mutant strain **(Fig. 11A)**, when the Δ*lpp* Δ*msbB* Δ*rbsA* triple mutant was complemented with the *rbsA* gene and used to infect mice, 80%

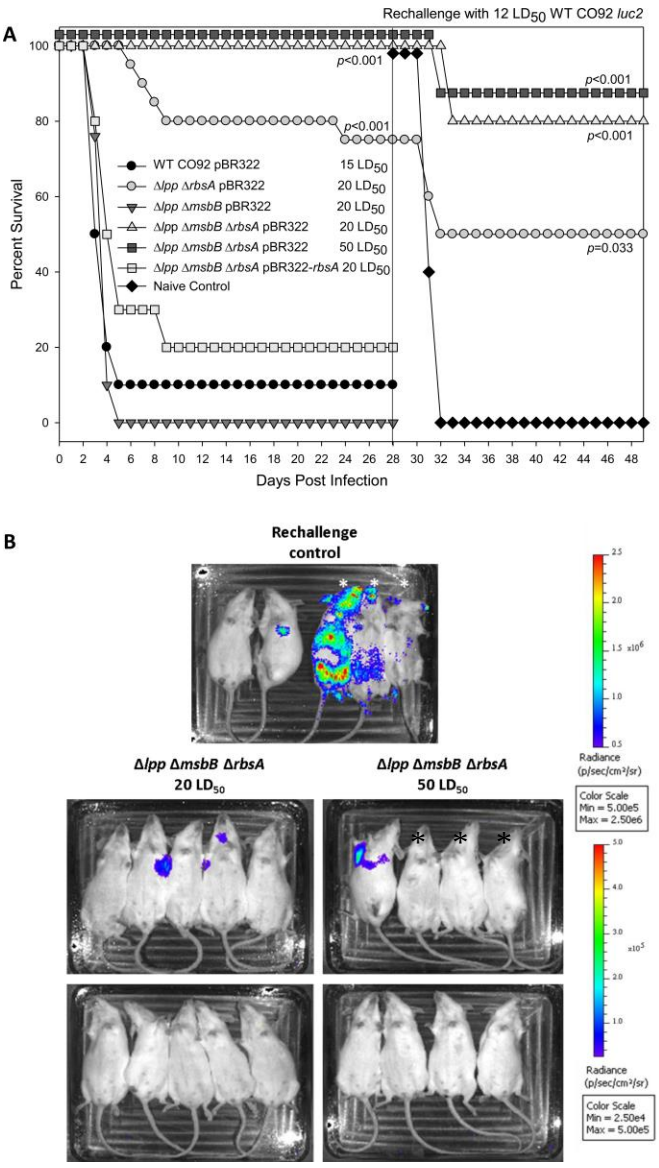

Figure 11. Survival of mice after initial infection with the Δ*rbsA* isogenic mutants of *Y. pestis* CO92 in a pneumonic plague model and subsequent re-challenge with WT CO92 *luc2* and evaluation of bacterial burden by IVIS.

(A) Adult Swiss-Webster mice were challenged at the indicated LD_{50}s by the i.n. route with WT CO92 pBR322 (n=10), Δ*lpp* Δ*rbsA* pBR322 (n=20), Δ*lpp* Δ*msbB* pBR322 (n=10), Δ*lpp* Δ*msbB* Δ*rbsA* pBR322 (20 LD_{50}, n=10), Δ*lpp* Δ*msbB* Δ*rbsA* pBR322 (50 LD_{50}, n=8), and Δ*lpp* Δ*msbB* Δ*rbsA* pBR322-*rbsA* (n=10) and observed for mortality over a period of 28 days. Surviving mice after the initial challenge with the mutants and the naïve control animals (n=5) were re-challenged with 12 LD_{50} of WT CO92 *luc2* (with luciferase gene) strain. Survival data were analyzed for significance by the Kaplan-Meier survival estimates with Bonferroni *post-hoc* test. The *p* values for each of the strains were compared to WT CO92 or naïve control re-challenge with WT CO92 *luc2*. **(B)** On day 3 post re-challenge, selected groups of mice were imaged by IVIS to determine relative bacterial burden. In WT CO92, three mice indicated by asterisks were found dead before imaging.

of the animals succumbed to infection with no significant difference in the survival pattern when compared to mice infected with the Δ*lpp* Δ*msbB* double mutant **(Fig. 11A)**.

As part of the evaluation for its inclusion as a component in a live-attenuated vaccine candidate, we were interested in testing the immune-protective potential of this strain. To accomplish this, we re-challenged the groups of mice that received a 20 LD_{50} of the Δ*lpp* Δ*rbsA* double mutant or the Δ*lpp* Δ*msbB* Δ*rbsA* triple mutant strain with a fully virulent bioluminescent *Y. pestis* CO92 strain on day 28 post initial challenge. Likewise, the group receiving a 50 LD_{50} of Δ*lpp* Δ*msbB* Δ*rbsA* triple mutant strain was subsequently challenged with bioluminescent *Y. pestis* CO92 strain **(Fig. 11B)**. This bioluminescent strain allowed us to evaluate progression of the disease as well as survival data from the same groups of mice. By day 3 p.i., 60% of naïve mice succumbed to the disease while 1 of the remaining 2 showed heavy infection in the lungs (**Fig. 11B**) and died on the following day. The remaining naïve mouse succumbed 2 days following imaging.

Only 2 of the 10 mice (20%) from the initial 20 LD_{50} challenge group with the Δ*lpp* Δ*msbB* Δ*rbsA* triple mutant strain showed bacterial burden and later succumbed to infection due to WT CO92 **(Fig. 11A&B)**. Only 1 out of the 8 mice (13%) from the initial 50 LD_{50} challenge group of the Δ*lpp* Δ*msbB* Δ*rbsA* triple mutant strain showed bacterial burden and succumbed to infection during re-challenge with WT CO92 **(Fig. 11A&B)**.

Interestingly, animals initially challenged with the Δ*lpp* Δ*rbsA* double mutant strain (75% protected) showed only a 50% survival after re-challenge **(Fig. 11A)**, indicating that the Δ*lpp* Δ*msbB* Δ*rbsA* triple mutant strain was better attenuated than the Δ*lpp* Δ*rbsA* double mutant and developed superior immunity in mice to subsequently protect animals from re-challenge with the WT CO92.

Third screen of selected signature-tagged transposon mutants of *Y. pestis* CO92 in a mouse model of pneumonic plague.

During the initial stage of pneumonic plague, *Y. pestis* suppresses the host immune system to down-regulate the inflammatory response, and, thereby, creating a highly permissive niche for the bacterium to multiply in an unrestrictive manner (48, 49). Subsequently, this accumulation of proliferating bacteria leads to the induction of a massive inflammatory reaction and that causes lung edema and death of the infected animals (48-50). Taken these findings together, it is likely that a *Y. pestis* mutant which is attenuated for dissemination to the peripheral organs after intranasal infection could still cause inflammatory changes in the lung tissue. Consequently, infected animals would succumb to infection due to pneumonia rather than the septicemic dissemination as noted during bubonic plague. Therefore, we further evaluated the extent of attenuation in causing pneumonic plague by the remaining 18 (Δ*vasK* and Δ*rbsA* isogenic mutants were already characterized) signature-tagged mutants (**Table 3**) identified during the screening process, and the animals were infected by the i.n. route at a dose equivalent to 12 LD_{50} of WT CO92 (**Table 3**).

In general, a delayed pattern of death was noted for all the mutants on day 3 after infection (**Table 3**). Nine out of 18 mutants exhibited between 40-100% survivals on day 9. The mutants 45-B9, 49-B1, 53-C3, and 53-G5 were unable to kill any mice, while 80% of mice survived challenge with mutants 52-B1, and 52-B5. These data implied that some mutants identified during the initial bubonic plague screen were attenuated in causing primary pneumonic plague as well and will be further characterized.

DISCUSSION

Knowledge on the virulence factors of *Y. pestis* is crucial to developing a new plague vaccine or to design a better therapeutic intervention. As no FDA approved plague vaccine is available for humans and the antibiotics have limited role when the disease progresses to a clinical stage, search for novel virulence factors of the organism becomes a compulsive need to combat plague in the future. Here, we chose high-throughput STM

approach, because this technique offers a power of analyzing multiple mutants simultaneously for attenuation in virulence either *in vitro* or *in vivo* assays (141, 147).

In this study, more than 5,000 transposon mutants of *Y. pestis* CO92, an isolate originally from a human case of pneumonic plague in the United States (161), were screened for impairment to disseminate to internal organs (e.g., spleen) in a mouse model of pneumonic plague (Fig. 5). Among these mutants, 118 were unable to reach in detectable numbers in the spleen as identified by comparing the presence or absence of signature tags between the input and output pools. The detection rate of such mutants (~2.4%) was close to that obtained in other studies using similar types of STM techniques (148, 162). We preferred to use pneumonic plague mouse model for our initial screening of the mutants for the following reasons: 1) pneumonic plague is the deadliest form with a high fatality rate compared to the bubonic form of plague, and 2) majority of the mice die due to pneumonic infection by day 3 p.i., with approximately 10^7 to 10^9 cfu of the plague bacterium in the peripheral organs (163). A high bacterial burden in the peripheral organs of mice is needed to obtain an adequate tag representation in the output pools during STM, and 10^4 cfu of bacteria is recommended as a threshold for obtaining authentic data (164). When animals are infected by the s.c. route to evoke bubonic plague, gauging consistent disease progression is somewhat challenging and the bacterial load in peripheral organs is relatively lower compared to that in the pneumonic plague mouse model (165, 166).

The complexity of the mutant pools during STM is a crucial parameter and has to be carefully considered for obtaining a high quality screen in the animal models (147). Although an increased pool complexity would enable more mutants to be screened simultaneously, one might also enhance the probability that some virulent mutants would not be present in sufficient numbers in the organs of an infected animal, and, thus, leading to false positive data. In addition, the quantity of a labeled tag for each transposon is inversely proportional to the complexity of the tag pool during

hybridization analysis (147). In our study, the number of signature tags was reduced from 56 to 53 due to cross-reaction noted for three tags during the prescreening step (148). The elimination of such tags is a pre-requisite in performing STM-based screens (141). At a challenge dose of 5 LD_{50} (used in our study), the inocula for the mutant pools with a complexity of 53 tags would provide ~50 cfu of the each tested mutant to ensure adequate bacterial number at the initial infection site, i.e., the lungs.

Unlike in other STM studies, we neither opted for a second round of animal infection-hybridization screening process nor used an *in vitro* assay to narrow down the number of selected mutants for further studies (148, 164). We rather chose bubonic plague mouse model and tested each of the 118 mutants individually and animals examined for mortality. While 20/118 mutants exhibited an attenuated phenotype at 8 LD_{50}, only 10 showed promising level of attenuation at an infectious dose of 40 LD_{50} (Tables 3&4). The false positive clones appeared in our initial screen were most likely due to technical artifacts associated with the STM technique. Indeed, hybridization signals for 3 tags (2, 9 and 19) were consistently missing from the blots of our input pools (Fig. 6), suggesting that these three tags were insufficiently PCR amplified and labeled from the complex DNA pools. These data correlated with an earlier report that STM mutants were frequently found to contain un-amplifiable tags or no tags at all (167). However, the genetic nature of the pathogen being studied may also play a role as the same 56 signature tags were successfully used in *Salmonella* Typhimurium and *Aeromonas veronii* (147, 148). Nevertheless, further reduction in the complexity of the pools should be highly recommended to improve specificity of the STM approach.

Our genomic characterization of the 10 mutants showed transposon insertion largely in uncharacterized genes (in 6 mutants) encoding hypothetical or putative proteins (Table 4). In the remaining four mutants (15-F2, 42-B8, 44-F11, and 52-B1), the interrupted genes encoded or were assigned some functions. In clone 15-F2, the interruption occurred in a well-known virulence gene *pla* located on the pPCP1 plasmid

of the plague bacterium. Pla plays an important role during bubonic plague, particularly in facilitating *Y. pestis* to disseminate systemically (64, 131), thus validating our screening process.

STM technique has previously been used to identify virulence factors in several pathogenic bacteria, including *Y. pestis* (164, 168). These studies employed either *Y. pestis* CO99-3015 strain lacking the pCD1 plasmid with a cell culture-based *in vitro* screen or *Y. pestis* Kimberley53 strain in a bubonic plague mouse model (infection dose of 100 cfu) as the initial screen (164, 168). Strain Kimberley53 was obtained by infecting mice by the s.c. route with *Y. pestis* Kimberley (164, 169). More recently, a laboratory reconstructed version of *Y. pestis* KIM10 strain, KIM1001, was used for transposon mutagenesis with a high-throughput sequencing (Tn-seq) to systematically probe the *Y. pestis* genome for elements contributing to fitness during infection. An intravenous route with an infection dose of 2.3×10^7 cfu of KIM1001 was used in order to preserve the diversity of the mutant pools (142). Although all of the above-mentioned studies yielded a set of genes associated with the virulence of *Y. pestis,* several of them belonged to the category of uncharacterized genes. Importantly, none of these genes were shared when compared with the interrupted genes identified in our mutant clones. This could be attributed to different strains and infection routes used as well as stringency of the screening procedures, and the threshold for accepting attenuated clones.

Two attenuated mutant clones were identified during our screens (44-B5 and 44-F11, Table 4) in which transposition occurred in the T6SS. Although the role of T6SS has been demonstrated in some pathogenic bacteria (170, 171), its involvement in the pathogenesis of *Y. pestis* infections has not been elucidated. Based on *in silico* analysis, six T6SS clusters have been predicated in the *Y. pestis* genome (170). Mutant 44-B5 was interrupted in an uncharacterized gene *ypo0498* and it is within the *ypo0495-ypo0518* locus, one of the six T6SS clusters found in *Y. pestis* CO92 (103, 170). Interestingly, the expression of the genes (*ypo0499-ypo0516*) in this T6SS locus was found to be up

regulated at 26ºC compared to that at 37ºC, and, therefore, its role in bacterial lifecycle in fleas has been speculated (103). However, deleting a portion (*ypo0499-ypo0516*) of this T6SS locus from WT CO92 did not affect the ability of the bacterium to infect the oriental rat flea, *Xenopsylla cheopis*, as well as its associated disease dynamics in both bubonic and pneumonic plague mouse models, although a decreased uptake by murine macrophage-like J774.A1 cells was noticed for the deletion mutant (103, 170).

Similarly, the expression of the *ypo0498* gene was up regulated approximately 3.7 folds when *Y. pestis* CO92 strain was exposed to human plasma, and was 14 folds higher at the mid-phase of the exponential growth compared to that at the stationary phase of bacterial growth. Interestingly, switching the growth temperature from 28ºC to 37ºC down-regulated the expression of the *ypo0498* gene to approximately 9 folds (138). Further, during infection in mice, the expression of the Δ*ypo0498* gene was down regulated (2-fold) in the lung tissues when compared to bacterial growth in the BHI broth at 37°C (27). Although we have shown a delayed time to death in mice infected with the Δ*ypo0498* isogenic mutant in a bubonic plague model, it is as virulent as the WT CO92 in a pneumonic plague mouse model (data not shown). Therefore, the role of YPO0498 and its associated T6SS locus in the pathogenesis of *Y. pestis* infections is still uncertain and needs further investigation.

In mutant 44-F11, the transposition occurred in the *ypo3603* gene which is homologous to the *vasK* gene and encodes a key component of the T6SS (155). The *ypo3603* gene belongs to another T6SS locus (*ypo3588-ypo3615*) in *Y. pestis* CO92 (170). Our earlier study showed that VasK mediated the secretion of T6SS effectors (e.g., Hcp) in *A. dhakensis* SSU, as the deletion of this gene led to a failure of the mutant to secrete Hcp to the extracellular medium and the mutant was attenuated in a septicemic mouse model of infection (155). Although six possible T6SS gene clusters have been predicted, BLAST search of the *hcp* gene sequence against the other predicted protein-encoding genes on *Y. pestis* CO92 genome revealed only one copy of the *hcp* gene.

Amino acid sequence of this *Y. pestis hcp* gene shares 82% and 81% homology with the Hcp of *Vibrio cholerae* and *A. dhakensis* strain SSU, respectively (http://blast.ncbi.nlm.nih.gov/Blast.cgi). Surprisingly, deletion of the *ypo3603* gene (Δ*vasK*) from *Y. pestis* CO92 did not prevent secretion of Hcp (Fig. 9B), suggesting that the secretion of Hcp might operate through other T6SS channels in *Y. pestis* CO92 and needs further studies. Nevertheless, our data demonstrated that the Δ*vasK* mutant of *Y. pestis* CO92 was attenuated in inducing both bubonic and pneumonic plague in mouse models. Importantly, the attenuated phenotype of the mutant Δ*vasK* could be fully complemented. To the best of our knowledge, this is the first report demonstrating a role of T6SS in the pathogenesis of *Y. pestis* infection.

In our screen, we did not identify so far any genes related to the T3SS which is an important virulence mechanism for *Y. pestis* (16). We would like to emphasize that our screening process for identifying *Y. pestis* mutants defective for dissemination to peripheral mouse organs in a pneumonic plague mouse model has not been completed as yet, and, thus far, only 50% of the total output pools have been successfully screened for this study. We expect that further screening of the remaining output pools would likely identify mutant clones related to the T3SS and its effectors as well as other known virulence factors of *Y. pestis*.

In addition to the above T6SS related mutants, clone 42-B8 was identified as having transposon insertion in the putative sugar transport system, ATP-binding protein, which is referred to as the *rbsA* gene. This gene is a part of the ribose transport (*rbs*) operon encoding ribose transport and modification system. The *rbs* operon in *Escherichia coli* consists of genes *rbsDACBK*, in which genes *rbsD* and *rbsK* are involved in phosphorylation of the ribose sugar. Based on the genomic composition, the *rbsACB* genes are organized in a polycistronic transcript and form the ribose transportation channel (172, 173). RbsA carries an ATP binding domain and possesses nucleotide-

binding property, while RbsB is a ribose-binding protein in the periplasmic space, and RbsC is a hydrophobic transmembrane protein (156, 157, 174).

In addition to transport ribose, RbsA was shown to mediate chemotaxis of ribose sugar for *E. coli*, and when this gene was mutated, the chemotactic activity as well as the ribose transportation across the bacterial membrane was significantly affected (156). We have shown for the first time that deletion of the *rbsA* gene attenuated the bacterium in both bubonic and pneumonic plague mouse models and clearly demonstrated the role of RbsA in the pathogenesis of *Y. pestis* infection. Although the underlying mechanism of attenuation is currently not clear, however, considering the primary role of RbsA in sugar transportation, it is most likely that failure to utilize ribose by the Δ*rbsA* mutant would have a negative effect on bacterial fitness and survival inside the hostile environment of the host.

Interestingly, the *rbs* operon has been reported to be regulated by quorum sensing (QS) AI-2 system, and RbsB shares structural resemblance with the sensor protein LuxP (171, 175). Therefore, RbsA may regulate bacterial virulence through QS. In addition, RbsB has been reported as a putative effector of T6SS in *Rhizobium leguminosarum* (171). In line with this finding, it is possible that the secretion of RbsB may be affected by the deletion of the *ypo3603* gene, a homolog of *vasK*. There could possibly be an interplay between RbsA and VasK which would constitute part of our future studies.

Similar to RbsA, a glucose importer (PtsG) from *Y. pestis* strain KIM1001 was recently reported as required for *in vivo* growth in mouse spleen tissues, although deletion of this gene did not change the pathodynamics of bubonic plague from its parental strain (142). Likewise, the *chvE-gguAB* operon in *Agrobacterium tumefaciens* encodes a glucose and galactose importer. Sugar binding to ChvE triggers a signaling response that results in virulence gene expression (176). These studies highlighted the importance of sugar transporter in bacterial pathogenesis.

We noted that the level of attenuation of the isogenic mutants (Fig. 8) in a mouse model of bubonic plague was on the lower side when compared to their respective transposon mutants (Tables 3 and 4). Likewise, Δ*ypo0498* mutant did not show any attenuation in a mouse pneumonic model (data not shown) while its corresponding STM mutant (44-B5) showed 60% survival of animals (Table 3). It is plausible that the presence of a kanamycin-resistant cassette in transposon mutants could contribute to the organism becoming more sensitive to host antibacterial defense mechanisms (168). For example, expression of the neomycin phosphotransferase-II (kanamycin resistant cassette) interferes with bacterial signaling pathways that would be detrimental for *Y. pestis* survivability during host infections. When the antibiotic cassette was removed while creating isogenic mutants, the mutant strains reflected their actual level of attenuation. It is also possible that the transposon mutant clones corresponding to the isogenic mutants carried more than one transposon insertions.

Although the transposon DNA constructs used in this study did not carry any known prokaryotic transcription termination sites, the level of mRNA transcription from the neighboring genes or from other genes of an operon (e.g., *rbs* operon) and their stability and secondary structure could be altered when the transposon insertion occurred. However, these transcriptional alternations would be minimal in isogenic mutants, and thus such mutants showed less attenuation than the corresponding transposon mutants.

Despite the reduced level of attenuation observed with each of the single isogenic mutants, they would be invaluable in the construction of a live-attenuated plague vaccine strain carrying deletion for multiple virulence genes. Evidently, when the *rbsA* gene was deleted from the Δ*lpp* mutant of CO92 strain, the level of attenuation increased synergistically in a mouse model of pneumonic plague (Fig. 11A). Similar synergistic attenuation for developing pneumonic plague was also noticed for the Δ*lpp* Δ*vasK* double mutant of CO92 (Fig. 9A). In agreement with these results, we have shown earlier that deletion of the *msbB* gene, encoding an acetyltransferase to modify lipid A portion of

LPS, from the Δ*lpp* background strain of CO92 further attenuated the Δ*lpp* Δ*msbB* double mutant in both models of plague (132). However, this synergistic augmentation of virulence attenuation was not noticed in the Δ*lpp* Δ*ypo0498* double mutant of CO92 in a mouse model of pneumonic plague (data not shown).

Lipoproteins play varying roles in different bacterial species such as their involvement in host cell colonization and adhesion, bacterial cell division, protein folding and signal transduction (177). In *Y. pestis* KIM/D27 strain (deleted for the pigmentation [*pgm*] locus), we reported that deletion of the *lpp* gene led to increased production of cytokines, such as interferon (IFN)-γ and interleukin (IL)-2 from mouse splenic T-cells, and IL-12 from macrophages. Further, this mutant caused less apoptotic changes and increased NF-kappa B signaling in both mouse splenocytes and macrophages (178). Similarly, we showed that the splenic T-cells from mice infected with the Δ*lpp* Δ*pla* double mutant of CO92 showed increased tumor necrosis factor (TNF)-α production when such immune cells were exposed *ex vivo* to heat-killed WT CO92 antigens (131). Further, the Δ*lpp* mutant of CO92 was defective in intracellular survival in RAW 264.7 murine macrophages, and it was attenuated in evoking both bubonic and pneumonic plague in a mouse model (132).

Therefore, it is likely that the deletion of *rbsA* and *vasK* genes from the Δ*lpp* background strain of CO92, or the deletion of the *rbsA* gene from the Δ*lpp* Δ*msbB* background strain would augment the host immune system to increase cytokine production. Both IFN-γ and TNF-α contribute to host survival by inhibiting bacterial multiplication *in vivo* and increasing bacterial clearance by macrophages (179). However, further detailed studies are needed to fully understand this cytokine interplay in synergistic attenuation of virulence by the double (Δ*lpp* Δ*vasK,* Δ*lpp* Δ*rbsA*) or triple (Δ*lpp* Δ*msbB* Δ*rbsA*) isogenic mutants during mouse models of plague infection.

In summary, we have identified 20 potential targets that could be associated with the full virulence of *Y. pestis* CO92 strain by using the STM approach. Among them, 15

mutants were either attenuated in a mouse model of bubonic plague at a higher infectious dose of 40 LD_{50} and/or in a pneumonic mouse model with an infectious dose equivalent to 12 LD_{50} of WT CO92. For the first time, we have demonstrated the role of VasK and RbsA in the pathogenesis of *Y. pestis* infections. The generated double mutants, Δ*lpp* Δ*vasK* and Δ*lpp* Δ*rbsA,* as well as the triple mutant Δ*lpp* Δ*msbB* Δ*rbsA* showed promising potential in their further development as live-attenuated vaccines. Our future study will continue to characterize the remaining genes that have been identified during this study and their roles in causing plague.

Chapter 3: New Paradigm in Autoinducer-2 Signaling: Potent *in vivo* Bacterial Virulence Regulator

INTRODUCTION

During the course of our investigation into novel virulence factors of *Y. pestis*, the causative agent of plague, we reported a dramatic increase in attenuation of the combinatorial deletion mutant, Δ*lpp*Δ*msbB*Δ*rbsA*, in a stringent pneumonic plague mouse model (180). Our earlier studies showed that deletions of *lpp*, a gene encoding Braun lipoprotein (Lpp), and *msbB*, a gene encoding lipopolysaccharide (LPS)-modifying acyltransferase (MsbB), attenuated a highly virulent *Y. pestis* CO92 strain (81, 133, 181). While Lpp activates toll-like receptor (TLR)-2 signaling, MsbB adds lauric acid to the lipid A moiety of LPS to modulate TLR-4 signaling (81). Additional deletion of *rbsA* (identified during our genome-wide transposon-based signature-tagged mutagenesis of *Y. pestis* CO92 (180)), encoding ribose ABC transporter ATP binding protein, led to a further attenuation in excess of 10 fold of the Δ*lpp*Δ*msbB* mutant (180). Investigation into the mechanism of attenuation due to deletion of *rbsA* within the *rbsBAC* operon showed that RbsA was necessary for efficient bacterial growth in a minimal medium limited to a ribose carbon source (180). While RbsA has ATPase activity, its coupling with RbsC, a bacterial membrane associated protein, actively transports ribose that has been shuttled through the periplasm of the organism by high affinity association with RbsB (156, 157).

In addition to the role in ribose utilization, orthologs of ribose transport proteins, such as RbsB in *Aggregatibacter actinomycetemcomitans*, efficiently interacts with autoinducer-2 (AI-2) in physiological relevant conditions (182, 183). The ribose transporter (Rbs) as well as the Lsr (LuxS-regulated) ATP binding cassette (ABC) transporter are responsible for the uptake of AI-2 quorum sensing (QS) signaling molecule into bacterial cells in many pathogenic bacteria which do not possess the

dedicated two-component circuit of *Vibrio harveyi* (184). *V. harveyi* produces three autoinducers: AI-1 (3-hydroxybutanoyl homoserine lactone), CAI-1 ((S)-3-hydroxytridecan-4-one), and AI-2 ((2S, 4S)-2-methyl-2, 3, 3, 4-tetrahydroxytetrahydrofuranborate) (185), which are detected extracellularly by their cognate transmembrane receptors: LuxN, CqsS, and LuxPQ, respectively (185). Signals through the autoinducer sensing pathways are then transduced through shared components LuxU and LuxO, and five small regulatory RNAs (sRNAs) to the master quorum-sensing regulator LuxR in *V. harveyi* (186, 187). AI-2, a QS molecule found widely among gram-positive and -negative bacteria, is associated with a diverse array of virulence mechanisms spanning from secretion systems to biofilm formation *in vitro* culture assays (182, 188-193). However, the physiological function of the AI-2 system has yet to be described.

AI-2 has a signaling pattern that is unique among the currently described QS systems (191). In *Enterobacteriaceae* family members, the AI-2 signal begins to increase in the extracellular compartment at the beginning of log phase growth. During late log phase growth, the signal peaks and is rapidly depleted from the extracellular compartment until there is no detectable AI-2 during mid-stationary phase (194). The pattern of signal has been correlated with metabolic activity in the bacterium, and as such, the AI-2 signal has been postulated to carry metabolic status information to the bacterial population (195). The expression of proteins associated with AI-2 activity is tightly regulated (195, 196). The *lsr* operon contains several genes that are involved in uptake (*lsrABCD*) of AI-2 from the extracellular milieu as well as regulation and downstream processing of the signal (*lsrKR*) (191, 194, 197). A repressor of transcription has been identified as LsrR that regulates the expression of the AI-2 uptake cassette (Fig 11). Interacting with a phosphorylated AI-2, LsrR undergoes a conformational shift that disassociates it with the promoter of the *lsr* operon allowing for efficient expression of the uptake proteins (194, 198, 199). In the orthologous system of *Escherichia coli,* prior

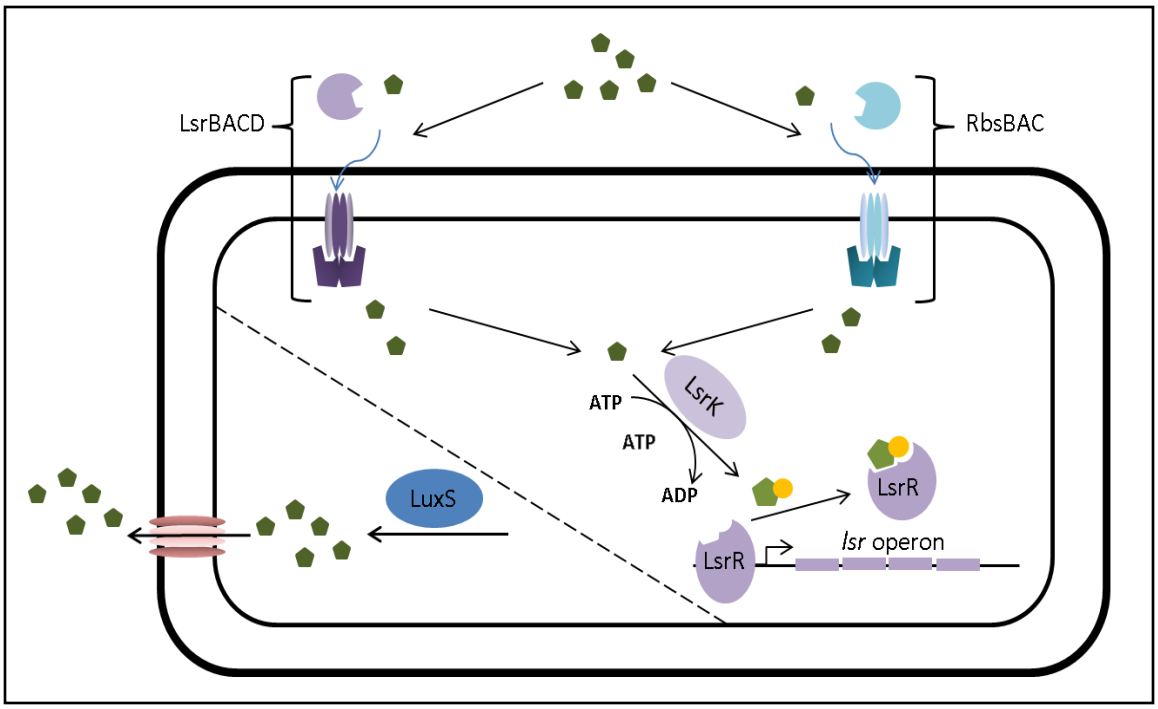

Figure 12. Schematic representation of autoinducer-2 signaling.

In bacteria, AI-2 is synthesized by an enzymatic reaction catalyzed by the protein LuxS. AI-2 (green hexagon) is then shuttled to the extracellular space by an unknown group of transporters. Once in the extracellular milieu, AI-2 is then taken back up by the bacteria primarily through one of two sets of transporters, the LsrBACD transporter or the RbsBAC transporter. As AI-2 is taken into the cell, it is phosphorylated by LsrK and then binds to LsrR, causing a conformational shift that disengages the repressor protein, LsrR, from the DNA upstream of the *lsr* operon allowing for enhanced expression of the *lsr* operon.

to expression of the specific Lsr proteins for uptake of the AI-2 signal, it has been shown that non-specific uptake of AI-2 occurs and that this uptake is regulated through the phosphotransferase system (PTS) that normally regulates sugar phosphorylation and transport (200). Deletion of an upstream regulator of PTS leads to an inability to remove AI-2 from the supernatant of bacterial cultures. Complementation of this *E. coli* strain with constitutive expression of Lsr proteins allowed for wild-type uptake of AI-2 and depletion of the AI-2 signal from culture supernatants (200). This evidence suggests that multiple mechanisms are present to take up AI-2 from the extracellular milieu and that these mechanisms may compensate for the loss of others.

Downstream of the uptake pathway, AI-2 is processed through LsrK, a phosphokinase, which phosphorylates AI-2 (197). Phospho-AI-2 then interacts with, at a minimum, with LsrR before degradation via several other Lsr components (**Fig. 12**). Downstream signaling has been implicated in many virulence mechanisms important to pathogenesis in a wide variety of bacteria (182, 188-193). Despite linking virulence mechanisms to AI-2 signaling, evidence of biological significance for these signaling pathways is limited *in vivo* models (183, 190, 193, 198). Generally, the AI-2 signaling is characterized in a given organism by deleting the gene encoding the primary synthetic enzyme for the AI-2 substrate, LuxS, and observing changes in bacterial virulence phenotypes (195).

An earlier study of AI-2 in an attenuated KIM 1001 *Y. pestis* strain (deleted for the pigmentation locus [*pgm*] required for iron uptake) revealed significant expression changes in large sets of genes as well as a diminished oxidative damage resistance when *luxS* was deleted from the above Δ*pgm* mutant (193). However, these changes in gene expression profile did not affect bacterial virulence in a bubonic mouse model of plague (193). In this study, we demonstrated for the first time that disrupting AI-2 transport from the extracellular milieu into *Y. pestis* CO92 due to the deletion of *rbsA* and *lsrA* genes resulted in a significant reduction of virulence of the mutant in a mouse model of

pneumonic plague. Furthermore, deletion of *luxS* compromised the attenuated phenotype of the Δ*rbsA*Δ*lsrA* mutant, thus establishing a new paradigm for AI-2 signaling.

MATERIALS AND METHODS

Bacterial strains, plasmids, and cell culture.

Bacterial strains and plasmids used in this study are provided in **Table 5**. *Y. pestis* strains were cultured overnight at 28°C, unless specifically noted, with shaking at 180 rpm in heart infusion broth (HIB) (Difco, Voigt Global Distribution Inc., Lawrence, KS) or grown for 48 h on 5% sheep blood agar (SBA) (Teknova, Hollister, CA) or HIB agar plates. As appropriate, the organisms were cultivated in the presence of antibiotics such as ampicillin, kanamycin, and polymyxin B at concentrations of 100, 50, and 35µg/ml, respectively. All of the experiments with *Y. pestis* were performed in the Centers for Disease Control and Prevention (CDC)-approved select agent laboratory in the Galveston National Laboratory (GNL), UTMB.

RAW 264.7 murine macrophage cell line (ATCC, Manassas, VA) was maintained in Dulbecco's modified eagle medium (DMEM) with 10% fetal bovine serum supplemented with 1% L-glutamine (Cellgro, Manassas) and 1% penicillin-streptomycin (Invitrogen, Carlsbad, CA) at 37°C with 5% CO_2.

Construction of Flippase expression plasmid

An easily curable plasmid for the expression of Flippase recombinase was constructed on a pCP20 backbone incorporating a levansucrase (*sacB*) gene derived from pDMS197 and eliminating the chloramphenicol resistance cassette. Construction of plasmid was accomplished using Infusion cloning (Clontech Laboratories Inc., Mountain View, CA) with dsDNA fragments generated by PCR with primers P1-P6 (**Table 6**).

Table 5. Bacterial strains used in this study

Strain Name	Genotype	Origin
WT CO92	Virulent *Y. pestis* biovar Orientalis strain isolated in 1992 from a fatal human pneumonic plague case and naturally resistant to polymyxin B	CDC
ΔrbsA	*rbsA* deletion mutant of *Y. pestis* CO92	*(11)*
Δlpp ΔrbsA	*lpp rbsA* double deletion mutant of *Y. pestis* CO92	*(11)*
Δlpp ΔmsbB ΔrbsA	*lpp msbB rbsA* triple deletion mutant of *Y. pestis* CO92	*(11)*
ΔlsrA	*lsrA* deletion mutant of *Y. pestis* CO92	This study
ΔrbsA ΔlsrA	*rbsA lsrA* double deletion mutant of *Y. pestis* CO92	This study
ΔluxS	*luxS* deletion mutant of *Y. pestis* CO92	This study
ΔrbsA ΔluxS	*rbsA luxS* double deletion mutant of *Y. pestis* CO92	This study
ΔlsrA ΔluxS	*lsrA luxS* double deletion mutant of *Y. pestis* CO92	This study
ΔrbsA ΔlsrA ΔluxS	*rbsA lsrA luxS* triple deletion mutant of *Y. pestis* CO92	This study
ΔrbsA ΔlsrA pBR-*luxS*	*rbsA lsrA* double deletion mutant of *Y. pestis* CO92 transformed with pBR-*luxS* (Tc^s)	This study
ΔrbsA ΔlsrA ΔluxS pBR-*luxS*	*rbsA lsrA luxS* triple deletion mutant of *Y. pestis* CO92 transformed with pBR-*luxS* (Tc^s)	This study
ΔrbsA ΔlsrA ΔluxS Tn*7*-*luxS*	*rbsA lsrA luxS* triple deletion mutant of *Y. pestis* CO92 integrated with a Tn*7* cassette carrying native promoter and gene *luxS*	This study
ΔrbsA ΔlsrA Tn*7*-*rbsA*	*rbsA lsrA* double deletion mutant of *Y. pestis* CO92 integrated with a Tn*7* cassette carrying native promoter and gene *rbsA*	This study
ΔrbsA ΔlsrA Tn*7*-*lsrA*	*rbsA lsrA* double deletion mutant of *Y. pestis* CO92 integrated with a Tn*7* cassette carrying native promoter and gene *lsrA*	This study
WT CO92::Tn*7*-luc	*Y. pestis* CO92 integrated with a Tn*7* cassette carrying the luciferase operon *luxCDABE* (*luc*) (Km^s)	This study
ΔrbsA::Tn7-luc	*rbsA* deletion mutant of *Y. pestis* CO92 integrated with a Tn*7* cassette carrying the luciferase operon *luxCDABE* (*luc*) (Km^s)	This study
Δlpp ΔrbsA::Tn7-luc	*lpp rbsA* double deletion mutant of *Y. pestis* CO92 integrated with a Tn*7* cassette carrying the luciferase operon *luxCDABE* (*luc*) (Km^s)	This study
Δlpp ΔmsbB ΔrbsA::Tn7-luc	*lpp msbB rbsA* triple deletion mutant of *Y. pestis* CO92 integrated with a Tn*7* cassette carrying the luciferase operon *luxCDABE* (*luc*) (Km^s)	This study
ΔlsrA::Tn7-luc	*lsrA* deletion mutant of *Y. pestis* CO92 integrated with a Tn*7* cassette carrying the luciferase operon *luxCDABE* (*luc*) (Km^s)	This study
ΔrbsA ΔlsrA::Tn7-luc	*rbsA lsrA* double deletion mutant of *Y. pestis* CO92 integrated with a Tn*7* cassette carrying the luciferase operon luxCDABE (*luc*) (Km^s)	This study
ΔluxS::Tn7-luc	*luxS* deletion mutant of *Y. pestis* CO92 integrated with a Tn*7* cassette carrying the luciferase operon *luxCDABE* (*luc*) (Km^s)	This study
ΔrbsA ΔluxS::Tn7-luc	*rbsA luxS* double deletion mutant of *Y. pestis* CO92 integrated with a Tn*7* cassette carrying the luciferase operon *luxCDABE* (*luc*) (Km^s)	This study
ΔlsrA ΔluxS::Tn7-luc	*lsrA luxS* double deletion mutant of *Y. pestis* CO92 integrated with a Tn*7* cassette carrying the luciferase operon *luxCDABE* (*luc*) (Km^s)	This study
ΔrbsA ΔlsrA ΔluxS::Tn7-luc	*rbsA lsrA luxS* triple deletion mutant of *Y. pestis* CO92 integrated with a Tn*7* cassette carrying the luciferase operon *luxCDABE* (*luc*) (Km^s)	This study

Table 6. Primers used in this study

Primer Designation	Description	Sequence 5' -> 3'
P1	FLP Amp Fwd	cgcctgtagtgccatttacc
P2	FLP Amp Rev	cattacgctgacttgacggg
P3	FLP Fwd	cccgtcaagtcagcgtaatg
P4	FLP Rev	ggtagcgttgccaatgatgt
P5	SacB FLP Fwd	aatggcactacaggcgtgggaattctgatccttttttaacccatcac
P6	SacB FLP Rev	tcattggcaacgctaccgccatttgcctgcttttatatagt
P7	λ red LsrA Fwd	atttgttcagtcccgtcagtcaacattgagggagcggaggcaacatgcaagtgtaggctggagctgcttc
P8	λ red LsrA Rev	ccggttattttggatgaatttcaacatgttgcctccgacgcaccatgttccggggatccgtcgacc
P9	λ red luxS Fwd	ttagaaaaatatgacttttttatgaggaggtaactaaatgccattattgggtgtaggctggagctgcttc
P10	λ red luxS Rev	cgccttttatcattctcctgcctactgatactgagcactaaatatgcaatattccggggatccgtcgacc
P11	lsrA Tn7 Fwd	ccaacactcgagagggcaaatagggtgagaatg
P12	lsrA Tn7 Rev	tccttcgaattcagccactgcgtaatgaatgttt
P13	LsrA Rev sequencing	atctatcaccccagactgcc
P14	LsrA Fwd sequencing	ccatcacgccgttcattgaa
P15	luxS pBR322/Tn7 Fwd	tccttcgaattcgctttgaagagtatttagcgct
P16	LuxS Tn7 Rev	ccaacaggtaccagctttactgaacccccagcc
P17	luxS pBR322 Rev	ccaacagtcgacaaagctttactgaacccccagcc
P18	LuxS Fwd sequencing	cagttatctgcagagcgcga
P19	LuxS Rev sequencing	gacgctttaatcagcgcctt

Construction of in-frame deletion mutants

To construct in-frame deletion mutants of *Y. pestis* CO92, λ-phage recombination system was used (150). Initially, the WT CO92 strain was transformed with plasmid pKD46 **(Table 3)** and grown in the presence of 1 mM L-arabinose to induce the expression of λ-phage recombination system. The above-mentioned *Y. pestis* culture was processed for the preparation of electroporation competent cells (150, 151). The latter were then transformed with 0.5 to 1.0 µg of the linear dsDNA constructs carrying the kanamycin resistance (Km^r) gene cassette that was immediately flanked by bacterial FRT (flippase recognition target) sequence followed by on either side by 50 bp of DNA sequences homologous to the 5' and 3'ends of the gene to be deleted from WT CO92. The plasmid pKD46 from the mutants that had successful Km^r gene cassette integration at the correct location was cured by growing the bacteria at 37°C. The latter mutants were transformed with plasmid pEF01 to excise the Km^r gene cassette. Eventually, the plasmid pEF01 was also cured from the kanamycin sensitive (Km^s) clones by growing them at 37°C followed by selection in a medium containing 5% sucrose (158). To confirm the in-frame deletion, mutants showing sensitivity to kanamycin and ampicillin were tested by PCR using appropriate primer pairs **(Table 6)** and sequencing of the PCR products.

Growth curves and AI-2 determination in mutants

To determine the AI-2 secretion profile, bacteria were inoculated in HIB medium at a dilution of 1:1000 and then aliquots of culture medium were taken at each hour. Culture medium was centrifuged briefly and then filtered through 0.1 µm micro-centrifuge filters (Corning Inc, Corning, NY), before storage at $^{-}$80°C prior to analysis. Analysis was performed as previously described (201), in brief, *Vibrio harveyi* BB170 (which is unable to synthesize AI-2, ATCC) was inoculated in Autoinducer Bioassay (AB) medium, incubated overnight at 30°C and then diluted 1:5000 in fresh AB medium. Freshly diluted *V. harveyi* BB170 was then mixed 9:1 with filtered culture supernatants

of *Y. pestis* strains and incubated for 5 h at 30°C (201). Samples were then analyzed for bioluminescence and AI-2 concentrations determined by standard curve with synthetic AI-2 (Omm Scientific, Dallas, TX).

Development of luminescent reporter strains

Electrocompetent cells of *Y. pestis* strains were prepared and electroporated with pTNS2 and pUC18r6kT mini-Tn*7*T::*lux*-FRT-kan (202) and selected by kanamycin resistance and luminescence. Following isolation, strains were electroporated with pEF01 to remove resistance cassette. Kanamycin sensitive mutants were grown at 37°C and selected for on 5% sucrose containing medium for removal of pEF01. Insertion of *lux* operon at the *att*Tn*7* region and appropriate removal of kanamycin cassette was confirmed by PCR and Sanger sequencing. Luminescence intensity of each strain was determined by serial dilution and RLU (relative luminescence unit) measurement (Spectramax M5e, Molecular Devices, Sunnyvale, CA).

Intracellular survival of *Y. pestis* CO92 strains in RAW 246.7 murine macrophages

Intracellular survival of *Y. pestis* strains was determined as previously described (203), in brief, luminescent *Y. pestis* strains were grown in HIB overnight to saturation at 28°C. RAW 264.7 macrophages were seeded in 96-well plates at a concentration of 2×10^4 cells/well for confluence. Plates were then infected with *Y. pestis* CO92-*lux* or its various mutant strains with *lux* at an MOI (multiplicity of infection) of 250 in DMEM, centrifuged, and incubated at 37°C and 5% CO_2 for 60 min. Infected macrophages were then washed with PBS, treated with gentamicin (50 μg/mL), washed again with PBS, and maintained in DMEM as described above. At 0 and 4 h, luminescence was measured in a Spectramax M5e microplate reader.

***Y. pestis* CO92 pneumonic plague mouse model**

All of the animal studies with *Y. pestis* were performed in an animal biosafety level 3 (ABSL-3) facility under an approved Institutional Animal Care and Use Committee (IACUC) protocol (UTMB). Six- to 8-week-old female Swiss Webster mice (17 to 20 g), purchased from Taconic Laboratories (Germantown, NY), were anesthetized by the intraperitoneal (i.p.) route with a mixture of ketamine and xylazine and subsequently challenged intranasally (i.n.) with 50% lethal doses (LD_{50}) (1 LD_{50} = 500 CFU) as described for WT *Y. pestis* CO92 (69). Mice were assessed for morbidity and/or mortality as well as clinical symptoms for the duration of each experiment (up to 21 days p.i.).

For the AI-2 complementation study, mice were anesthetized by isofluorane and dosed intranasally at time of infection, 24 h and 48 h postinfection with 20 μL of PBS with added synthetic AI-2 calculated to result in a 0, 0.2, 2, 25 μM concentration of AI-2 in the lung volume of a six- to 8-week old female Swiss Webster mouse (~500 μL).

AI-2 uptake by *Y. pestis*

AI-2 uptake was determined as previously described (200), in brief, strains were grown to saturation overnight in HIB at 37°C. Bacteria were washed twice with PBS and diluted 1:100 in fresh HIB supplemented with 50 μM AI-2. Culture aliquots were sampled and assayed for AI-2 activity as described above.

Hydrogen peroxide resistance of *Y. pestis* strains

Luminescent reporter *Y. pestis* strains were cultured as described for AI-2 analysis but bacteria were harvested at time of maximal AI-2 production, washed twice in PBS, and resuspended at an OD_{600} of 1 in HIB supplemented with 0.3% H_2O_2 (Thermo Fisher Scientific, Waltham, MA). Luminescence was measured in a Spectramax M5e microplate reader.

Growth curves in modified minimal medium

Overnight cultures of various *Y. pestis* strains were washed in PBS and then normalized by OD_{600}. Flasks of 20 mL modified M9 medium (1 x M9 salts [22 mM KH_2PO_4, 33.7 mM Na_2HPO_4, 8.55 mM NaCl, 9.35 mM NH_4Cl], 1 mM $MgSO_4$, 2.5 mM $CaCl_2$, 0.001 mg/mL $FeSO_4$, 0.0001% thiamine, 0.1% casamino acids) (all chemicals obtained from Sigma-Aldrich, St. Louis, MO) were supplemented with 0.4% glucose, and were inoculated with approximately 1 x 10^7 CFU of various bacterial strains and incubated at 37°C with shaking at 180 rpm. Samples were taken every hour and absorbance measured at OD_{600}.

RNA-seq and expression analysis

Cultures were grown as described for AI-2 growth curve analysis and RNA was isolated at peak time of AI-2 production using TRIzol (Thermo Fisher Scientific) and extracting with chloroform and ethanol. Total RNA was purified and DNase treated using Quick-RNA kit (Zymo Research, Irvine, CA) followed by mRNA enrichment using MicrobeExpress (Ambion, Thermo Fisher Scientific, Waltham, MA).

Library construction and sequencing. RNA (1-3 µg) was fragmented by incubation at 94°C for 8 min. in 19.5 µl of fragmentation buffer (Illumina 15016648). Sequencing libraries were prepared using an Illumina TruSeq Stranded RNA v2 kit following the manufacturer's protocol. The indexed samples were sequenced on a single lane of an Illumina HiSeq 1500 using the 2x50 paired-end protocol. The resulting BCL files were converted to fastq files using Illumina bcl2fastq2 software, version 2.17. Reads were checked for quality using FastQC and aligned to the *Y. pestis* CO92 genome using BWA Aligner *via* Illumina BaseSpace. Transcript counts were generated using the Bioconductor Genomic Alignments package (204) and differential expression was determined using DESeq2 (205). Euclidean distance mapping was performed using distance function in R from the regularized-logarithm transformed counts. Poisson

distance mapping was performed using the method described by Witten et al. (206) and heat maps were generated in R.

Western blotting for T3SS

Western blotting for *Y. pestis* secreted factors was performed as previously described (203), in brief, overnight cultures of *Y. pestis* CO92 or its mutants, grown in HIB at 28°C, were diluted 1:20 in 5 ml HIB supplemented with 5 mM EGTA to trigger the low-calcium response. The cultures were incubated at 28°C for 2 h before being shifted to 37°C (to activate the T3SS) for an additional 3 h of growth. Supernatants were precipitated with 20% (vol/vol) trichloroacetic acid (TCA) on ice for 2 h. The TCA precipitates were then washed and dissolved in SDS-PAGE buffer and analyzed by immunoblotting using antibodies to YopE or LcrV (Santa Cruz Biotechnology, Santa Cruz, CA). Secondary antibodies were anti-rabbit IgG or anti-mouse IgG as appropriate (Southern Biotech, Birmingham, AL). Blots were developed using SuperSignal West Dura (Pierce Biotechnology, Thermo Fisher Scientific). Protein loading normalization was accomplished through visualization of total protein on blots using Stain-free technology (Bio-Rad, Hercules, CA).

Pla protease activity

Pla protease activity measurement was performed as previously described (203), in brief, bacteria were grown as described above for AI-2 analysis and collected at time of maximal AI-2 levels. Cultures were centrifuged, washed twice, and resuspended in PBS to obtain a final OD_{600} of 0.1 in a spectrophotometer (SmartSpec 300; Bio-Rad). For each sample, 50-µl suspensions were added to wells of a black microtiter plate (Costar Corning Inc.) in triplicate. The hexapeptide substrate DABCYL-Arg-Arg-Ile-Asn-Arg-Glu (EDANS)-NH_2, synthesized on Sieber amide resin (207), was added to the wells at a final concentration of 2.5 µg/50 µl. The kinetics of substrate cleavage by Pla was

measured every 10 min for 3 h by a fluorometric assay (excitation/emission wavelengths, 360/460 nm) at 37°C on a BioTek Synergy HT spectrophotometer (BioTek Instruments Inc., Winooski, VT).

RESULTS

Deletions of *rbsA* and *lsrA* in *Y. pestis* CO92 disrupt autoinducer-2 signaling

The initial finding we reported, that the deletion of *rbsA* synergistically attenuated *Y. pestis* CO92 in association with deletions of *lpp* and *msbB* (Chapter 2), led us to investigate mechanisms of attenuation beyond the impairment of ribose transport and utilization (180). Since orthologs of Rbs operon are associated with AI-2 transport, we measured the effect of in-frame deletions of *rbsA* on the concentration of AI-2 in the culture supernatants of mutants versus the wild type (WT) CO92 using a standardized bioreporter assay (**Fig. 13**). At both 28°C (flea) and 37°C (human body) temperatures, representing two lifestyles of *Y. pestis* (208), there were major aberrations in the patterns of AI-2 in the mutants compared to WT CO92.

As shown in **Fig. 13A**, single deletion of *rbsA* resulted in no discernable effect on the AI-2 pattern when compared to WT CO92. However, both Δ*lpp*Δ*msbB* and Δ*lpp*Δ*msbB*Δ*rbsA* mutant strains showed a sharp increase in free AI-2 in the culture supernatants during mid-to-late log phase of bacterial growth. Deletion of *rbsA* from the Δ*lpp*Δ*msbB* mutant further augmented available AI-2 in the extracellular milieu. These altered AI-2 levels in the culture supernatants of Δ*lpp*Δ*msbB* and Δ*lpp*Δ*msbB*Δ*rbsA* mutants were not attributable to differences in bacterial growth rates (**Fig. 13A**) or changes in the membrane topology (133). These data suggested that a previously unknown defect in AI-2 signaling, due to deletions in *lpp* and *msbB*, combined with deletion of *rbsA*, led to reduced virulence of these two mutants in *in vivo* models of *Y. pestis* infection (81).

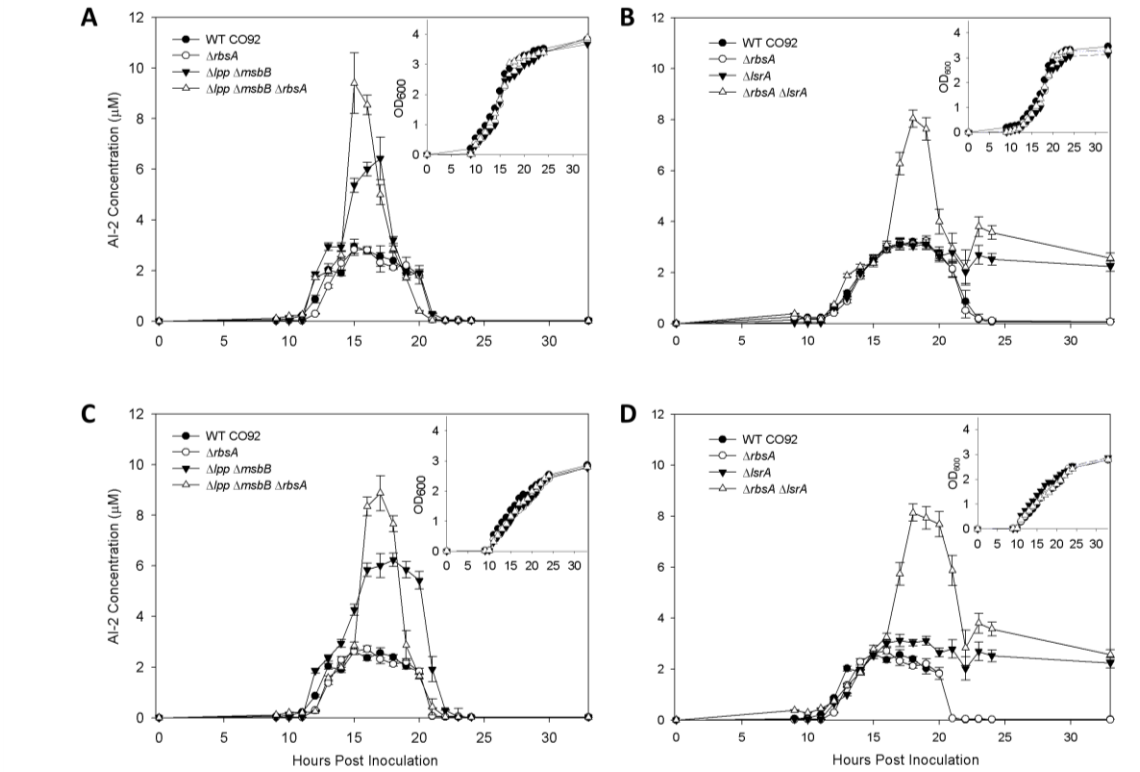

Figure 13. AI-2 levels in cell free supernatants of WT *Y. pestis* CO92 and its various mutant strains.

Concentration of AI-2 in culture supernatants with absorbance of culture at 600nm inset for 28°C (**A & B**) or 37°C (**C & D**). Data are representative of three independent experiments and error bars represent arithmetic means ± standard deviations.

To further evaluate the effect of changes in AI-2 signaling on *Y. pestis* CO92 virulence, deletion mutants of the canonical AI-2 transport system were constructed both singly and in combination with *rbsA,* and the effects on AI-2 levels in the culture supernatants observed. As previously reported (193), *lsrA* deletion resulted in stationary phase aberration of AI-2 levels (after 22 h); however, when combined with *rbsA* deletion, the Δ*rbsA*Δ*lsrA* strain exhibited significant increases in AI-2 during mid-to-late-log phase growth (**Fig. 13B**) similar to the Δ*lpp*Δ*msbB*Δ*rbsA* strain (**Fig. 13A**). In addition, the level of AI-2 in the stationary phase was further augmented (**Fig. 13B**).

Changes in AI-2 signaling correlate to *in vitro* and *in vivo* attenuation of *Y. pestis* CO92

Following the confirmation of AI-2 substrate aberrations, we determined whether there was any correlation between changes in AI-2 signaling and *in vitro* virulence as measured by intracellular survival (ICS) of the mutants in RAW 264.7 murine macrophages compared to that of WT CO92 (**Fig. 14A**). The ability to survive and replicate within macrophages and the recruitment of early immune effector cells during *Y. pestis* infection, contribute to pathogenicity *in vivo* models, and as such, are important measures of virulence (2, 41). We found that single deletions in either of the transport protein encoding genes (*rbsA* or *lsrA*) had minimal effects on ICS, but when combined, the Δ*rbsA*Δ*lsrA* mutant was significantly less resistant to the macrophage intracellular environment (**Fig. 14A**). We also observed that increasing magnitude of aberration in the AI-2 levels tightly correlated with the observed decreases in ICS, as the Δ*lpp*Δ*msbB*Δ*rbsA* mutant strain had significantly lower ICS than the Δ*rbsA*Δ*lsrA* strain (**Fig. 14A&B**). All of the tested mutants exhibited similar levels of phagocytosis when compared to WT CO92 (**Fig. 14B**).

The data thus far have been consistent with previous studies of AI-2 signaling in various pathogenic bacteria, showing changes in bacterial virulence related to *in vitro*

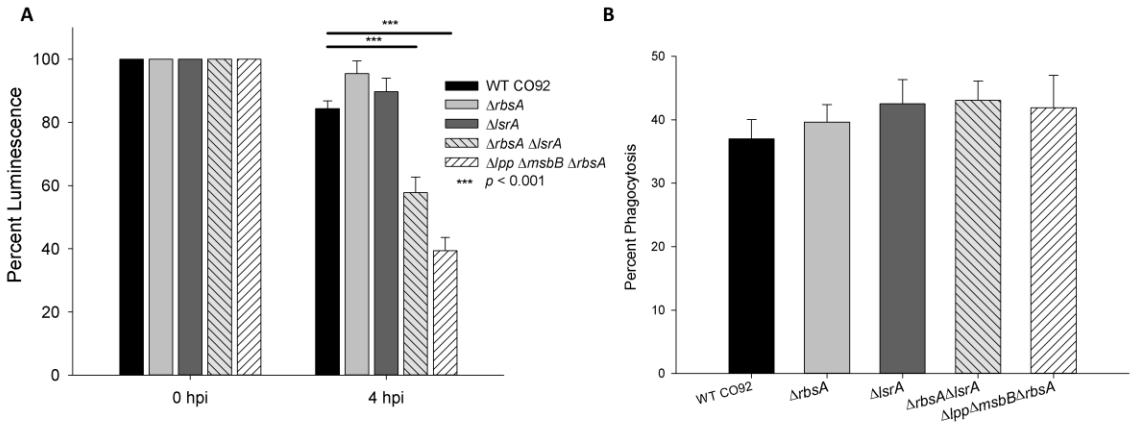

Figure 14. Intracellular survival of WT *Y. pestis* CO92 and its various mutant strains in macrophages.

The intracellular survival of WT *Y. pestis* and its various mutants in a RAW 264.7 murine macrophage cell line was evaluated at 0 and 4 h post infection (**A**). Luminescent reporter strains of each background culture were utilized to evaluate real-time reporting of bacterial survival in macrophages. Phagocytosis of bacteria was determined by comparing luminescence of infectious dose to luminescence at 0 h (**B**). Data are representative of three independent experiments. Statistical analysis was performed using one-way ANOVA with Tukey *post-hoc* correction.

assays. However, when we challenged mice in a pneumonic plague model to determine if these changes in AI-2 signaling correlated with alteration in *in vivo* virulence, our findings diverged from the previous literature (**Fig. 15**). Single gene deletions of either *rbsA* or *lsrA* showed only modest decreases in virulence in a mouse model; Δ*rbsA* reached statistical significance at 30% survival after a challenge dose equivalent to 9 LD_{50} of WT CO92, while Δ*lsrA* was not significantly different (20% survival) from that of the WT CO92-challenged group of mice. Combinatorial deletions of Δ*rbsA*Δ*lsrA* resulted in significant decreases in virulence of the mutant with 80% of mice surviving a challenge dose of up to 50 LD_{50} equivalent of WT CO92 (**Fig. 15**). These data for the Δ*rbsA*Δ*lsrA* mutant were comparable to our published virulence attenuation of the Δ*lpp*Δ*msbB*Δ*rbsA* strain with 100% survival at 50 LD_{50} equivalent of WT CO92 (180). The attenuating phenotype of the Δ*rbsA*Δ*lsrA* mutant could be complemented through a site-specific, single-copy, mini-Tn*7* transposon insertion of the native gene, along with the promoter, of either *rbsA* or *lsrA* (**Fig. 16**). The significant decrease in virulence of the above mutants (Δ*rbsA*Δ*lsrA* and Δ*lpp*Δ*msbB*Δ*rbsA* (180)) that we observed in animals was unexpected given extensive literature indicating negligible role for AI-2 in regulating *in vivo* virulence (190, 193, 195, 198, 209). As such, our results merited a more thorough investigation and we decided to determine the additional role that *luxS* played in virulence.

Masking phenotype of *luxS* deletion in the Δ*rbsA*Δ*lsrA* background strain of *Y. pestis* CO92

To characterize the effect *luxS* deletion had on the AI-2 signaling pathway, we constructed single and combinatorial deletions of *luxS* in the background strain of Δ*rbsA*Δ*lsrA*, in addition to developing various complemented and overexpressing strains. When these strains were evaluated in a mouse pneumonic plague model, we found a significant trend not reported before in the literature (**Fig. 17**). While the Δ*luxS* mutant

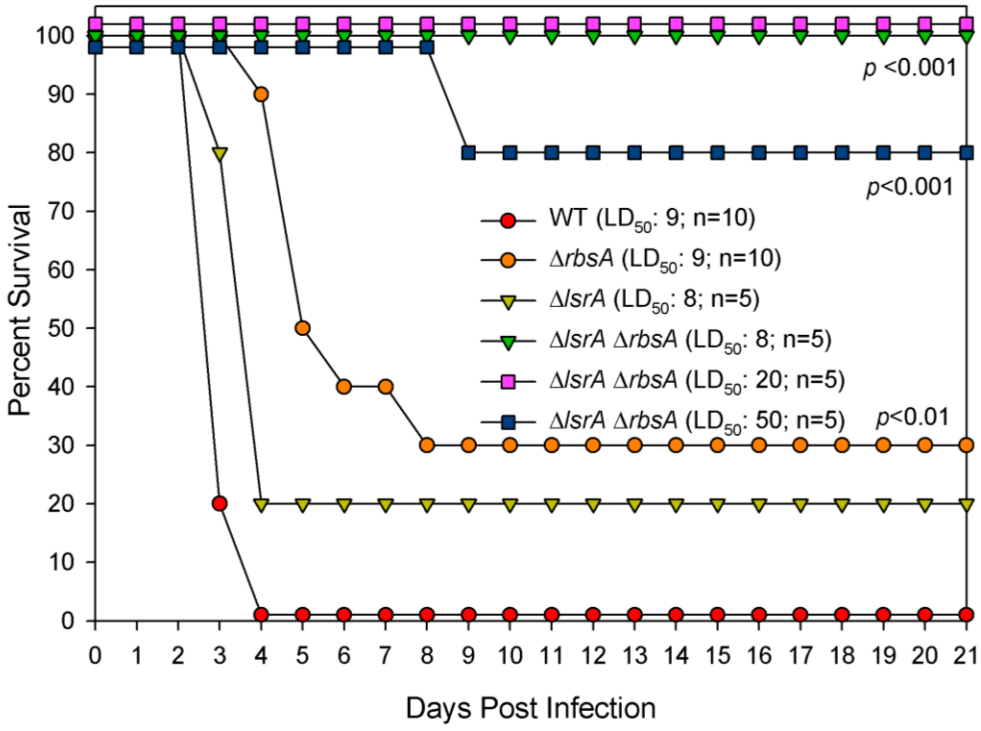

Figure 15. *In vivo* virulence of Δ*rbsA*Δ*lsrA* mutants.

The survival of female Swiss-Webster mice (n=5-10) in a pneumonic plague model challenged with the stated dose equivalent to WT *Y. pestis* CO92 LD_{50} where 1 LD_{50} is 500 colony forming units (CFU), was monitored. Statistical analysis was performed using Kaplan Meier survival curve analysis.

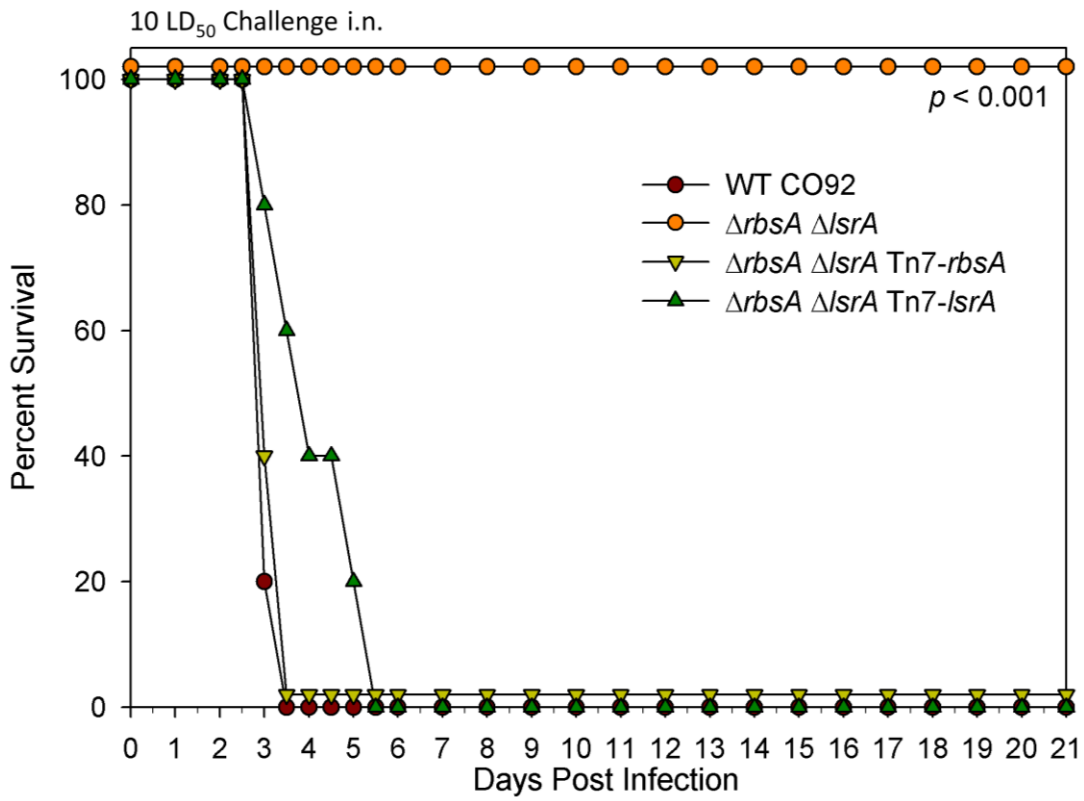

Figure 16. Complemented mutants in a pneumonic plague model.

The survival of female Swiss-Webster mice (n=5) in a pneumonic plague model challenged with 10 LD_{50} equivalent of WT CO92 where 1 LD_{50} is 500 CFU was monitored. Statistical analysis was performed using Kaplan Meier survival curve analysis. i.n.=intranasal.

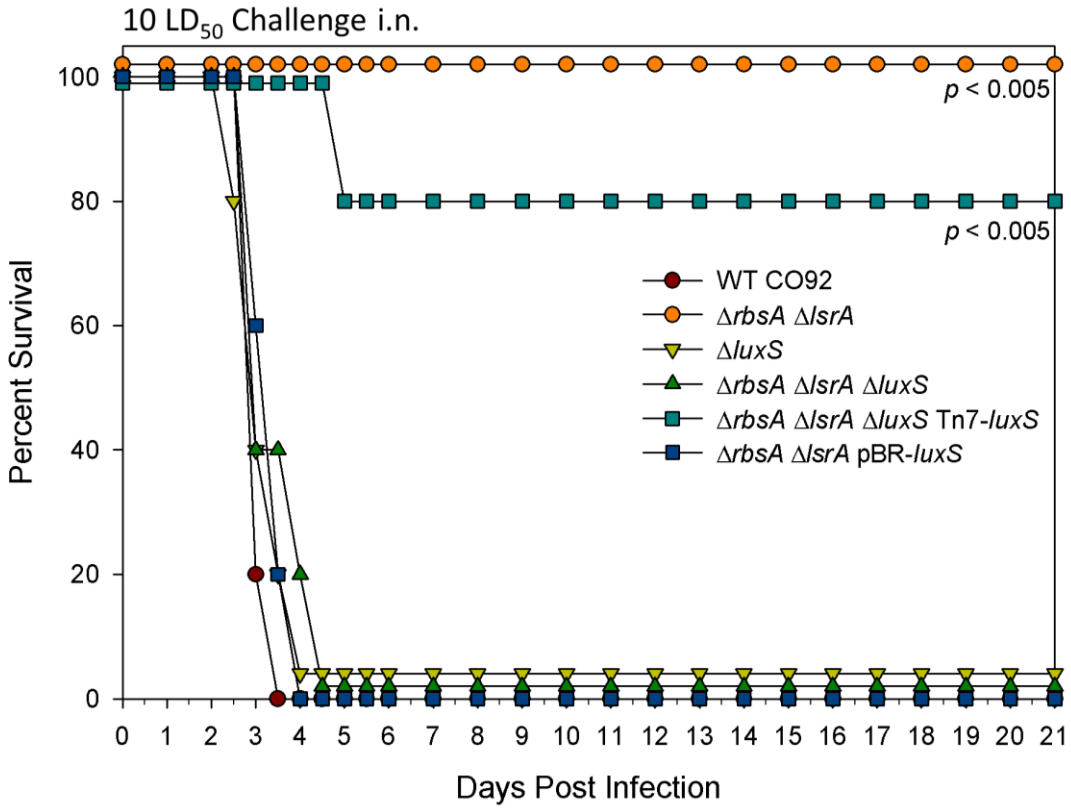

Figure 17. *In vivo* virulence of Δ*luxS* mutants.

The survival of female Swiss-Webster mice (n=10) in a pneumonic plague model challenged with 10 LD_{50} equivalent of WT CO92 where 1 LD_{50} is 500 CFU. Statistical analysis was performed using Kaplan Meier survival curve analysis. i.n.=intranasal.

was as virulent as the WT CO92, deletion of *luxS* resulted in a masking phenotype that reverted the attenuated Δ*rbsA*Δ*lsrA* background strain to a fully virulent form similar to that of WT CO92 (**Fig. 17**). These intriguing data accounted for much of the divergence from the literature, as the *luxS* deletion is used extensively as a model for evaluating AI-2 signaling disruption.

Interestingly, we found that copy number of *luxS* was critical during complementation of this gene in the Δ*rbsA*Δ*lsrA*Δ*luxS* mutant. A *trans*-complementation strategy using a low-copy number plasmid (pBR322) resulted in a virulent phenotype (**Fig. 17**), while *cis*-complementation of the Δ*rbsA*Δ*lsrA*Δ*luxS* mutant with *luxS* using the Tn*7* system led to an avirulent phenotype in a mouse model. Overall, our data in context of Δ*rbsA*Δ*lsrA* indicated that both loss of *luxS*, as in Δ*rbsA*Δ*lsrA*Δ*luxS*, and overexpression of *luxS*, as in Δ*rbsA*Δ*lsrA*-pBR-*luxS*, led to virulent phenotypes *in vivo* (**Fig. 17**). Similarly, when we examined the ICS of these strains we found a similar trend where single *luxS* deletion induced a phenotype similar to that of WT CO92 and masked attenuating characteristics of the Δ*rbsA*Δ*lsrA* strain (**Fig. 18A)**. Deletion of *luxS* allowed us to measure the transport of AI-2 into the bacteria distinctly from bacterial synthesis of AI-2. The Δ*luxS* mutant was able to uptake synthetic AI-2 from the culture medium during *in vitro* growth, however, the Δ*rbsA*Δ*lsrA*Δ*luxS* mutant was impaired in its ability to transport AI-2 from the medium as measured by using the *V. harveyi* reporter strain (**Fig. 18B**).

The paradigm of equating LuxS with AI-2 function has been questioned in the past, particularly due to LuxS' multiple roles beyond AI-2 substrate production (195). However, the difficulty in linking AI-2 signaling to particular gene products and the lack of evidence indicating a substantial biological impact of AI-2 signaling *in vivo* have forestalled further study. Thus far, we have shown a correlation between disruptions in AI-2 signaling due to aberrant transport of AI-2 within the bacterial cell and attenuating

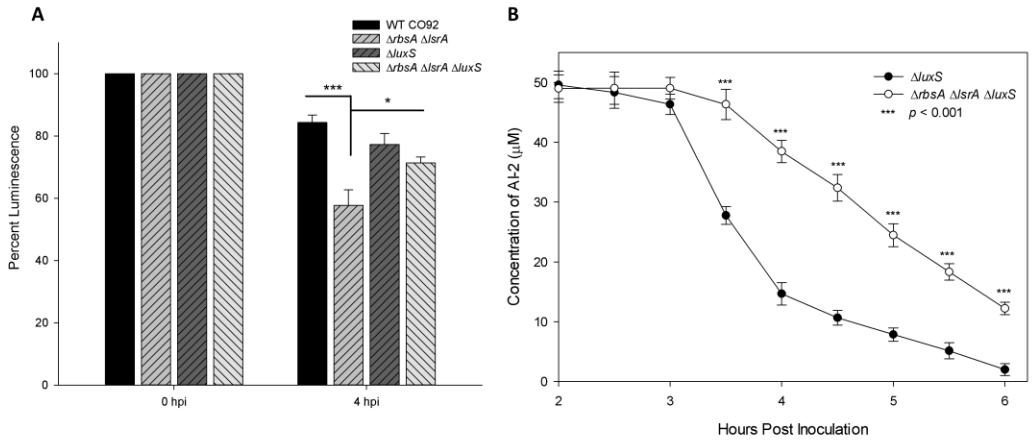

Figure 18. *In vitro* characterization of *luxS* deletion mutants.

Intracellular survival of deletion mutants for *luxS* (**A**). The intracellular survival of WT *Y. pestis* CO92 and its various mutants in a RAW 264.7 murine macrophage cell line was evaluated at 0 and 4 h post infection (hpi). Luminescent reporter strains of each background culture were utilized to evaluate real-time reporting of bacterial survival in macrophages. Statistical analysis was performed using one-way ANOVA with Tukey *post-hoc* correction. Uptake of AI-2 from culture supernatants (**B**). The time course of AI-2 concentration in culture supernatants of mutants deficient for AI-2 production. AI-2 concentration was measured by using *V. harveyi* BB170 reporter strain. Statistical analysis was performed by using multiple *t*-test using the Holm-Sidak method correcting for multiple comparisons. Data (arithmetic means ± standard deviations) are representative of three independent experiments.

phenotypes in both *in vitro* and *in vivo* models of plague and that deletion of *luxS* disrupted these attenuating features.

Transcriptomic profiles of AI-2 perturbed strains of *Y. pestis* CO92

To identify potential mechanism(s) of attenuation and further link the changes observed in AI-2 concentrations to attenuated phenotypes in the mutants, we subjected each of the major mutant strains to RNAseq analysis. RNA was isolated from the bacterial strains at peak AI-2 levels during mid-to-late exponential phase of growth, when the most significant aberrations in AI-2 signaling were observed (**Fig. 13A&B**). A heat map of the top 100 most variable genes showed similar expression patterns within each strain and common expression patterns shared between AI-2 perturbed strains, as well as isolated groupings unique to the attenuated Δ*rbsA*Δ*lsrA* strain (**Fig. 19A**). Distance mapping of the strains revealed a hierarchical grouping of the samples within their strains, exhibiting low variance between samples, as well as showing commonalities between Δ*rbsA*Δ*lsrA*Δ*luxS* and Δ*luxS* strains (**Fig. 19B&C**).

Of the approximately 4000 genes in the *Y. pestis* genome, 219 genes were differentially expressed greater than 2 fold, up or down, at a significance level of $p_{adj} < 0.05$ between Δ*rbsA*Δ*lsrA* and WT CO92; 119 genes between Δ*luxS* and WT CO92; 46 genes between Δ*luxS* and Δ*rbsA*Δ*lsrA*Δ*luxS*; and 78 genes between Δ*luxS* and Δ*rbsA*Δ*lsrA* (**Appendix A, Tables 7-10**). From these data, multiple comparisons could be derived and the most enlightening were those that highlighted attenuating expression phenotypes, those changes that masked attenuation, and, lastly, a comparison identifying a set of regulated genes in all AI-2 perturbed strains.

The attenuating phenotype was identified by sorting for significant changes in Δ*rbsA*Δ*lsrA* versus WT CO92 and excluding any common significant changes from Δ*luxS* or Δ*rbsA* Δ*lsrA*Δ*luxS* versus WT CO92 (**Appendix A, Table 11**). Attenuating

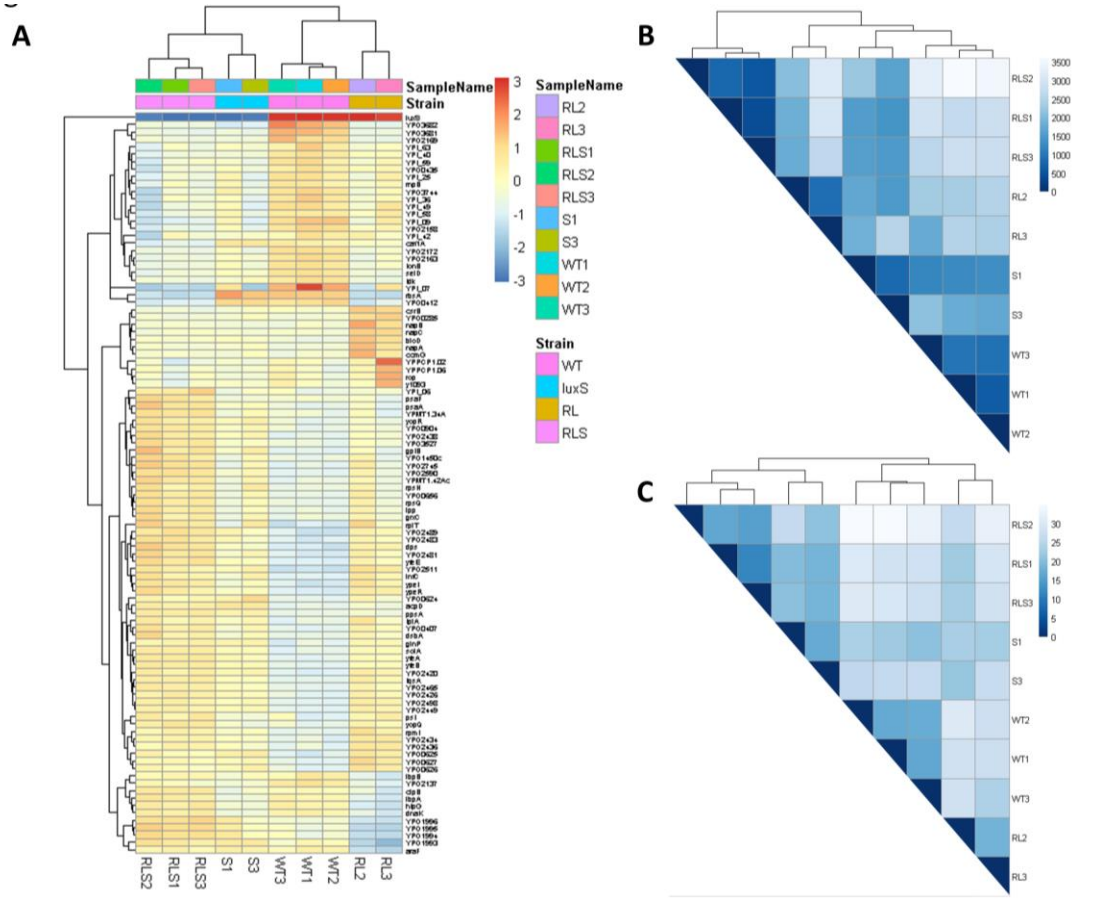

Figure 19. Analysis of AI-2 mutant transcriptomes.

A heatmap was constructed against mean counts of the top 100 most variable genes across all samples including WT CO92 (WT), Δ*rbsA*Δ*lsrA* (RL), Δ*luxS* (S), and Δ*rbsA*Δ*lsrA*Δ*luxS* (RLS) mutants (**A**). A distance map was created using poisson (**B**) or euclidean (**C**) distance against the transcriptome of each mutant examined.

expression changes included 249 genes with a $p_{adj} < 0.1$, and comprised of ABC transporter families specific to arabinose, *araCFGH* (mean fold change = -1.8 - -5.9) and galactose, *mglABC* (-1.6 - -1.8); chaperone-encoding genes *dnaJK* (-2.4 - -2.5), *ibpAB* (-2.6), and *htpG* (-3.2); oxidative phosphorylation gene family *atpABEFGH* (1.6-2.2); anaerobic nitrogen metabolism gene family, *napABC* (3.5-5.3); a catalase *katY* (-2.42); and 44 genes encoding hypothetical proteins.

Interestingly, this pattern of expression included both aerobic and anaerobic metabolic pathway upregulation in addition to decreases in expression of key stress response/resistance pathways. A gene encoding a key transcriptional regulator of anaerobic metabolism, *arcA,* (mean fold change = 1.52) responds to changes in redox flux inhibiting downstream glucose transporter encoding gene, *ptsG* (-2.14). Genes encoding key functional regulators of the phosphotransferase system (PTS) immediately upstream of *ptsG*, i.e., *ptsIH*, were both upregulated (1.45-1.81). An earlier study with *luxS* deletion in *Y. pestis* Δ*pgm* strain showed decreases in hydrogen peroxide resistance with disruption of AI-2 signaling in association with decreased *katY* expression when compared to the parental strain (193). Consequently, we also performed a hydrogen peroxide resistance assay and found minimal decreases with either the Δ*rbsA* or the Δ*lsrA* strain and a significant alteration in hydrogen peroxide resistance in the Δ*rbsA*Δ*lsrA* mutant strain (**Fig. 20A**), consistent with decreased expression of the *katY* gene (**Appendix A, Table 7**).

To determine if changes in metabolic gene expression could be altering the growth pattern of the Δ*rbsA*Δ*lsrA* mutant in a restricted nutrient environment, the mutant and the WT CO2 strain were grown in a modified defined medium based on M9 salts. The Δ*rbsA*Δ*lsrA* mutant exhibited delayed growth kinetics using glucose as the primary carbon source (**Fig. 20B**). There was an extended lag phase of growth for the mutant, although reaching a final optical density equivalent to WT CO92.

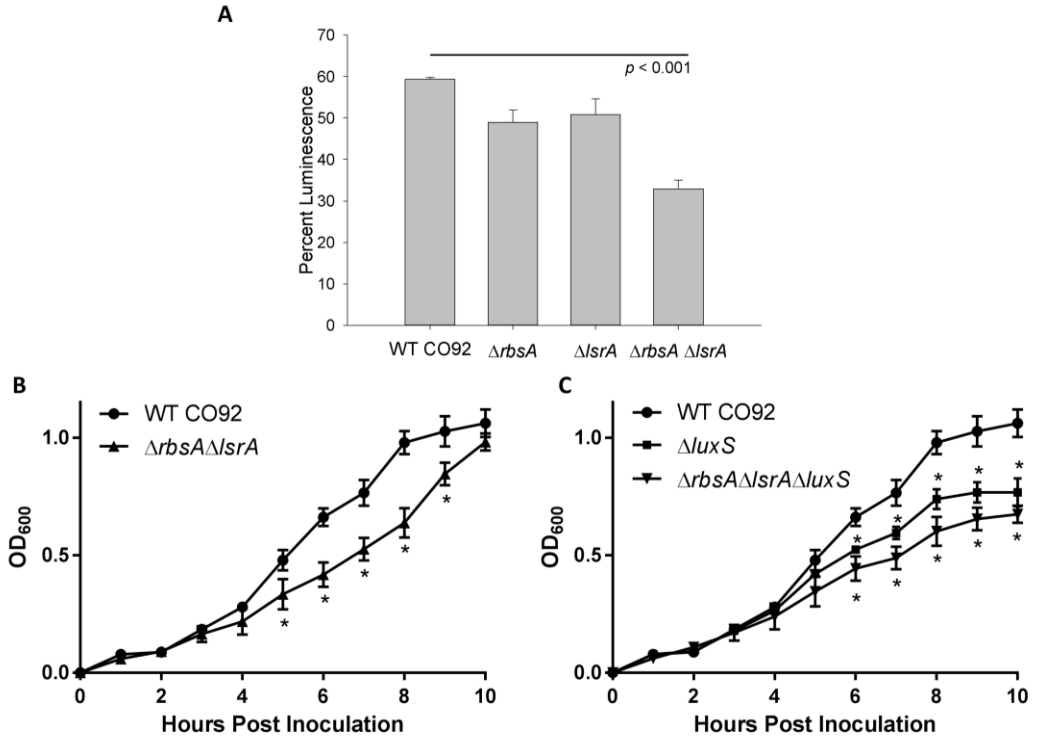

Figure 20. Functional assays of significant expression changes.

Resistance to killing by hydrogen peroxide (**A**). The resistance of bacterial strains to killing by a 0.3% H_2O_2 containing medium through measurement of luminescence reporter in real-time was evaluated. Measurements were taken 15 min post addition of hydrogen peroxide. Statistical analysis was performed via one-way ANOVA with Tukey *post-hoc* correction. Growth of *Y. pestis* strains in carbon source restricted minimal medium measured by absorbance (**B**). *Y. pestis* strains were inoculated in a modified M9 medium and samples were measured for absorbance at a wavelength of 600nm every hour. Asterisks denote time point at which WT and mutant are statistically significant with $p < 0.001$. Statistical analysis was performed using multiple t-tests with the Holm-Sidak method correcting for multiple comparisons. Growth of *Y. pestis* strains in iron source restricted minimal medium (**C**). *Y. pestis* strains were inoculated in a modified M9 medium and samples were measured for absorbance at a wavelength of 600nm every hour. Asterisks denote time point at which WT and mutant are statistically significant with $p < 0.001$. Statistical analysis was performed using multiple t-tests with the Holm-Sidak method correcting for multiple comparisons. Data (arithmetic means ± standard deviations) are representative of three independent experiments.

The attenuation masking phenotype of gene expression changes were identified by sorting for duplicate changes between Δ*luxS* or Δ*rbsA*Δ*lsrA*Δ*luxS* versus WT CO92 and excluding those changes that were also displayed between Δ*rbsA*Δ*lsrA* versus WT CO92 (**Appendix A, Table 12**). Through this analysis, 220 genes with a $p_{adj} < 0.1$ were selected and included a large segment of the genes encoding type III secretion system (T3SS) structural, *yscABCDGLOPRSTUVXY* (1.3-2.6), and effector proteins, encoded by *yopBDHJMQRT* (1.4-2.9), and all of these genes were upregulated. The T3SS in *Y. pestis* has been extensively characterized as an essential virulence system with functions ranging from targeted cell lysis to immune evasion (88). We confirmed changes in expression profiles of T3SS effectors, i.e., *Yersinia* outer membrane protein E, YopE, and the structural low calcium response antigen V, LcrV, by Western blot analysis in *luxS*-associated and Δ*rbsA*Δ*lsrA* mutants, as well as WT CO92. Both of these proteins were secreted at higher levels in Δ*luxS* and Δ*rbsA*Δ*lsrA*Δ*luxS* mutants when compared to either WT CO92 or the Δ*rbsA*Δ*lsrA* mutant under inducing *in vitro* growth conditions, i.e., low calcium and at 37°C (88) (**Fig. 21)**. Other characterized virulence factor encoding genes such as *ail*, the attachment invasion locus, and *pla*, plasminogen-activator protease, were not significantly differentially expressed in any of the strains examined compared to WT CO92. For confirmation, we examined levels of Pla by Western blot analysis and evaluated Pla protease activity (**Fig. 22**), which remained unaltered across the strains examined.

To determine the impact of AI-2 on gene regulation, we focused on common changes between comparisons of Δ*rbsA*Δ*lsrA* and Δ*luxS* versus WT CO92 (**Appendix A, Table 13**). This analysis identified 348 differentially expressed genes with a $p_{adj} < 0.1$ and included several iron transport gene families as well as autoinducer-1 (AI-1) quorum sensing components. There were significant changes to expression in iron transport related genes. Inorganic chelated iron transport, *yfeABCDE* (2.15- 3.75), was upregulated while organic iron transport, *tonB* (-2.8) and siderophore yersiniabactin synthesis,

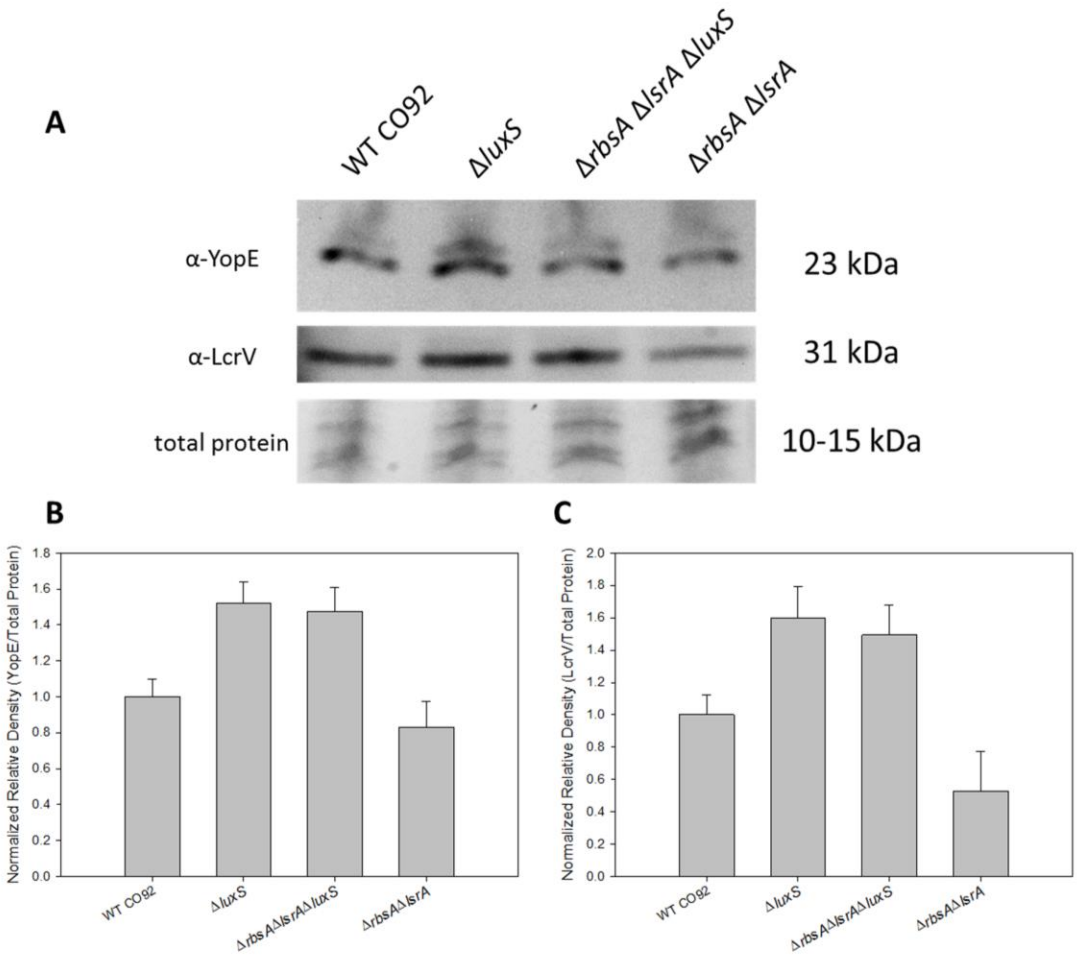

Figure 21. Type III secretion system function.

Western blots of anti-LcrV and anti-YopE from concentrated culture supernatants normalized against total protein visualized on the blot (**A**). Densities of anti-YopE (**B**) and anti-LcrV (**C**) were measured and plotted. Western blot image is representative of three independent experiments. Arithmetic means ± standard deviations are shown.

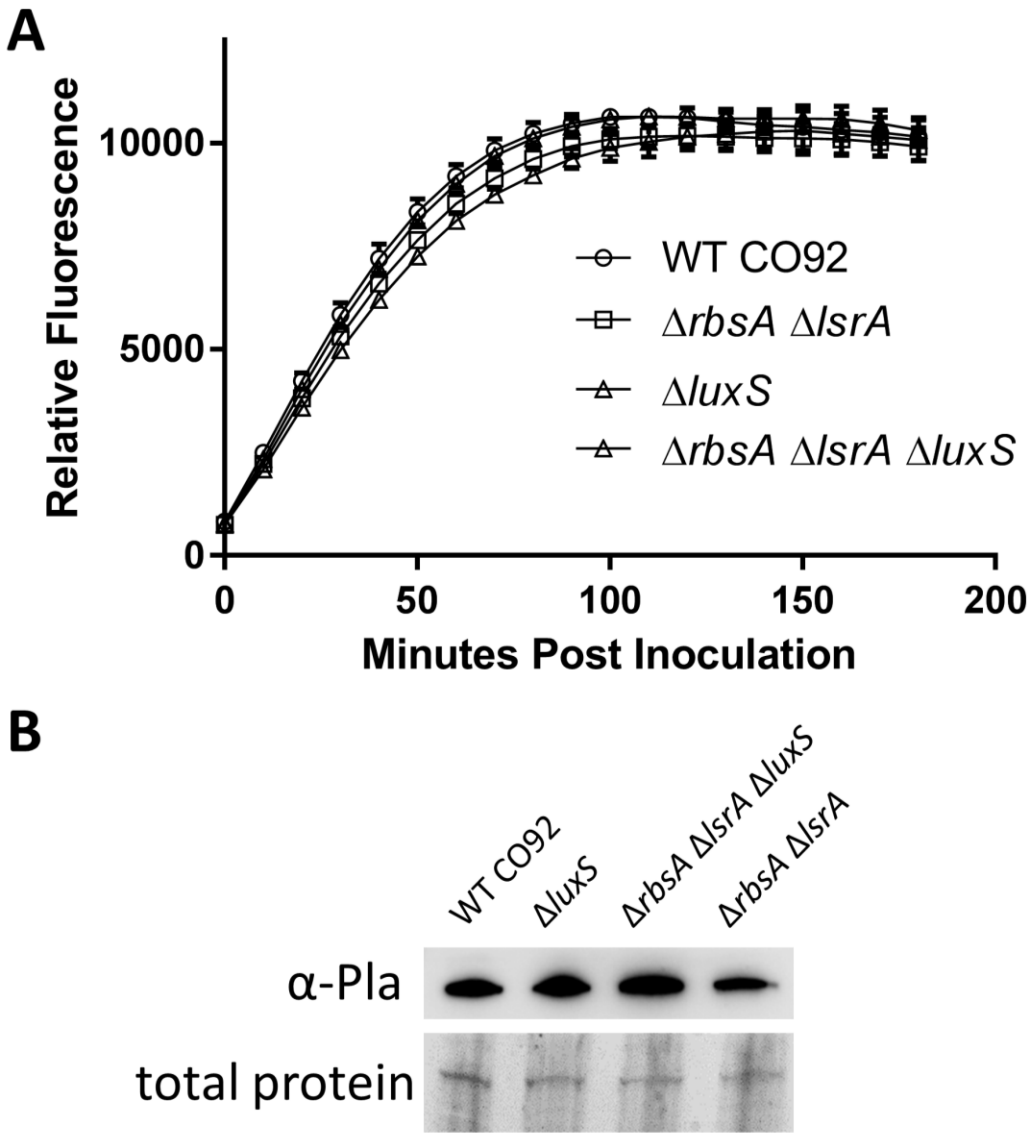

Figure 22. Pla protease activity.

The activity of Pla protease was measured for several strains using a fluorescent reporter assay (**A**). The protein levels of Pla were determined by immunoblotting using polyclonal anti-Pla antibodies and loading controlled by total protein visualization using Stain-Free technology (**B**). Data are representative of three independent cultures per strain. Arithmetic means ± standard deviations are shown.

irp1/2/3/4/5/6/7/8 (-1.83 - -3.29), were both uniformly repressed. Growth in restricted nutrient medium with a sole iron source of non-chelated inorganic iron, $FeSO_4$, resulted in delayed growth of the above-mentioned mutants compared to WT CO92 as well as a lower final bacterial density, indicating a functional consequence of expression changes (**Fig. 20C**). In addition to the alteration in iron uptake mechanisms that was observed across AI-2 perturbed strains, we also observed uniform upregulation of AI-1 system components, *ypeIR* (4.14-4.35) and *yspI* (2.02), including synthetic genes for both of the *acyl*-homoserine lactones used by the AI-1 system as well as the downstream receptor.

Finally, as is the gold standard in the field, we attempted to complement phenotypes of the mutants with exogenous AI-2. In the mouse pneumonic plague model, we partially complemented the Δ*rbsA*Δ*lsrA*Δ*luxS* mutant with exogenous AI-2 to an attenuated phenotype (at doses of 0.2 and 2 μM) characterized by the Δ*rbsA*Δ*lsrA* strain (**Fig. 23**). This complementation was achieved *via* intranasal dosing with exogenous AI-2 resulting in AI-2 lung concentrations equivalent to an order of magnitude below typical levels achieved in *in vitro* rich medium culture. Equivalent dosing of mice with AI-2 that were infected with WT CO92 strain showed no difference in virulence (**Fig. 23**), suggesting the change in virulence is specific to the Δ*rbsA*Δ*lsrA*Δ*luxS* strain and due to the availability of AI-2.

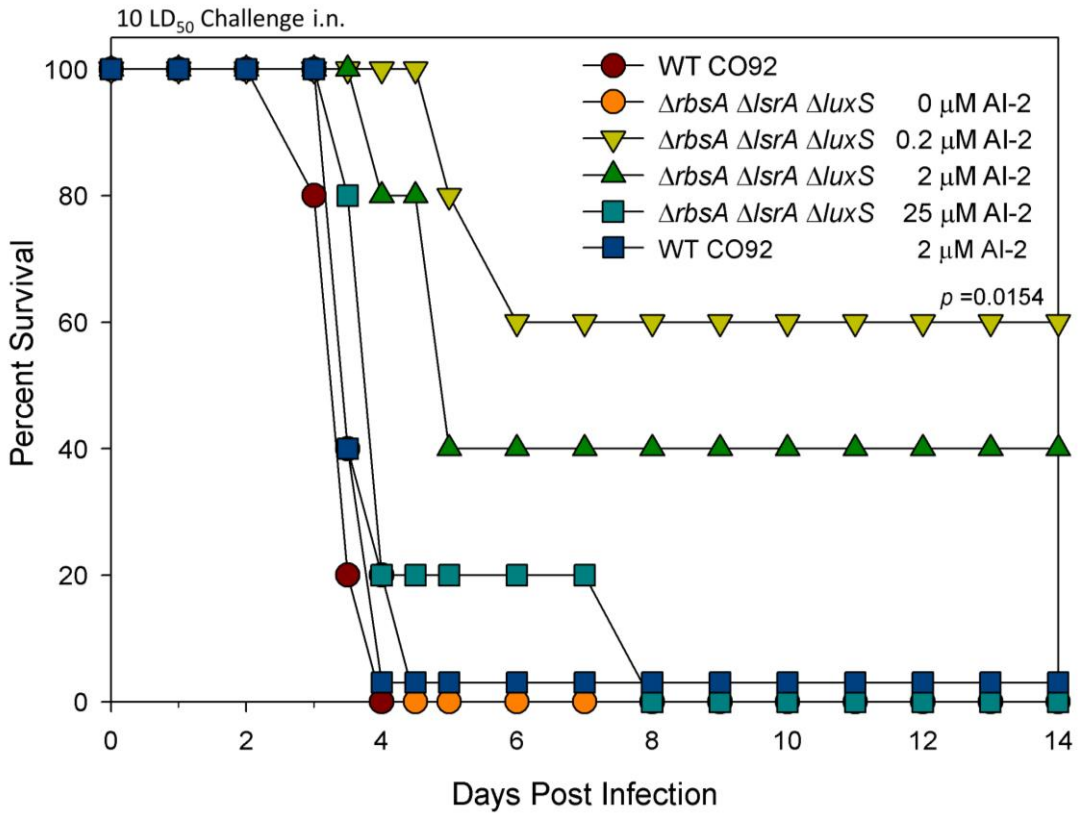

Figure 23. *In vivo* complementation of the Δ*rbsA*Δ*lsrA*Δ*luxS* mutant with exogenous synthetic AI-2.

The survival of female Swiss-Webster mice (n=5) in a pneumonic plague model challenged with 10 LD_{50} equivalent of WT CO92 where 1 LD_{50} is 500 CFU. Mice were dosed with the stated concentration of synthetic AI-2 in phosphate-buffered saline (PBS) at the time of infection, 24 h, and 48 h post infection (PI) *via* the intranasal (i.n.) route. Statistical analysis was performed using Kaplan Meier survival curve analysis.

DISCUSSION

AI-2 has been purported to be an interspecies metabolic status signaling mechanism in bacteria allowing adaptive regulation to environmental conditions. AI-2 controls a diverse array of traits in a just as diverse array of bacterial species, both non-pathogenic and pathogenic. In fully virulent *Y. pestis*, we showed that decoupling of the AI-2 signaling mechanism resulted in a drastic reduction in virulence, requiring over 50 fold greater challenge doses to cause disease. This contrasts greatly with previous reports of AI-2 regulation in both *Y. pestis* as well as in other pathogenic bacteria. We also demonstrated a basis for the reported differences observed in AI-2 *in vivo* virulence through the deletion of *luxS* and its accompanying virulence masking phenotype. As has been discussed often in the literature, the role of LuxS in the cycling of homocysteine could have significant effects beyond the loss of AI-2 production or alternately be necessary for endogenous AI-2 signal propagation that is distinct from exogenous signal propagation (210). The impact of these pleiotropic effects is apparent in the upregulation of the T3SS of *Y. pestis* observed in this study that paralleled similar secretion phenotypes described in both *Aeromonas* and *Salmonella* Δ*luxS* strains (190, 211). We suggest that AI-2 signaling may require reevaluation in many of the previously characterized bacterial species in light of our results.

The metabolic regulation observed with AI-2 perturbation, especially the PTS system, indicates a strong role for AI-2 in the adaptive response to different environmental niches. The PTS system regulates preferred sugar uptake and depends on flux of sugars to balance the phosphorylation state of two major regulatory kinases, PtsIH, that influence both transcription and function of non-PTS transporters. The diminished expression of *ptsG* could influence the phosphorylation states of these kinases in addition to the expression changes, allowing further dysregulation. Previous studies have indicated that PtsI is essential for the uptake of AI-2 *via* a regulatory function (200),

thus the reciprocal changes in expression of PTS regulators suggest a complex and strictly controlled dynamics utilizing AI-2 as a powerful environmental signal. Taken together, the attenuated phenotype of *Y. pestis* CO92 mutant that is unable to transport AI-2 and modulation of expression profile of genes suggest a decoupling of metabolic status from regulatory control, resulting in a maladaptive metabolic and stress response profile. This aberrant response possibly contributes to the attenuating phenotype of the Δ*rbsA*Δ*lsrA* mutant.

Finally, a high conservation of AI-2 transport mechanisms and signaling pathway in microbes present a significant opportunity for small molecule intervention (212). Current inhibitors of AI-2 have unknown activity in *in vivo* models of disease which is in part due to paucity of *in vivo* data in conjunction with the lack of attenuation previously observed for the *luxS* deletion strains for several pathogenic bacteria. The inhibitors characterized thus far, and the development of potential drug targets in the RbsBAC and LsrABCD family of proteins, represent an untapped resource in the fight against antibacterial resistance.

Chapter 4: Summary and Future Directions

INTRODUCTION

Plague is a significant disease caused by the pathogenic bacteria, *Y. pestis*. There are several manifestations of disease including bubonic, septicemic, and pneumonic plague. Bubonic and septicemic plague have moderately high case fatality rates approaching 50% without prompt antibiotic treatment and approximately 16% even with aggressive treatment. Pneumonic plague is almost universally fatal if untreated or if the treatment is delayed beyond 24 hours of first symptoms. *Y. pestis* has caused disease in humans throughout recorded history with potential outbreaks reaching back into pre-Christian eras. Three pandemics have devastated populations across the globe with the first, the Justinian plague, beginning in the 6th century and killing an estimated 100 million. The second plague pandemic began in the 14th century and resulted in the deaths of a quarter of Europe's population. Finally, the third pandemic began in the late 19th century with plague classified as a re-emerging pathogen in modern times. In the United States, a handful of cases occur naturally each year, with most resulting from exposures to *Y. pestis* in geographic areas known to be endemic for *Y. pestis.* As recently as 2014, an outbreak of pneumonic plague occurred from exposure to an infected dog and may have been the first human-to-human transmission of pneumonic plague in almost a century. The potential application of *Y. pestis* as a bioweapon is especially concerning. The long history of *Y. pestis* being used as a bioweapon and its warfare development by the Japanese in World War II as well as by the former USSR during the 1970's, present a strong case for preparing countermeasures. To this end, several antibiotics are approved for the specific treatment of *Y. pestis* infection, however, the rise of antibiotic resistance could spell trouble for this approach. Vaccines are currently under development,

however, none are approved for use in the United States at this time. Research into the correlates of immunity necessary for protection against *Y. pestis* have suggested that a combination of humoral and cell mediated immunity is necessary for robust protection. A live-attenuated vaccine would best fulfill this requirement while also providing the cheapest and most scalable platform. Rational development of live-attenuated vaccines require specific knowledge of virulence factors for the pathogen in question. To address this gap in knowledge, we proposed to identify novel virulence factors, particularly as they relate to pneumonic plague and to characterize these factors for both function and mechanism to identify targets for future vaccine and therapeutic development.

HIGH-THROUGHPUT SIGNATURE-TAGGED MUTAGENIC APPROACH TO IDENTIFY NOVEL VIRULENCE FACTORS OF *YERSINIA PESTIS* CO92 IN A MOUSE MODEL OF INFECTION.

Towards the goal of identifying novel virulence factors, we used a strategy of signature tagged mutagenesis in *Y. pestis*. Over 5000 transposon mutants were generated and subsequently used to infect mice. Following isolation of bacteria that had disseminated in the mouse model to the spleen, hybridization blots assessed the fitness of the mutants to reach peripheral organs and to represent potential virulence factor mutants. This screening method identified 118 mutant clones that had decreased fitness. Each mutant that passed the first bottleneck was then individually examined for virulence in a bubonic plague model in a second screening. Of the original 118, 20 mutants were attenuated at biological relevant levels and 10 of those 20 mutants were also attenuated at a high challenge dose of 40 LD_{50}.

The 20 mutants identified to be attenuated in a bubonic plague model were characterized to determine the location of genomic disruption. Of the 20 mutants 18 had transposon insertion locations appropriately identified. Several were found to have disruptions in known virulence factors such as insertions in the *pla* gene encoding Pla protease or in the gene encoding F1 capsular antigen. Several of the most highly

attenuated clones had genomic disruptions in *rbsA*, *vasK*, or *ypo0498*. These genes were then targeted for isogenic deletion to confirm their status as virulence determinants. When tested in a bubonic plague model, deletions in *rbsA* or in *vasK* both resulted in significant attenuation while a moderate decrease in virulence was noted in the *ypo0498* deletion strain but did not reach significance. Orthologs of VasK, encoded by *vasK*, have been characterized as essential components of the T6SS and are necessary for secretion of effectors such as Hcp. Deletion of *vasK* from *Y. pestis* failed to decrease secretion of Hcp as determined by Western blot; however, in combination with deletion of *lpp,* resulted in 90 percent survival in a pneumonic plague model at a challenge dose of 12 LD_{50}. Deletion of *rbsA* was found to impact the growth of *Y. pestis* in a minimal medium limited to a ribose carbon source, providing confirmation of the annotated function of the *rbs* operon as a ribose transporter. Additionally, isogenic deletion of *rbsA* led to a significant decrease in virulence in a pneumonic plague model. When combined with deletion of *lpp* and *msbB*, the triple deletion strain was highly attenuated with 100 percent survival at challenge doses up to 50 LD_{50}. Further, this initial challenge with attenuated bacteria provided 80 percent protection against re-challenge with a fully virulent strain CO92 of *Y. pestis*. Through a signature-tagged mutagenic strategy, we identified multiple novel virulence factors in *Y. pestis* as well as characterized several isogenic deletions. This study has therefore led to the identification of several potential targets for inclusion in a combinatorial attenuated vaccine candidate.

NEW PARADIGM IN AUTOINDUCER-2 SIGNALING: POTENT IN VIVO BACTERIAL VIRULENCE REGULATOR

The signature tagged mutagenesis study identified several candidate novel virulence factors, one of which was encoded by the gene *rbsA*. We sought to further characterize the function and mechanism of attenuation afforded by deletion of *rbsA*. Early studies with *rbsA* suggested that deletion of the gene resulted in deficits with ribose

utilization by *Y. pestis*. There was also literature that suggested that orthologs of RbsA protein could efficiently interact with AI-2. To further characterize the attenuating deletion of *rbsA*, AI-2 signaling was investigated. The concentration of AI-2 present in the supernatants of cultures was determined for several strains including a deletion in *rbsA*. Aberrations in the concentration of AI-2 were discovered with the highly attenuated triple deletion mutant Δ*lpp*Δ*msbB*Δ*rbsA*. As there is a characterized transport operon specific for AI-2, the *lsr* operon, we isogenically deleted the analogous gene to *rbsA* from this *lsr* operon. Single deletions in either *rbsA* or *lsrA* had no significant effect at mid-log phase on AI-2 levels in the culture supernatant, however, double deletion of both *rbsA* and *lsrA* resulted in a similar defect (increased AI-2 levels) observed in the original triple mutant. Further, this double mutant was significantly attenuated in mouse models of pneumonic plague with 80 percent survival at challenges up to 50 LD_{50}. Interestingly, this attenuation was reversed upon deletion of the gene encoding the synthetic enzyme for the AI-2 signal, *luxS*. Deletions of *luxS* had previously been the primary method of determining AI-2 signaling changes in the literature.

We sought to uncover the differences in gene expression downstream of AI-2 that resulted in both the attenuating phenotype observed with the Δ*rbsA*Δ*lsrA* deletion mutant as well as the masking, virulent phenotype observed with the Δ*rbsA*Δ*lsrA*Δ*luxS* deletion mutant. To accomplish this, we used RNAseq to determine the transcriptomes of WT CO92, Δ*rbsA*Δ*lsrA*, Δ*luxS,* and the Δ*rbsA*Δ*lsrA*Δ*luxS* strain. Through this analysis, several gene clusters were observed to be differentially regulated. Most notably, genes associated with stress responses such as *dnaJK*, *ibpAB*, and *htpG* as well as the catalase encoding gene *katY* were all downregulated in the attenuated Δ*rbsA*Δ*lsrA* strain. Also, the well characterized T3SS that is essential for virulence was upregulated in the masking phenotype of the Δ*rbsA*Δ*lsrA*Δ*luxS* strain. Further functional assays confirmed these transcriptomic changes to be biologically relevant by *in vitro* assays. Finally, we used a

synthetic AI-2 to partially complement the Δ*rbsA*Δ*lsrA*Δ*luxS* strain *in vivo* resulting in a significantly attenuated phenotype in the pneumonic plague model.

These results all suggest that the AI-2 system is an active regulator of *Y. pestis* virulence in both *in vitro* and *in vivo* models. Further, these results also suggest that studies of AI-2 in other pathogenic organisms should be re-examined in light of the disadvantageous response from deletions of *luxS*. The highly conserved nature of the AI-2 system in a large number of pathogenic bacteria makes this a prime target for therapeutic intervention, highlighted by the significant response that dysregulation of the AI-2 system had on attenuating the virulent phenotype of *Y. pestis*.

CONCLUSIONS AND FUTURE DIRECTIONS

Through the course of this study, we have accomplished the goal of identifying novel virulence factors in *Y. pestis* as well as characterizing the function and a partial mechanism by which the attenuation is developed. The signature-tagged mutagenesis study identified at least 10 highly attenuated mutants, several of which harbored mutations in putative or hypothetical protein encoding genes. Moving forward, the studies of *rbsA* and the larger role of AI-2 in virulence hold promise for targeted therapeutic interventions as well as potential for inclusion in a combinatorial live-attenuated vaccine(s). The potential for therapeutic intervention utilizing an anti-virulence approach is gaining popularity as antibiotic resistance continues to rise. The utility of targeting AI-2 as an anti-virulence strategy lies in several factors: there are multiple compounds that have already been identified as AI-2 inhibitors, AI-2 is highly conserved system throughout the bacterial kingdom and inhibition of AI-2 may have broad spectrum efficacy, and lastly, the large impact that dysregulation of AI-2 has on attenuation makes it a highly attractive target. Our findings describing an *in vivo* model in which AI-2 dysregulation impacts *in vivo* virulence provides a platform on which to test inhibitors of AI-2 function.

Other directions of inquiry would include further screening of mutants from the STM pool derived from this study. Approximately half of the total mutants were screened in this study, leaving a pool of over 2000 mutants from which a further group of novel virulence candidates could be pulled. Additionally, several of the genes identified through the STM study were annotated as putative or hypothetical. These genes encode proteins of unknown function that may have orthologs in other pathogens representing an entire new area of research.

Appendix A: Transcriptomic results

Table 7. Significant differentially expressed genes Δ*rbsA*Δ*lsrA* v. WT CO92 and Δ*luxS* v. WT CO92

Δ*rbsA*Δ*lsrA* vs. WT CO92			
Gene Symbol	**log fold change**	***padj***	**Genome Annotation**
accC	-0.627	5.563E-02	acetyl-CoA carboxylase biotin carboxylase subunit
adhE	-0.577	2.944E-04	bifunctional acetaldehyde-CoA/alcohol dehydrogenase
ansA	-0.926	1.787E-07	cytoplasmic asparaginase I
araC	-0.573	2.417E-02	DNA-binding transcriptional regulator AraC
araF	-0.573	2.417E-02	L-arabinose-binding protein
araG	-0.573	2.417E-02	L-arabinose transporter ATP-binding protein
arnT	1.367	1.599E-23	4-amino-4-deoxy-L-arabinose transferase
atpF	-0.485	4.442E-02	ATP synthase F0F1 subunit B
atpH	0.592	3.478E-03	ATP synthase F0F1 subunit delta
bioD	0.438	5.255E-02	dithiobiotin synthetase
btuE	1.472	8.976E-18	glutathione peroxidase
ccmA	0.591	6.228E-02	cytochrome c biogenesis protein CcmA
ccmD	-0.549	9.220E-02	heme exporter protein D
ccmE	-0.549	9.220E-02	cytochrome c-type biogenesis protein CcmE
ccmF	-0.549	9.220E-02	cytochrome c-type biogenesis protein
ccmG	-0.549	9.220E-02	thiol:disulfide interchange protein DsbE
ccmH	-0.549	9.220E-02	cytochrome c-type biogenesis protein
clpB	0.663	7.864E-03	Clp ATPase
cls	-1.077	1.771E-08	cardiolipin synthetase
cpxP	1.025	8.999E-07	periplasmic stress adaptor protein CpxP
csrB	-0.434	2.173E-02	#N/A
cysT	-0.841	6.566E-04	sulfate/thiosulfate transporter subunit
dadA	-1.291	8.502E-15	D-amino acid dehydrogenase small subunit
dksA	1.317	8.477E-09	RNA polymerase-binding transcription factor
dnaJ	-0.335	5.012E-02	molecular chaperone DnaJ
dnaK	-0.335	5.012E-02	molecular chaperone DnaK
dps	2.556	9.163E-47	DNA starvation/stationary phase protection protein Dps
fis	1.189	1.003E-07	Fis family transcriptional regulator
fklB	1.189	1.003E-07	peptidyl-prolyl cis-trans isomerase
flgG	-0.772	2.039E-04	flagellar basal body rod protein FlgG
fliH	-0.767	5.874E-02	flagellar assembly protein H
ftn	1.218	7.921E-07	ferritin
gapA	-0.762	1.757E-04	glyceraldehyde 3-phosphate dehydrogenase A
glnP	1.683	2.126E-13	glutamine ABC transporter permease
glnQ	1.449	1.671E-12	glutamine ABC transporter ATP-binding protein
greA	1.343	1.849E-11	transcription elongation factor GreA
hcaT	-0.973	1.249E-03	3-phenylpropionic acid transporter
hdeB	1.457	2.376E-20	acid-resistance protein
htpG	0.704	1.330E-03	heat shock protein 90
ibpA	0.377	8.126E-02	heat shock protein IbpA
ibpB	0.377	8.126E-02	heat shock chaperone IbpB
ihfA	0.379	9.252E-02	integration host factor subunit alpha
ihfB	1.114	2.313E-08	integration host factor subunit beta
infC	1.767	2.558E-12	translation initiation factor IF-3
irp1	-1.719	9.119E-07	yersiniabactin biosynthetic protein
irp2	-1.081	7.403E-04	yersiniabactin biosynthetic protein
irp3	-1.375	4.403E-03	yersiniabactin biosynthetic protein YbtU
lplA	1.579	4.750E-24	lipoate-protein ligase A
marC	1.715	5.326E-23	multiple drug resistance protein MarC

"-" indicates down regulation of expression

Δ*rbsA*Δ*lsrA* vs. WT CO92

Gene Symbol	log fold change	*padj*	Genome Annotation
menF	-0.710	4.296E-02	menaquinone-specific isochorismate synthase
mipB	-1.088	4.479E-04	fructose-6-phosphate aldolase
mrpA	1.219	1.572E-06	mannose-resistant fimbrial protein
napA	1.109	4.581E-08	nitrate reductase catalytic subunit
napB	1.109	4.581E-08	citrate reductase cytochrome c-type subunit
napC	1.109	4.581E-08	cytochrome c-type protein NapC
napD	1.109	4.581E-08	assembly protein for periplasmic nitrate reductase
napF	1.109	4.581E-08	ferredoxin-type protein NapF
nhaB	-1.284	1.417E-11	sodium/proton antiporter
nirB	0.991	2.197E-05	nitrite reductase
nqrB	-0.710	2.471E-04	Na(+)-translocating NADH-quinone reductase subunit B
nqrC	-0.710	2.471E-04	Na(+)-translocating NADH-quinone reductase subunit C
nqrD	-0.710	2.471E-04	Na(+)-translocating NADH-quinone reductase subunit D
nudG	-1.433	5.901E-05	pyrimidine (deoxy)nucleoside triphosphate pyrophosphohydrolase
opdA	1.014	6.365E-09	oligopeptidase A
oppF	-1.172	1.010E-06	oligopeptide transport ATP-binding protein
pheS	0.805	3.318E-06	phenylalanyl-tRNA synthetase subunit alpha
pheT	0.520	1.202E-02	phenylalanyl-tRNA synthetase subunit beta
pmrF	1.517	8.834E-21	undecaprenyl phosphate 4-deoxy-4-formamido-L-arabinose transferase
priB	0.550	6.102E-04	primosomal replication protein N
ptsG	0.570	1.894E-03	PTS system glucose-specific transporter subunits IIBC
rbsA	-5.047	2.214E-47	sugar transport system ATP-binding protein
rhaA	-1.239	4.257E-03	L-rhamnose isomerase
rplS	1.211	5.847E-05	50S ribosomal protein L19
rplT	1.757	5.262E-05	50S ribosomal protein L20
rpmG	0.941	2.788E-04	50S ribosomal protein L33
rpmI	1.424	3.513E-13	50S ribosomal protein L35
selD	-1.626	1.057E-18	selenophosphate synthetase
solA	1.818	5.053E-26	N-methyltryptophan oxidase
tauA	-0.487	7.032E-02	taurine transporter substrate binding subunit
tauD	-0.644	4.019E-02	taurine dioxygenase
tdk	-1.528	2.575E-17	thymidine kinase
thrS	1.075	1.749E-05	threonyl-tRNA synthetase
tig	-0.347	3.181E-02	trigger factor
tonB	-1.690	9.903E-18	transport protein TonB
topB	-1.048	3.311E-11	DNA topoisomerase III
tpiA	1.390	4.471E-08	triosephosphate isomerase
tqsA	1.683	1.264E-27	transport protein
xylF	0.829	6.203E-07	D-xylose transporter subunit XylF
yecC	-0.694	8.225E-04	amino-acid ABC transporter ATP-binding protein YecC
yecS	-0.780	2.231E-03	amino-acid ABC transporter permease
yfeA	1.965	3.266E-40	substrate-binding protein
yfeB	1.915	8.948E-35	ATP-binding transport protein
yfeC	1.357	7.281E-10	chelated iron transport system membrane protein
yfeD	1.188	4.872E-10	chelated iron transport system membrane protein

"-" indicates down regulation of expression

Δ*rbsA*Δ*lsrA* vs. WT CO92

Gene Symbol	log fold change	*padj*	Genome Annotation
yfeE	2.343	2.143E-42	yfeABCD locus regulator
yfgD	0.471	6.103E-03	arsenate reductase
yhjA	-0.544	5.237E-02	cytochrome C peroxidase
yopQ	1.523	1.731E-13	Yop targeting protein (plasmid)
ypeI	2.192	5.649E-23	N-acylhomoserine lactone synthase
ypeR	2.140	1.284E-24	quorum-sensing transcriptional activator YpeR
YPMT1.01	0.445	6.360E-03	putative transposase (plasmid)
YPMT1.04c	-0.743	2.885E-04	putative phage tail protein (plasmid)
YPMT1.11c	-1.623	3.547E-05	hypothetical protein YPMT1.11c (plasmid)
YPMT1.35c	-1.517	3.050E-05	hypothetical protein YPMT1.35c (plasmid)
YPMT1.45c	1.201	1.329E-02	hypothetical protein YPMT1.45c (plasmid)
YPMT1.46c	0.874	7.318E-02	hypothetical protein YPMT1.46c (plasmid)
YPMT1.55c	1.759	1.871E-11	hypothetical protein YPMT1.55c (plasmid)
YPMT1.59c	-1.801	5.220E-05	putative DNA-binding protein (plasmid)
YPMT1.75c	-1.164	1.168E-02	reverse transcriptase (plasmid)
YPMT1.79c	-1.553	1.373E-11	transposase (plasmid)
YPO0127	0.386	7.035E-02	DNA uptake protein
YPO0147	-1.185	4.057E-04	hypothetical protein YPO0147
YPO0148	-1.459	5.842E-04	hypothetical protein YPO0148
YPO0285	0.970	1.914E-04	hypothetical protein YPO0285
YPO0286	0.970	1.914E-04	coproporphyrinogen III oxidase
YPO0397	-1.125	8.544E-04	hypothetical protein YPO0397
YPO0400	0.713	6.441E-06	hypothetical protein YPO0400
YPO0407	1.857	3.011E-18	autoinducer-2 (AI-2) modifying protein LsrG
YPO0412	-2.897	1.465E-26	ABC transporter ATP-binding protein
YPO0624	1.246	1.053E-07	hypothetical protein YPO0624
YPO0625	1.468	4.344E-13	hypothetical protein YPO0625
YPO0626	1.080	8.688E-07	hypothetical protein YPO0626
YPO0627	1.193	1.744E-10	translational inhibitor protein
YPO0640	0.721	2.858E-04	hypothetical protein YPO0640
YPO0950	1.249	4.336E-07	hypothetical protein YPO0950
YPO1316	-0.628	3.200E-02	iron/ascorbate oxidoreductase family protein
YPO1318	-1.197	5.867E-04	ABC transporter ATP-binding protein
YPO1500	1.277	1.320E-04	hypothetical protein YPO1500
YPO1718	1.039	8.337E-09	hypothetical protein YPO1718
YPO1736	1.603	2.242E-14	hypothetical protein YPO1736
YPO1941	1.377	2.161E-11	hypothetical protein YPO1941
YPO1942	1.066	3.542E-10	hypothetical protein YPO1942
YPO1993	-2.104	2.585E-17	dehydrogenase
YPO1994	-1.270	5.646E-07	hypothetical protein YPO1994
YPO1995	-1.418	7.043E-10	hypothetical protein YPO1995
YPO1996	-1.084	1.938E-05	hypothetical protein YPO1996
YPO2055	1.039	1.040E-06	hypothetical protein YPO2055
YPO2095	1.535	1.616E-04	hypothetical protein YPO2095
YPO2096	1.455	9.429E-09	hypothetical protein YPO2096
YPO2128	1.112	6.652E-04	phage-like lipoprotein
YPO2137	-1.827	6.540E-13	hypothetical protein YPO2137
YPO2138	-1.550	3.909E-04	aminotransferase
YPO2139	-1.147	3.372E-02	hypothetical protein YPO2139
YPO2148	-1.779	1.543E-14	multidrug resistance protein
YPO2151	-1.265	1.799E-06	hypothetical protein YPO2151
YPO2152	-1.160	7.955E-08	hypothetical protein YPO2152
YPO2153	-1.086	1.172E-06	hypothetical protein YPO2153
YPO2163	-1.563	1.398E-08	hypothetical protein YPO2163
YPO2169	-3.199	9.937E-18	LysR family transcriptional regulator
YPO2172	-1.422	3.911E-09	hypothetical protein YPO2172

"-" indicates down regulation of expression

Δ*rbsA*Δ*lsrA* vs. WT CO92

Gene Symbol	log fold change	*padj*	Genome Annotation
YPO2173	-1.707	7.411E-17	response regulator of RpoS
YPO2192	-1.229	4.457E-05	hypothetical protein YPO2192
YPO2398	1.270	3.174E-11	murein L,D-transpeptidase
YPO2400	1.044	7.715E-07	bifunctional cysteine desulfurase/selenocysteine lyase
YPO2410	1.366	5.855E-09	hypothetical protein YPO2410
YPO2416	1.418	1.912E-11	hypothetical protein YPO2416
YPO2419	1.561	2.012E-14	hypothetical protein YPO2419
YPO2420	1.788	1.193E-23	bifunctional UDP-glucuronic acid decarboxylase/UDP-4-amino-4-deoxy-L-arabinose formyltransferase
YPO2422	1.456	4.609E-16	UDP-4-amino-4-deoxy-L-arabinose--oxoglutarate aminotransferase
YPO2426	1.465	8.920E-11	hypothetical protein YPO2426
YPO2434	1.924	2.877E-17	hypothetical protein YPO2434
YPO2436	1.779	5.095E-16	hypothetical protein YPO2436
YPO2446	1.355	1.352E-06	2-deoxyglucose-6-phosphatase
YPO2449	1.641	2.255E-24	LuxR family transcriptional regulator
YPO2451	1.077	1.802E-08	hypothetical protein YPO2451
YPO2455	1.004	1.698E-03	hypothetical protein YPO2455
YPO2459	1.057	6.961E-03	transporter protein
YPO2462	1.274	6.821E-05	hypothetical protein YPO2462
YPO2464	1.256	8.559E-06	hypothetical protein YPO2464
YPO2465	1.353	2.932E-12	hypothetical protein YPO2465
YPO2467	1.114	5.388E-07	hypothetical protein YPO2467
YPO2470	1.102	7.158E-03	hypothetical protein YPO2470
YPO2476	1.280	4.455E-05	sugar ABC transporter permease
YPO2481	1.840	3.343E-10	hypothetical protein YPO2481
YPO2482	1.075	1.215E-03	hypothetical protein YPO2482
YPO2483	1.705	2.175E-10	hypothetical protein YPO2483
YPO2484	1.474	1.563E-03	hypothetical protein YPO2484
YPO2489	1.821	3.770E-15	hypothetical protein YPO2489
YPO2490	1.076	1.217E-07	hemolysin
YPO2494	1.173	3.285E-04	transporter
YPO2495	1.254	2.028E-04	hypothetical protein YPO2495
YPO2496	1.004	9.254E-04	tartrate dehydrogenase
YPO2498	1.724	2.481E-23	LacI family transcriptional regulator
YPO2504	1.781	7.524E-10	hypothetical protein YPO2504
YPO2511	2.530	8.532E-30	hypothetical protein YPO2511
YPO2515	1.317	1.897E-10	chemotactic transducer
YPO2563	1.253	5.064E-10	hypothetical protein YPO2563
YPO2590	1.014	8.688E-04	hypothetical protein YPO2590
YPO2675	1.124	1.830E-06	voltage-gated potassium channel
YPO2855	1.286	1.184E-08	protease
YPO3048	1.226	4.067E-11	ABC transporter ATP-binding protein
YPO3050	1.037	3.082E-05	hypothetical protein YPO3050
YPO3121	1.093	5.580E-04	hypothetical protein YPO3121
YPO3136	1.165	3.015E-06	hypothetical protein YPO3136
YPO3170	1.286	7.196E-08	nucleotide-binding protein
YPO3213	1.043	1.584E-06	hypothetical protein YPO3213
YPO3343	1.112	1.496E-05	ABC transporter substrate-binding protein
YPO3387	-1.042	4.758E-07	iron-sulfur cluster insertion protein ErpA
YPO3518	-1.282	3.111E-06	hypothetical protein YPO3518
YPO3617	1.460	9.233E-12	hypothetical protein YPO3617
YPO3618	1.159	1.646E-05	oxidoreductase

"-" indicates down regulation of expression

Δ*rbsA*Δ*lsrA* vs. WT CO92			
Gene Symbol	**log fold change**	***padj***	**Genome Annotation**
YPO3655	1.004	9.815E-08	tRNA-dihydrouridine synthase B
YPO3681	-2.421	4.626E-31	insecticial toxin
YPO3682	-3.170	2.008E-29	LysR family transcriptional regulator
YPO3784	1.070	1.860E-09	carbon starvation protein
YPO3874	1.126	4.400E-05	hypothetical protein YPO3874
YPO3908	1.027	2.065E-05	periplasmic protein
YPO3957	-1.099	2.424E-02	hypothetical protein YPO3957
YPO3967	1.042	1.991E-05	phosphate transport protein
YPO4050	1.129	5.580E-04	hypothetical protein YPO4050
YPO4109	-1.055	1.197E-04	amino acid transport system permease
YPO4110	-1.527	1.173E-07	ABC transporter permease
YPPCP1.02	1.364	7.389E-03	transposase/IS protein (plasmid)
YPPCP1.06	1.028	4.144E-02	hypothetical protein YPPCP1.06 (plasmid)
YPt_02	-1.087	4.383E-02	#N/A
YPt_29	-1.267	2.096E-04	#N/A
YPt_53	1.252	2.982E-03	#N/A
YPt_63	-1.246	2.279E-03	#N/A
zntA	-1.087	2.797E-05	zinc/cadmium/mercury/lead-transporting ATPase

Table 8. Significant differentially expressed genes Δ*luxS* v. WT CO92

Δ*luxS* vs. WT CO92			
Gene Symbol	**log fold change**	***padj***	**Genome Annotation**
aceA	1.309	4.894E-09	isocitrate lyase
acpD	1.843	9.745E-23	azoreductase
ansA	-1.069	1.894E-07	cytoplasmic asparaginase I
arnT	1.107	4.376E-12	4-amino-4-deoxy-L-arabinose transferase
astA	1.067	1.017E-02	arginine succinyltransferase
cls	-1.058	2.354E-06	cardiolipin synthetase
cysP	-1.272	3.853E-08	thiosulfate transporter subunit
dps	1.236	1.019E-08	DNA starvation/stationary phase protection protein Dps
dsbB	-1.202	2.045E-07	disulfide bond formation protein B
fadA	1.069	3.096E-08	3-ketoacyl-CoA thiolase
fadB	1.037	4.423E-09	multifunctional fatty acid oxidation complex subunit alpha
fliY	-1.124	5.495E-08	cystine transporter subunit
gapA	-1.069	2.380E-06	glyceraldehyde 3-phosphate dehydrogenase A
glnP	1.614	7.424E-10	glutamine ABC transporter permease
glnQ	1.341	1.822E-08	glutamine ABC transporter ATP-binding protein
gptB	1.126	2.338E-02	PTS system mannose-specific transporter subunit IIAB
hslV	-1.104	2.416E-05	ATP-dependent protease peptidase subunit
infC	1.240	5.295E-05	translation initiation factor IF-3
irp1	-1.034	2.541E-02	yersiniabactin biosynthetic protein
irp3	-1.261	2.292E-02	yersiniabactin biosynthetic protein YbtU
irp4	-1.374	1.168E-02	yersiniabactin biosynthetic protein YbtT
lplA	1.160	3.422E-10	lipoate-protein ligase A
luxS	-8.422	8.167E-205	S-ribosylhomocysteinase
mtlK	1.012	2.554E-03	mannitol transport ATP-binding protein
nhaB	-1.148	2.344E-07	sodium/proton antiporter
nudG	-1.198	6.031E-03	pyrimidine (deoxy)nucleoside triphosphate pyrophosphohydrolase
ompF	-1.125	8.481E-08	porin

"-" indicates down regulation of expression

Δ*luxS* vs. WT CO92

Gene Symbol	log fold change	*padj*	Genome Annotation
pmrF	1.442	8.276E-15	undecaprenyl phosphate 4-deoxy-4-formamido-L-arabinose transferase
pncA	-1.000	6.487E-04	nicotinamidase/pyrazinamidase
ppsA	1.335	1.197E-15	phosphoenolpyruvate synthase
pspG	-1.190	1.544E-02	phage shock protein G
purK	-1.151	2.231E-02	phosphoribosylaminoimidazole carboxylase ATPase subunit
rhaA	-1.092	4.774E-02	L-rhamnose isomerase
rimI	-1.055	1.179E-02	ribosomal-protein-alanine N-acetyltransferase
selD	-1.140	1.891E-07	selenophosphate synthetase
solA	1.248	1.218E-09	N-methyltryptophan oxidase
sufA	1.069	5.099E-07	iron-sulfur cluster assembly scaffold protein
sufC	1.349	3.333E-10	cysteine desulfurase
tam	1.071	2.483E-04	trans-aconitate 2-methyltransferase
tauA	-1.177	1.342E-03	taurine transporter substrate binding subunit
tdk	-1.048	1.268E-06	thymidine kinase
tonB	-1.156	8.408E-07	transport protein TonB
tpiA	1.020	1.408E-03	triosephosphate isomerase
xthA	-1.107	1.036E-05	exonuclease III
yecS	-1.320	2.568E-06	amino-acid ABC transporter permease
yfeA	1.287	1.948E-13	substrate-binding protein
yfeB	1.279	3.618E-12	ATP-binding transport protein
yfeE	1.331	7.091E-11	yfeABCD locus regulator
yopR	1.109	1.157E-05	secreted protein (plasmid)
ypeI	1.181	1.743E-05	N-acylhomoserine lactone synthase
ypeR	1.262	5.750E-07	quorum-sensing transcriptional activator YpeR
YPO0148	-1.116	3.959E-02	hypothetical protein YPO0148
YPO0407	1.102	2.813E-05	autoinducer-2 (AI-2) modifying protein LsrG
YPO0419	1.043	3.409E-03	hypothetical protein YPO0419
YPO0435	-1.023	7.075E-03	Na+ dependent nucleoside transporter family protein
YPO0623	1.370	1.197E-15	aminotransferase
YPO0624	1.788	3.618E-12	hypothetical protein YPO0624
YPO0625	1.813	1.171E-15	hypothetical protein YPO0625
YPO0626	1.305	1.569E-07	hypothetical protein YPO0626
YPO0627	1.226	1.401E-08	translational inhibitor protein
YPO1061	1.045	2.231E-02	hypothetical protein YPO1061
YPO1096	1.141	8.865E-05	hypothetical protein YPO1096
YPO1409	1.122	1.893E-07	metallo-beta-lactamase superfamily protein
YPO1465	-1.179	4.446E-02	hypothetical protein YPO1465
YPO1941	1.084	6.858E-07	hypothetical protein YPO1941
YPO1975	1.371	4.188E-04	hypothetical protein YPO1975
YPO2137	-1.265	2.581E-06	hypothetical protein YPO2137
YPO2138	-1.639	3.091E-04	aminotransferase
YPO2139	-1.609	2.075E-03	hypothetical protein YPO2139
YPO2140	-1.149	3.579E-07	hypothetical protein YPO2140
YPO2158	-1.378	6.733E-06	methionine sulfoxide reductase B
YPO2163	-1.333	3.779E-06	hypothetical protein YPO2163
YPO2169	-2.648	1.132E-12	LysR family transcriptional regulator
YPO2171	-1.069	5.444E-08	formyltetrahydrofolate deformylase
YPO2172	-1.341	8.865E-08	hypothetical protein YPO2172
YPO2313	1.235	3.667E-03	hypothetical protein YPO2313
YPO2398	1.176	3.448E-09	murein L,D-transpeptidase
YPO2400	1.127	1.569E-07	bifunctional cysteine desulfurase/selenocysteine lyase

"-" indicates down regulation of expression

Δ*luxS* vs. WT CO92

Gene Symbol	log fold change	*padj*	Genome Annotation
YPO2401	1.302	2.803E-10	cysteine desulfurase
YPO2403	1.095	9.086E-07	cysteine desulfurase
YPO2406	1.002	9.330E-05	hypothetical protein YPO2406
YPO2419	1.400	3.947E-11	hypothetical protein YPO2419
YPO2420	1.548	3.544E-17	bifunctional UDP-glucuronic acid decarboxylase/UDP-4-amino-4-deoxy-L-arabinose formyltransferase
YPO2422	1.223	6.020E-11	UDP-4-amino-4-deoxy-L-arabinose--oxoglutarate aminotransferase
YPO2426	1.233	2.244E-07	hypothetical protein YPO2426
YPO2438	1.211	2.206E-06	membrane-bound lytic murein transglycosylase
YPO2446	1.011	1.371E-03	2-deoxyglucose-6-phosphatase
YPO2449	1.313	2.824E-15	LuxR family transcriptional regulator
YPO2462	1.278	1.236E-04	hypothetical protein YPO2462
YPO2464	1.060	5.847E-04	hypothetical protein YPO2464
YPO2465	1.106	7.137E-08	hypothetical protein YPO2465
YPO2476	1.033	3.446E-03	sugar ABC transporter permease
YPO2478	1.048	6.927E-05	LacI family transcriptional regulator
YPO2481	1.542	6.482E-07	hypothetical protein YPO2481
YPO2482	1.025	4.252E-03	hypothetical protein YPO2482
YPO2483	1.493	1.385E-07	hypothetical protein YPO2483
YPO2484	1.450	3.516E-03	hypothetical protein YPO2484
YPO2489	1.601	2.742E-11	hypothetical protein YPO2489
YPO2498	1.270	3.071E-12	LacI family transcriptional regulator
YPO2504	1.219	2.133E-04	hypothetical protein YPO2504
YPO2511	1.900	2.081E-16	hypothetical protein YPO2511
YPO2590	1.044	1.083E-03	hypothetical protein YPO2590
YPO3681	-2.388	2.239E-30	insecticial toxin
YPO3682	-3.732	5.334E-38	LysR family transcriptional regulator
YPO4109	-1.074	1.712E-04	amino acid transport system permease
YPO4110	-1.624	4.817E-08	ABC transporter permease
YPO4111	-1.346	7.349E-13	substrate-binding protein
YPt_02	-1.331	1.544E-02	#N/A
YPt_03	-1.186	8.469E-03	#N/A
YPt_16	-1.012	6.261E-03	#N/A
YPt_26	-1.131	8.567E-03	#N/A
YPt_29	-1.769	1.931E-07	#N/A
YPt_34	-1.286	8.443E-03	#N/A
YPt_40	-1.682	1.650E-07	#N/A
YPt_43	-1.175	2.266E-03	#N/A
YPt_44	-1.365	6.380E-03	#N/A
YPt_55	-1.122	4.061E-02	#N/A
YPt_59	-1.415	2.037E-04	#N/A
YPt_63	-1.183	7.458E-03	#N/A

"-" indicates down regulation of expression

Table 9. Significant differentially expressed genes Δ*luxS* v. Δ*rbsA*Δ*lsrA*Δ*luxS*

Δ*luxS* vs. Δ*rbsA*Δ*lsrA*Δ*luxS*			
Gene Symbol	**log fold change**	***padj***	**Genome Annotation**
caf1A	-1.978	1.129E-27	putative F1 capsule anchoring protein (plasmid)
clpB	1.212	1.489E-05	Clp ATPase
ddg	-1.056	3.674E-03	lipid A biosynthesis palmitoleoyl acyltransferase
dnaJ	1.037	9.843E-07	molecular chaperone DnaJ
dnaK	1.208	5.107E-08	molecular chaperone DnaK
dps	1.320	2.453E-09	DNA starvation/stationary phase protection protein Dps
hslU	1.256	3.388E-07	ATP-dependent protease ATP-binding subunit HslU
htpG	1.155	3.626E-08	heat shock protein 90
ibpA	1.365	9.097E-10	heat shock protein IbpA
lpp	1.092	8.362E-04	major outer membrane lipoprotein
mrpA	1.240	1.149E-04	mannose-resistant fimbrial protein
psaA	1.167	8.906E-05	pH 6 antigen (antigen 4) (adhesin)
psaE	1.229	5.954E-07	regulatory protein
psaF	1.681	1.075E-08	hypothetical protein YPO1302
rbsA	-5.340	9.187E-50	sugar transport system ATP-binding protein
rpsO	1.004	2.397E-03	30S ribosomal protein S15
sbp1	1.007	4.501E-07	sulfate transporter subunit
sopB	1.039	2.041E-06	plasmid-partitioning protein (plasmid)
yfeE	1.012	4.158E-06	yfeABCD locus regulator
yfiA	1.273	3.626E-08	sigma 54 modulation protein
yopQ	1.251	6.978E-07	Yop targeting protein (plasmid)
ypeI	1.011	7.592E-04	N-acylhomoserine lactone synthase
YPMT1.06c	-1.032	4.392E-04	host specificity protein J (plasmid)
YPMT1.32	-1.109	1.389E-02	putative lipoprotein (plasmid)
YPMT1.33	-1.046	3.563E-02	putative transcriptional regulator (plasmid)
YPMT1.34A	1.312	4.626E-03	hypothetical protein YPMT1.34A (plasmid)
YPMT1.54	1.042	4.984E-05	hypothetical protein YPMT1.54 (plasmid)
YPMT1.55c	1.656	3.316E-07	hypothetical protein YPMT1.55c (plasmid)
YPMT1.66c	-1.108	1.557E-05	putative DNA-binding protein (plasmid)
YPMT1.74	-1.028	2.407E-05	toxin protein (plasmid)
YPMT1.79c	-1.143	1.063E-04	transposase (plasmid)
YPMT1.84	-1.241	3.626E-08	F1 capsule antigen (plasmid)
YPO0412	-2.976	1.326E-23	ABC transporter ATP-binding protein
YPO0415	-1.055	2.288E-03	autoinducer-2 (AI-2) kinase
YPO0623	-1.080	3.810E-09	aminotransferase
YPO0882	1.308	6.455E-06	hypothetical protein YPO0882
YPO1107	1.071	1.109E-05	heat shock protein GrpE
YPO1453	1.394	1.118E-03	hypothetical protein YPO1453
YPO2280	-1.088	5.954E-03	phage-like secreted protein
YPO2481	1.082	1.622E-03	hypothetical protein YPO2481
YPO2483	1.028	8.956E-04	hypothetical protein YPO2483
YPO2973	-1.030	3.159E-02	hypothetical protein YPO2973
YPO3527	1.179	6.828E-08	hypothetical protein YPO3527
YPO4111	1.164	4.700E-09	substrate-binding protein
YPt_06	1.487	1.216E-04	#N/A
yscA	1.306	5.452E-08	hypothetical protein YPCD1.50 (plasmid)

"-" indicates down regulation of expression

Table 10. Significant differentially expressed genes Δ*luxS* v. Δ*rbsA*Δ*lsrA*

Δ*luxS* vs. Δ*rbsA*Δ*lsrA*			
Gene Symbol	**log fold change**	***padj***	**Genome Annotation**
acpD	-1.342	4.649E-10	azoreductase
araC	-1.154	1.641E-04	DNA-binding transcriptional regulator AraC
araF	-2.661	8.900E-21	L-arabinose-binding protein
araG	-1.155	1.639E-04	L-arabinose transporter ATP-binding protein
atpB	1.106	9.760E-06	ATP synthase F0F1 subunit A
atpE	1.153	3.316E-05	ATP synthase F0F1 subunit C
bioD	1.481	5.759E-10	dithiobiotin synthetase
caf1A	-1.017	3.546E-06	putative F1 capsule anchoring protein (plasmid)
ccmA	1.065	1.370E-03	cytochrome c biogenesis protein CcmA
ccmF	1.380	7.286E-04	cytochrome c-type biogenesis protein
ccmG	1.573	3.590E-06	thiol:disulfide interchange protein DsbE
cpxP	1.265	1.390E-06	periplasmic stress adaptor protein CpxP
csrB	1.620	1.478E-15	#N/A
dksA	1.691	6.966E-20	RNA polymerase-binding transcription factor
efp	1.212	1.965E-11	elongation factor P
fis	1.301	9.368E-10	Fis family transcriptional regulator
gpt	1.137	9.956E-07	xanthine-guanine phosphoribosyltransferase
htpG	-1.016	1.550E-05	heat shock protein 90
ibpB	-1.022	1.397E-03	heat shock chaperone IbpB
katY	-1.379	8.379E-10	catalase-peroxidase
luxS	8.238	2.232E-185	S-ribosylhomocysteinase
menF	1.517	7.083E-05	menaquinone-specific isochorismate synthase
metK	1.049	3.830E-05	S-adenosylmethionine synthetase
mrpA	1.158	7.152E-04	mannose-resistant fimbrial protein
napA	1.599	1.888E-08	nitrate reductase catalytic subunit
napB	2.514	1.780E-12	citrate reductase cytochrome c-type subunit
napC	1.877	1.271E-14	cytochrome c-type protein NapC
nirB	1.265	6.975E-05	nitrite reductase
poxB	-1.272	4.177E-06	pyruvate dehydrogenase
ptsG	-1.104	4.625E-07	PTS system glucose-specific transporter subunits IIBC
putP	1.017	2.451E-04	proline permease
qacE	1.518	4.466E-08	quaternary ammonium compound-resistance protein
rbsA	-4.958	3.429E-41	sugar transport system ATP-binding protein
rdgC	1.089	1.244E-07	recombination associated protein
rop	1.207	3.537E-02	putative replication regulatory protein (plasmid)
rplU	1.150	2.717E-08	50S ribosomal protein L21
rpmA	1.138	1.173E-06	50S ribosomal protein L27
rpmB	1.397	1.234E-08	50S ribosomal protein L28
rpmF	1.037	2.051E-04	50S ribosomal protein L32
rpmG	1.140	4.863E-04	50S ribosomal protein L33
rpsF	1.004	3.774E-05	30S ribosomal protein S6
rpsI	1.195	2.087E-04	30S ribosomal protein S9
tig	1.257	5.790E-13	trigger factor
ureC	-1.033	2.253E-03	urease subunit alpha
yaaH	1.353	3.316E-05	hypothetical protein YPO0467
yhjA	1.338	2.611E-06	cytochrome C peroxidase
YPCD1.01	1.193	1.349E-02	putative transposase (plasmid)
YPMT1.01	1.216	9.160E-03	putative transposase (plasmid)
YPMT1.55c	1.370	1.200E-04	hypothetical protein YPMT1.55c (plasmid)
YPMT1.58c	1.082	3.129E-02	transposase (plasmid)

"-" indicates down regulation of expression

Δ*luxS* vs. Δ*rbsA*Δ*lsrA*			
Gene Symbol	**log fold change**	***padj***	**Genome Annotation**
YPO0285	1.454	5.931E-08	hypothetical protein YPO0285
YPO0412	-2.880	2.381E-19	ABC transporter ATP-binding protein
YPO1233	1.028	1.935E-04	prophage repressor protein
YPO1385	1.018	7.426E-04	hypothetical protein YPO1385
YPO1594	1.053	3.349E-08	hypothetical protein YPO1594
YPO1655a	-1.016	5.251E-03	#N/A
YPO1942	1.098	1.850E-08	hypothetical protein YPO1942
YPO1993	-2.788	8.551E-26	dehydrogenase
YPO1994	-2.083	4.194E-15	hypothetical protein YPO1994
YPO1995	-2.186	2.581E-19	hypothetical protein YPO1995
YPO1996	-1.831	3.128E-12	hypothetical protein YPO1996
YPO2096	1.036	8.897E-04	hypothetical protein YPO2096
YPO2148	-1.091	1.507E-04	multidrug resistance protein
YPO2173	-1.044	3.316E-05	response regulator of RpoS
YPO2282	-1.108	1.225E-04	hypothetical protein YPO2282
YPO2563	1.052	1.221E-05	hypothetical protein YPO2563
YPO2855	1.042	1.284E-04	protease
YPO3010	1.002	1.630E-03	hypothetical protein YPO3010
YPO3170	1.390	3.472E-07	nucleotide-binding protein
YPO3617	1.082	3.210E-05	hypothetical protein YPO3617
YPO3655	1.145	7.856E-08	tRNA-dihydrouridine synthase B
YPO3784	1.075	1.293E-07	carbon starvation protein
YPO3839	-1.009	5.934E-05	hypothetical protein YPO3839
YPO3967	1.182	2.405E-05	phosphate transport protein
YPO4111	1.208	1.015E-08	substrate-binding protein
YPPCP1.01	1.041	3.687E-02	putative transposase (plasmid)
YPPCP1.02	1.520	4.676E-03	transposase/IS protein (plasmid)
YPPCP1.06	1.117	4.999E-02	hypothetical protein YPPCP1.06 (plasmid)

Table 11. Significant differentially expressed genes indicating an attenuated phenotype

Attenuated Phenotype			
Gene Symbol	**log fold change**	***padj***	**Genome Annotation**
ampG	-0.539	3.689E-02	muropeptide transporter
apbE	0.428	8.778E-02	thiamine biosynthesis lipoprotein
araC	-1.357	1.658E-07	DNA-binding transcriptional regulator AraC
araF	-2.523	1.644E-21	L-arabinose-binding protein
araG	-1.190	7.187E-06	L-arabinose transporter ATP-binding protein
araH	-0.980	7.083E-03	L-arabinose transporter permease
artI	0.550	9.001E-02	arginine-binding periplasmic protein 1
atpA	0.924	1.689E-07	ATP synthase F0F1 subunit alpha
atpB	0.989	7.309E-06	ATP synthase F0F1 subunit A
atpE	0.747	4.081E-03	ATP synthase F0F1 subunit C
atpF	1.131	1.638E-11	ATP synthase F0F1 subunit B
atpG	0.716	2.493E-03	ATP synthase F0F1 subunit gamma
atpH	1.160	2.716E-08	ATP synthase F0F1 subunit delta
bglA	-0.819	5.101E-05	6-phospho-beta-glucosidase
bioD	2.046	4.452E-23	dithiobiotin synthetase
bioH	-0.856	3.202E-02	biotin biosynthesis protein
bipA	0.703	3.650E-02	GTPase
carA	0.483	8.928E-02	carbamoyl phosphate synthase small subunit
carB	0.501	5.044E-02	carbamoyl phosphate synthase large subunit
ccmA	1.603	2.023E-09	cytochrome c biogenesis protein CcmA
ccmF	1.269	4.300E-04	cytochrome c-type biogenesis protein
ccmG	1.806	6.950E-10	thiol:disulfide interchange protein DsbE

"-" indicates down regulation of expression

Attenuated Phenotype

Gene Symbol	log fold change	*padj*	Genome Annotation
cdd	-0.826	5.998E-04	cytidine deaminase
cfa	-0.588	2.184E-02	cyclopropane fatty acyl phospholipid synthase
clpX	0.379	8.276E-02	ATP-dependent protease ATP-binding subunit ClpX
coaA	0.783	6.523E-04	pantothenate kinase
cpxR	0.843	2.181E-04	DNA-binding transcriptional regulator CpxR
cru	-0.501	9.176E-02	nucleoside permease
csrB	1.514	1.500E-16	#N/A
cybB	-0.766	2.240E-04	cytochrome b561
cyoA	0.625	5.750E-03	cytochrome o ubiquinol oxidase subunit II
cyoB	0.493	2.182E-02	cytochrome O ubiquinol oxidase subunit I
cysA	-0.746	4.379E-03	sulfate/thiosulfate transporter subunit
cysB	-0.536	3.799E-02	transcriptional regulator CysB
cysI	-0.439	8.140E-02	sulfite reductase subunit beta
dcrA	0.574	4.670E-02	#N/A
dksA	1.428	2.045E-17	RNA polymerase-binding transcription factor
dxs	0.571	1.316E-02	1-deoxy-D-xylulose-5-phosphate synthase
efp	0.774	4.888E-06	elongation factor P
fabF	0.585	3.515E-02	3-oxoacyl-ACP synthase
fabG	0.512	7.677E-02	3-ketoacyl-ACP reductase
fdhD	-0.645	7.211E-02	formate dehydrogenase accessory protein
fis	1.516	1.281E-16	Fis family transcriptional regulator
fklB	1.039	8.771E-05	peptidyl-prolyl cis-trans isomerase
fkpA	0.877	4.461E-06	FKBP-type peptidylprolyl isomerase
flgG	-1.123	4.284E-03	flagellar basal body rod protein FlgG
flhB	-0.468	6.673E-02	flagellar biosynthesis protein FlhB
focA	0.680	6.960E-03	formate transporter
gpt	0.626	4.855E-03	xanthine-guanine phosphoribosyltransferase
gyrB	0.403	4.582E-02	DNA gyrase subunit B
hflK	0.513	2.053E-02	FtsH protease regulator HflK
hpaI	-0.855	2.538E-02	2,4-dihydroxyhept-2-ene-1,7-dioic acid aldolase
ibpB	-1.749	5.391E-12	heat shock chaperone IbpB
ihfA	1.044	2.939E-06	integration host factor subunit alpha
katY	-0.958	4.813E-06	catalase-peroxidase
lemA	0.823	1.017E-02	hypothetical protein YPO2732
livJ	-0.527	8.509E-02	branched-chain amino acid-binding protein
lpxA	0.490	3.133E-02	UDP-N-acetylglucosamine acyltransferase
menF	1.119	1.138E-03	menaquinone-specific isochorismate synthase
metK	0.973	8.128E-06	S-adenosylmethionine synthetase
metN	0.649	3.133E-02	DL-methionine transporter ATP-binding protein
mglA	-0.593	1.031E-03	sugar transport ATP-binding protein
mglB	-0.737	1.640E-03	galactose-binding protein
mglC	-0.474	6.673E-02	beta-methylgalactoside transporter inner membrane protein
mltD	0.840	8.830E-06	membrane-bound lytic murein transglycosylase D
mnmC	-0.599	3.875E-02	5-methylaminomethyl-2-thiouridine methyltransferase
mntH	-0.554	2.936E-02	manganese transport protein MntH
moaA	-0.617	8.968E-02	molybdenum cofactor biosynthesis protein A
moaE	-0.780	2.839E-02	molybdopterin guanine dinucleotide biosynthesis protein MoaE

"-" indicates down regulation of expression

Attenuated Phenotype			
Gene Symbol	**log fold change**	***padj***	**Genome Annotation**
modF	-0.595	6.048E-02	molybdenum transport ATP-binding protein ModF
mrcA	0.477	3.980E-02	peptidoglycan synthetase
mtr	-0.579	6.169E-02	tryptophan-specific transport protein
mutM	0.557	6.117E-02	formamidopyrimidine-DNA glycosylase
nanT	-0.617	5.920E-02	sialic acid transporter
napA	2.030	1.281E-16	nitrate reductase catalytic subunit
napB	2.396	3.239E-14	citrate reductase cytochrome c-type subunit
napC	1.776	1.281E-16	cytochrome c-type protein NapC
ndk	0.959	2.077E-03	nucleoside diphosphate kinase
nirB	1.503	1.647E-08	nitrite reductase
nqrC	1.212	6.696E-10	Na(+)-translocating NADH-quinone reductase subunit C
nqrD	1.037	4.787E-06	Na(+)-translocating NADH-quinone reductase subunit D
nrdD	0.880	6.075E-05	anaerobic ribonucleoside triphosphate reductase
nrdE	-0.764	1.985E-03	ribonucleotide-diphosphate reductase subunit alpha
nrdI	-0.911	9.001E-02	ribonucleotide reductase stimulatory protein
ompC	-0.975	4.813E-06	porin
ompH	0.555	2.353E-02	periplasmic chaperone
parA	-0.720	2.873E-03	partitioning protein A (plasmid)
pcnB	0.492	5.203E-02	poly(A) polymerase
pepT	0.655	5.613E-03	peptidase T
pheT	1.105	1.916E-07	phenylalanyl-tRNA synthetase subunit beta
poxB	-0.896	5.498E-04	pyruvate dehydrogenase
ppa	0.652	1.126E-04	inorganic pyrophosphatase
ppiC	0.606	2.762E-02	peptidyl-prolyl cis-trans isomerase C
prfA	0.541	3.906E-02	peptide chain release factor 1
priB	1.057	2.384E-08	primosomal replication protein N
proS	0.862	2.000E-04	prolyl-tRNA synthetase
prsA	0.811	1.878E-04	ribose-phosphate pyrophosphokinase
pstB	-0.351	4.718E-01	phosphate transporter ATP-binding protein
ptsG	-1.100	9.821E-09	PTS system glucose-specific transporter subunits IIBC
ptsH	0.856	6.141E-04	PTS system phosphohistidinoprotein-hexose phosphotransferase subunit Hpr
purF	0.502	1.112E-02	amidophosphoribosyltransferase
putP	0.730	4.463E-03	proline permease
qacE	0.955	2.322E-04	quaternary ammonium compound-resistance protein
rdgC	0.748	7.746E-05	recombination associated protein
recC	-0.384	6.254E-02	exonuclease V subunit gamma
rimM	0.491	3.689E-02	16S rRNA-processing protein RimM
rnfD	-0.528	4.362E-02	electron transport complex protein RnfD
rnhB	0.748	2.111E-03	ribonuclease HII
rodA	0.556	3.689E-02	cell wall shape-determining protein
rph	0.419	6.014E-02	ribonuclease PH
rpiA	0.581	2.330E-02	ribose-5-phosphate isomerase A
rplI	0.803	1.570E-04	50S ribosomal protein L9
rplJ	0.651	1.784E-03	50S ribosomal protein L10
rplK	0.388	9.747E-02	50S ribosomal protein L11
rplM	0.733	2.420E-04	50S ribosomal protein L13
rplU	0.568	6.227E-03	50S ribosomal protein L21

"-" indicates down regulation of expression

Attenuated Phenotype			
Gene Symbol	**Gene Symbol**	**Gene Symbol**	**Gene Symbol**
rpmA	0.921	1.342E-05	50S ribosomal protein L27
rpmB	0.953	3.077E-05	50S ribosomal protein L28
rpmF	0.675	1.056E-02	50S ribosomal protein L32
rpmH	0.662	9.150E-02	50S ribosomal protein L34
rpsF	0.760	5.384E-04	30S ribosomal protein S6
rpsJ	0.723	4.375E-03	30S ribosomal protein S10
rpsP	0.502	7.999E-03	30S ribosomal protein S16
secF	0.614	1.460E-03	preprotein translocase subunit SecF
slyD	0.468	4.545E-02	FKBP-type peptidylprolyl isomerase
smpB	0.550	6.297E-03	SsrA-binding protein
speD	0.731	1.934E-04	S-adenosylmethionine decarboxylase
tap	-0.738	8.814E-02	RepA leader peptide Tap (plasmid)
terX	0.828	2.936E-02	tellurium resistance protein
thiI	0.572	1.763E-02	thiamine biosynthesis protein ThiI
tig	1.090	4.133E-12	trigger factor
tsf	0.538	5.613E-03	elongation factor Ts
tuf	0.572	2.982E-03	elongation factor Tu
ugpB	-0.824	4.206E-02	glycerol-3-phosphate transporter substrate-binding protein
ugpQ	-0.776	2.838E-02	cytoplasmic glycerophosphodiester phosphodiesterase
upp	0.841	2.923E-04	uracil phosphoribosyltransferase
uup	0.579	3.226E-03	ABC transporter ATPase
valS	0.511	3.004E-02	valyl-tRNA synthetase
virG	-0.483	6.644E-02	needle complex outer membrane lipoprotein precursor (plasmid)
yaaH	0.861	4.667E-03	hypothetical protein YPO0467
ybiT	0.526	7.465E-02	ABC transporter ATP-binding protein
yfgA	0.500	4.540E-02	cytoskeletal protein RodZ
yfgD	1.426	1.619E-17	arsenate reductase
yfgL	0.441	3.875E-02	outer membrane protein assembly complex subunit YfgL
yhjA	1.656	4.677E-12	cytochrome C peroxidase
yhjW	0.510	5.750E-03	phosphoethanolamine transferase
yidC	0.664	5.840E-04	inner membrane protein translocase component YidC
YPCD1.01	0.972	2.730E-02	putative transposase (plasmid)
YPCD1.92	-0.736	1.592E-02	hypothetical protein YPCD1.92 (plasmid)
YPMT1.01	1.081	8.760E-03	putative transposase (plasmid)
YPMT1.57c	0.813	4.416E-02	transposase/IS protein (plasmid)
YPMT1.58c	0.801	8.220E-02	transposase (plasmid)
YPMT1.70	-0.725	2.856E-02	putative resolvase (plasmid)
YPO0043	0.448	6.061E-02	hypothetical protein YPO0043
YPO0096	0.735	7.254E-02	transposase/IS protein
YPO0100	0.544	9.533E-02	hypothetical protein YPO0100
YPO0141	-0.593	7.755E-02	hypothetical protein YPO0141
YPO0163	-0.958	7.243E-05	hypothetical protein YPO0163
YPO0285	1.824	2.094E-15	hypothetical protein YPO0285
YPO0302	-0.523	2.313E-02	outer membrane fimbrial usher protein
YPO0327	-0.938	4.072E-02	alcohol dehydrogenase
YPO0400	1.180	1.659E-12	hypothetical protein YPO0400
YPO0507	-0.728	3.123E-02	hypothetical protein YPO0507
YPO0527	0.730	7.547E-02	transposase/IS protein
YPO0749	0.718	6.290E-03	hypothetical protein YPO0749
YPO0875	-0.998	6.606E-02	hypothetical protein YPO0875

"-" indicates down regulation of expression

Attenuated Phenotype			
Gene Symbol	**Gene Symbol**	**Gene Symbol**	**Gene Symbol**
YPO0878	-1.033	6.013E-02	regulatory protein
YPO0900	-0.953	2.984E-03	hemolysin III
YPO0913	-0.548	8.923E-02	5-formyltetrahydrofolate cyclo-ligase
YPO0923	0.799	3.739E-02	transposase/IS protein
YPO0940	-0.482	9.445E-02	hypothetical protein YPO0940
YPO1007	-0.512	4.129E-02	hypothetical protein YPO1007
YPO1074	0.480	3.720E-02	D,D-heptose 1,7-bisphosphate phosphatase
YPO1085	0.718	8.384E-02	transposase/IS protein
YPO1237	-0.531	9.955E-02	transcriptional regulator
YPO1291	-0.779	6.668E-02	carbohydrate kinase
YPO1317	-0.536	9.316E-02	hypothetical protein YPO1317
YPO1385	0.739	6.331E-03	hypothetical protein YPO1385
YPO1426	0.680	9.150E-02	transposase/IS protein
YPO1454	-0.844	3.803E-02	(3R)-hydroxymyristoyl-ACP dehydratase
YPO1567	-0.558	3.792E-02	racemase
YPO1594	0.854	7.198E-07	hypothetical protein YPO1594
YPO1622	0.747	5.129E-02	transposase/IS protein
YPO1637	0.766	1.032E-02	hypothetical protein YPO1637
YPO1648	-0.669	5.432E-03	phosphoanhydride phosphorylase
YPO1655a	-0.618	8.305E-02	#N/A
YPO1683	0.805	2.371E-05	N-acetylmuramoyl-L-alanine amidase
YPO1684	-0.725	6.420E-02	surface protein
YPO1688	0.460	4.775E-02	hypothetical protein YPO1688
YPO1738	0.782	6.701E-03	hypothetical protein YPO1738
YPO1745a	0.792	5.980E-07	#N/A
YPO1751a	-0.494	6.535E-02	PAS/PAC domain-containing protein
YPO1942	1.066	3.542E-10	hypothetical protein YPO1942
YPO1943	0.704	2.877E-02	hypothetical protein YPO1943
YPO1946	0.735	9.342E-03	ABC transporter ATP-binding protein
YPO2025	0.787	2.991E-02	transposase/IS protein
YPO2173	-1.707	7.411E-17	response regulator of RpoS
YPO2177	0.752	5.395E-02	transposase/IS protein
YPO2228	-0.819	2.402E-04	translation initiation factor Sui1
YPO2252	-0.555	8.997E-02	toxin transport protein
YPO2262	0.463	2.831E-02	hypothetical protein YPO2262
YPO2282	-0.779	4.116E-03	hypothetical protein YPO2282
YPO2289	-0.829	6.741E-02	virulence factor
YPO2305	0.499	9.377E-03	hypothetical protein YPO2305
YPO2312	-0.437	7.736E-02	insecticidal toxin complex
YPO2517	0.793	4.234E-02	transposase/IS protein
YPO2559	0.636	4.765E-03	hypothetical protein YPO2559
YPO2560	0.604	6.502E-02	hypothetical protein YPO2560
YPO2563	1.253	5.064E-10	hypothetical protein YPO2563
YPO2568	-0.769	2.132E-02	LacI family transcriptional regulator
YPO2581	0.792	9.308E-02	sugar-binding protein
YPO2642	0.776	6.229E-02	transposase/IS protein
YPO2794	0.691	8.063E-02	hypothetical protein YPO2794
YPO2809	0.738	6.151E-02	transposase/IS protein
YPO2811	-0.873	4.822E-02	hypothetical protein YPO2811
YPO2855	1.286	1.184E-08	protease
YPO2873	0.932	3.792E-02	hypothetical protein YPO2873
YPO2897	-0.444	7.135E-02	DNA-binding transcriptional regulator IscR
YPO2922	0.672	1.107E-02	transglycosylase
YPO2937	0.839	4.687E-02	hypothetical protein YPO2937
YPO2972	-0.828	9.220E-02	lipoprotein

"-" indicates down regulation of expression

Attenuated Phenotype			
Gene Symbol	**log fold change**	***padj***	**Genome Annotation**
YPO3010	0.665	2.838E-02	hypothetical protein YPO3010
YPO3048	1.226	4.067E-11	ABC transporter ATP-binding protein
YPO3170	1.286	7.196E-08	nucleotide-binding protein
YPO3207	0.556	3.126E-02	hypothetical protein YPO3207
YPO3208	0.774	6.308E-02	transposase/IS protein
YPO3257	-0.862	9.445E-02	amino acid ABC transporter substrate-binding protein
YPO3387	-1.042	4.758E-07	iron-sulfur cluster insertion protein ErpA
YPO3445	0.470	4.064E-02	hypothetical protein YPO3445
YPO3518	-1.282	3.111E-06	hypothetical protein YPO3518
YPO3556	0.871	3.468E-02	hypothetical protein YPO3556
YPO3617	1.460	9.233E-12	hypothetical protein YPO3617
YPO3618	1.159	1.646E-05	oxidoreductase
YPO3655	1.004	9.815E-08	tRNA-dihydrouridine synthase B
YPO3708	0.617	5.241E-02	hypothetical protein YPO3708
YPO3773	0.702	7.082E-02	transposase/IS protein
YPO3838	-0.577	5.648E-02	hypothetical protein YPO3838
YPO3839	-0.933	2.347E-05	hypothetical protein YPO3839
YPO3957	-1.099	2.424E-02	hypothetical protein YPO3957
YPO3967	1.042	1.991E-05	phosphate transport protein
YPO4005	-0.540	7.129E-02	hemolysin activator protein
YPPCP1.01	0.965	2.580E-02	putative transposase (plasmid)
YPPCP1.02	1.364	7.389E-03	transposase/IS protein (plasmid)
YPPCP1.06	1.028	4.144E-02	hypothetical protein YPPCP1.06 (plasmid)
YPPCP1.09c	0.627	9.445E-02	hypothetical protein YPPCP1.09c (plasmid)
yscK	-0.617	6.981E-03	type III secretion apparatus component (plasmid)
zntA	-1.087	2.797E-05	zinc/cadmium/mercury/lead-transporting ATPase
zwf	-0.484	4.299E-02	glucose-6-phosphate 1-dehydrogenase

"-" indicates down regulation of expression

Table 12. Significant differentially expressed genes indicating an attenuation masking phenotype

Attenuation Masking Phenotype			
Gene Symbol	**log fold change**	***padj***	**Genome Annotation**
aceB	0.800	5.524E-05	malate synthase
aceE	0.521	3.881E-03	pyruvate dehydrogenase subunit E1
acrA	0.666	1.733E-03	multidrug efflux protein
acrB	0.403	4.907E-02	multidrug efflux protein
astA	0.845	1.588E-02	arginine succinyltransferase
atpI	-1.177	1.491E-06	F0F1 ATP synthase subunit I
bfr	1.458	2.754E-12	bacterioferritin
bioB	-1.023	2.409E-02	biotin synthase
ccmB	-1.061	3.185E-03	heme exporter protein B
ccrB	1.210	1.176E-03	camphor resistance protein CrcB
cheB	-1.447	1.493E-03	chemotaxis-specific methylesterase
clpB3	-1.335	3.572E-03	Clp ATPase
copB	-0.573	1.057E-02	replication protein (plasmid)
cysZ	-0.517	2.265E-02	sulfate transport protein CysZ
ddhC	1.268	2.823E-09	CDP-4-keto-6-deoxy-D-glucose-3-dehydratase
edd	-1.026	1.323E-02	phosphogluconate dehydratase
endA	-0.716	4.795E-02	endonuclease I
fadA	1.289	2.351E-15	3-ketoacyl-CoA thiolase
fadB	1.227	2.486E-16	multifunctional fatty acid oxidation complex subunit alpha
fadE	0.947	1.426E-05	acyl-CoA dehydrogenase
fhuB	-1.008	8.051E-04	iron-hydroxamate transporter permease
fhuC	-1.009	2.086E-02	iron-hydroxamate transporter ATP-binding protein
fldA	-0.772	2.039E-04	flavodoxin FldA
fliG	-1.106	5.370E-03	flagellar motor switch protein G
fliI	-0.954	1.525E-02	flagellum-specific ATP synthase
fliP	-1.016	1.269E-02	flagellar biosynthesis protein FliP
frsA	1.065	2.762E-05	fermentation/respiration switch protein
ftsZ	0.751	1.267E-04	cell division protein FtsZ
fyuA	-1.090	1.381E-04	pesticin/yersiniabactin receptor protein
galF	1.034	6.503E-07	UTP-glucose-1-phosphate uridylyltransferase
glnA	0.420	2.137E-02	glutamine synthetase
gltC	-0.744	8.544E-04	sodium/glutamate symport carrier protein
gptB	1.898	4.143E-07	PTS system mannose-specific transporter subunit IIAB
grxC	1.307	9.375E-04	glutaredoxin 3
hemY	-0.864	5.809E-04	protoheme IX biogenesis protein
hns	-0.435	8.228E-02	global DNA-binding transcriptional dual regulator H-NS
infA	-0.970	3.867E-08	translation initiation factor IF-1
irp4	-0.901	8.090E-02	yersiniabactin biosynthetic protein YbtT
irp5	-1.006	3.447E-02	yersiniabactin siderophore biosynthetic protein
irp8	-1.564	2.299E-04	signal transducer
kdpB	-1.040	2.724E-04	potassium-transporting ATPase subunit B
kdsA	0.856	4.395E-03	2-dehydro-3-deoxyphosphooctonate aldolase
lcrV	0.859	4.507E-09	secreted effector protein (plasmid)
lpxK	-1.005	3.391E-04	tetraacyldisaccharide 4\'-kinase

"-" indicates down regulation of expression

Attenuation Masking Phenotype			
Gene Symbol	**log fold change**	***padj***	**Genome Annotation**
luxS	-8.909	2.075E-242	S-ribosylhomocysteinase
malK	-1.271	4.482E-03	maltose ABC transporter ATP-binding protein
manY	1.035	8.685E-06	PTS system mannose-specific transporter subunit C
manZ	0.766	7.408E-05	PTS system mannose-specific transporter subunit IID
mda66	-0.944	6.764E-06	modulator of drug activity
mltB	-0.497	6.562E-02	murein hydrolase B
modC	-1.309	3.266E-04	molybdate transporter ATP-binding protein
nagB	1.490	7.038E-09	glucosamine-6-phosphate deaminase
nuoE	0.755	1.893E-03	NADH dehydrogenase subunit E
obgE	0.522	1.007E-03	GTPase ObgE
ompF	-0.750	7.310E-05	porin
oxyR	-0.623	1.357E-02	DNA-binding transcriptional regulator OxyR
pdxA	-1.029	4.099E-06	4-hydroxythreonine-4-phosphate dehydrogenase
phoH	1.311	4.351E-13	hypothetical protein YPO1957
pldA	-0.474	2.152E-02	phospholipase A
proB	0.574	4.344E-02	gamma-glutamyl kinase
psaA	1.940	5.220E-17	pH 6 antigen (antigen 4) (adhesin)
psaE	1.169	1.451E-08	regulatory protein
psaF	1.510	7.281E-10	hypothetical protein YPO1302
psiF	1.127	1.027E-04	starvation-inducible protein
purK	-1.019	1.366E-02	phosphoribosylaminoimidazole carboxylase ATPase subunit
rffG	-1.002	1.277E-05	dTDP-D-glucose-4,6-dehydratase
rhaB	-1.145	4.504E-03	rhamnulokinase
rimI	-0.604	8.919E-02	ribosomal-protein-alanine N-acetyltransferase
rnpB	-1.102	4.993E-03	#N/A
rplA	-0.470	2.260E-02	50S ribosomal protein L1
rpsH	1.148	6.963E-03	30S ribosomal protein S8
rpsO	1.100	1.936E-05	30S ribosomal protein S15
rpsU	-0.369	6.339E-02	30S ribosomal protein S21
sopB	1.164	7.753E-11	plasmid-partitioning protein (plasmid)
ssuC	-1.108	9.657E-03	aliphatic sulfonates transporter permease
sucC	0.686	1.606E-03	succinyl-CoA synthetase subunit beta
surE	-1.088	1.454E-04	stationary phase survival protein SurE
thiD	-1.170	3.881E-03	phosphomethylpyrimidine kinase
tktA	0.715	8.165E-04	transketolase
treC	1.066	5.074E-04	trehalose-6-phosphate hydrolase
trpD	-1.272	3.242E-03	anthranilate phosphoribosyltransferase
trpH	-1.283	3.653E-06	hypothetical protein YPO2211
uppP	-1.028	7.234E-03	undecaprenyl pyrophosphate phosphatase
wrbA	0.624	1.180E-03	TrpR binding protein WrbA
yfcA	-1.301	7.558E-07	hypothetical protein YPO2753
yfeN	-0.386	4.114E-02	hypothetical protein YPO3163
yfiA	1.505	2.852E-15	sigma 54 modulation protein
yggE	1.140	8.361E-07	hypothetical protein YPO0917
yicN	1.057	3.965E-03	hypothetical protein YPO2654

"-" indicates down regulation of expression

Attenuation Masking Phenotype			
Gene Symbol	**log fold change**	***padj***	**Genome Annotation**
ylpB	0.782	2.233E-06	needle complex inner membrane lipoprotein (plasmid)
ymoA	1.183	5.036E-07	hemolysin expression-modulating protein
ynbB	-1.107	6.578E-03	phosphatidate cytidylyltransferase
yopB	0.540	1.116E-02	secreted effector protein (plasmid)
yopD	0.838	1.233E-06	secreted effector protein (plasmid)
yopH	1.041	5.446E-10	putative secreted protein-tyrosine phosphatase (plasmid)
yopJ	1.135	2.084E-12	targeted effector protein (plasmid)
yopM	1.130	1.306E-09	secreted effector protein (plasmid)
yopO	1.130	1.306E-09	#N/A
yopR	1.566	6.587E-14	secreted protein (plasmid)
yopT	0.759	2.043E-05	Yop targeted effector (plasmid)
YPCD1.07	1.273	6.864E-13	hypothetical protein YPCD1.07 (plasmid)
YPCD1.91n	1.139	4.694E-06	hypothetical protein YPCD1.91n (plasmid)
YPCD1.94	0.675	1.512E-04	putative transposase (plasmid)
YPMT1.07c	-1.157	2.030E-02	putative phage tail protein (plasmid)
YPMT1.13c	-1.027	4.343E-02	hypothetical protein YPMT1.13c (plasmid)
YPMT1.18c	-1.057	9.937E-03	hypothetical protein YPMT1.18c (plasmid)
YPMT1.24c	-1.162	1.473E-02	hypothetical protein YPMT1.24c (plasmid)
YPMT1.26c	-1.379	7.604E-04	hypothetical protein YPMT1.26c (plasmid)
YPMT1.28c	-1.170	1.932E-02	hypothetical protein YPMT1.28c (plasmid)
YPMT1.34A	1.819	3.788E-07	hypothetical protein YPMT1.34A (plasmid)
YPMT1.43c	1.158	6.348E-04	hypothetical protein YPMT1.43c (plasmid)
YPMT1.60c	-1.417	3.166E-03	hypothetical protein YPMT1.60c (plasmid)
YPMT1.61c	-1.600	4.911E-04	antirestriction protein (plasmid)
YPMT1.63c	-1.067	2.817E-02	hypothetical protein YPMT1.63c (plasmid)
YPMT1.76A	-1.165	1.301E-02	hypothetical protein YPMT1.76A (plasmid)
YPO0001	-0.550	4.584E-03	flavodoxin
YPO0013a	0.745	2.724E-04	hypothetical protein YPO0013a
YPO0102	-1.061	6.111E-03	hypothetical protein YPO0102
YPO0237	1.054	2.625E-03	hypothetical protein YPO0237
YPO0267	-1.125	1.955E-02	type III secretion system ATPase
YPO0352	-1.328	1.384E-10	lipoprotein
YPO0368	-0.961	1.634E-04	hypothetical protein YPO0368
YPO0403	-1.194	1.080E-02	PTS system fructose family transporter subunit IIB
YPO0435	-1.488	4.756E-07	Na+ dependent nucleoside transporter family protein
YPO0516	1.003	7.148E-07	hypothetical protein YPO0516
YPO0536	-1.046	7.823E-03	hypothetical protein YPO0536
YPO0622	1.056	2.414E-02	hypothetical protein YPO0622
YPO0647	-0.691	5.458E-03	glycerol-3-phosphate acyltransferase PlsY
YPO0819	1.135	1.239E-07	carbonic anhydrase
YPO0840	-1.108	1.215E-02	hypothetical protein YPO0840
YPO0862	1.333	1.498E-06	hypothetical protein YPO0862
YPO0899	-0.404	6.623E-02	hypothetical protein YPO0899
YPO0904	1.673	1.265E-14	hypothetical protein YPO0904
YPO0936	-1.281	1.080E-06	hypothetical protein YPO0936
YPO0970	-1.025	2.319E-02	hypothetical protein YPO0970
YPO0973	-1.216	9.298E-04	hypothetical protein YPO0973
YPO0976	-1.070	2.948E-02	hypothetical protein YPO0976
YPO0978	-1.544	7.477E-04	hypothetical protein YPO0978
YPO0982	1.198	2.095E-03	lipoprotein
YPO0988	-0.912	3.494E-02	hypothetical protein YPO0988

"-" indicates down regulation of expression

Attenuation Masking Phenotype			
Gene Symbol	**log fold change**	***padj***	**Genome Annotation**
YPO1011	0.929	2.483E-04	TonB-dependent outer membrane receptor
YPO1033	0.570	5.333E-03	hypothetical protein YPO1033
YPO1061	1.116	2.083E-03	hypothetical protein YPO1061
YPO1064a	-0.961	4.180E-03	hypothetical protein YPO1064a
YPO1090	-1.357	7.464E-04	prophage DNA primase
YPO1097	1.064	3.381E-06	hypothetical protein YPO1097
YPO1158	-1.112	9.422E-05	hypothetical protein YPO1158
YPO1244	-1.212	1.301E-02	hypothetical protein YPO1244
YPO1277	0.620	5.264E-03	cobalamin synthesis protein
YPO1288	-1.151	1.007E-02	D-isomer specific 2-hydroxyacid dehydrogenase family protein
YPO1315	0.876	3.682E-06	hydrolase
YPO1348	-1.062	1.015E-02	hypothetical protein YPO1348
YPO1423	-1.048	1.768E-02	hypothetical protein YPO1423
YPO1446	1.390	3.883E-05	acylphosphatase
YPO1453	1.750	1.560E-07	hypothetical protein YPO1453
YPO1465	-1.023	3.849E-02	hypothetical protein YPO1465
YPO1469	-1.209	1.468E-02	hypothetical protein YPO1469
YPO1470	-1.010	6.350E-03	hypothetical protein YPO1470
YPO1471	-1.386	4.400E-03	ATPase subunit of ATP-dependent protease
YPO1474	1.041	2.192E-03	hypothetical protein YPO1474
YPO1483	-1.067	3.056E-02	hypothetical protein YPO1483
YPO1496	0.933	5.728E-05	heme-binding protein
YPO1534	-1.070	1.892E-02	iron-siderophore transporter membrane permease
YPO1568	0.936	2.801E-05	hypothetical protein YPO1568
YPO1649	0.461	2.368E-02	hypothetical protein YPO1649
YPO1669	1.284	1.723E-03	hypothetical protein YPO1669
YPO1694	1.235	2.165E-07	hypothetical protein YPO1694
YPO1707	1.279	2.921E-04	fimbrial protein
YPO1747	-1.022	6.398E-06	hypothetical protein YPO1747
YPO1788	1.529	2.813E-07	acyl carrier protein
YPO1818	-1.012	2.086E-02	hypothetical protein YPO1818
YPO1975	1.030	3.036E-03	hypothetical protein YPO1975
YPO2031	-1.083	2.365E-02	binding-protein-dependent transporter membrane protein
YPO2051	0.921	2.724E-04	hypothetical protein YPO2051
YPO2187	-0.666	6.059E-03	dsDNA-mimic protein
YPO2277	0.602	8.760E-02	hypothetical protein YPO2277
YPO2331	0.957	1.735E-03	lipoprotein
YPO2379	0.610	6.564E-03	N-ethylmaleimide reductase
YPO2385	0.827	1.477E-04	hypothetical protein YPO2385
YPO2653	1.045	3.428E-04	hypothetical protein YPO2653
YPO2683	1.061	1.530E-02	hypothetical protein YPO2683
YPO2792	1.479	6.089E-04	hypothetical protein YPO2792
YPO2806	1.367	1.918E-08	aldo/keto reductase
YPO2822	1.165	1.557E-03	hypothetical protein YPO2822
YPO2842	-1.001	3.388E-02	ABC transporter permease
YPO2864	1.153	2.158E-02	hypothetical protein YPO2864
YPO2923	1.283	2.408E-04	tRNA-specific adenosine deaminase
YPO3137	1.401	1.941E-09	hypothetical protein YPO3137
YPO3150	0.668	1.421E-03	queuosine biosynthesis protein QueC
YPO3348	1.575	5.950E-11	transcriptional regulator
YPO3476	-1.206	5.470E-07	acetyltransferase

"-" indicates down regulation of expression

Attenuation Masking Phenotype			
Gene Symbol	**log fold change**	***padj***	**Genome Annotation**
YPO3498	-0.858	5.916E-05	hypothetical protein YPO3498
YPO3549	-1.327	2.832E-07	hypothetical protein YPO3549
YPO3613	-1.199	1.079E-02	Rhs accessory genetic element
YPO3699	-0.370	2.781E-02	hypothetical protein YPO3699
YPO3799	-1.055	2.157E-02	hypothetical protein YPO3799
YPO3801	-1.013	4.571E-02	hypothetical protein YPO3801
YPO3828	0.605	1.651E-02	hypothetical protein YPO3828
YPO3885	1.114	1.435E-03	hypothetical protein YPO3885
YPO3902	-1.108	5.710E-03	magnesium chelatase family protein
YPO3904	1.243	1.306E-05	transcriptional regulator HdfR
YPO3956	0.723	2.100E-02	hypothetical protein YPO3956
YPO3963	-1.316	4.467E-03	sugar transport system permease
YPO3965	-0.549	4.701E-02	hybrid two-component system regulatory protein
yscA	1.367	4.912E-12	hypothetical protein YPCD1.50 (plasmid)
yscB	0.525	2.281E-02	type III secretion apparatus component (plasmid)
yscC	0.440	1.128E-02	outer membrane secretin precursor (plasmid)
yscD	0.836	5.383E-07	virulence protein (plasmid)
yscG	1.139	1.201E-09	type III secretion apparatus component (plasmid)
yscL	1.139	1.201E-09	type III secretion system protein (plasmid)
yscO	0.450	9.335E-03	type III secretion apparatus component (plasmid)
yscP	0.484	3.715E-03	type III secretion apparatus component (plasmid)
yscR	0.593	6.103E-05	type III secretion system protein (plasmid)
yscS	0.521	4.370E-03	needle complex export protein (plasmid)
yscT	0.508	1.843E-02	needle complex export protein (plasmid)
yscU	0.653	9.754E-05	needle complex export protein (plasmid)
yscV	0.506	9.350E-04	low calcium response protein D (plasmid)
yscX	0.434	1.137E-01	hypothetical protein YPCD1.36c (plasmid)
yscY	-0.687	1.140E-01	hypothetical protein YPCD1.35c (plasmid)
zipA	0.682	1.141E-01	cell division protein ZipA

"-" indicates down regulation of expression

Table 13. Significant differentially expressed genes in response to autoinducer-2 dysregulation

Autoinducer-2 dysregulation			
Gene Symbol	**log fold change**	***padj***	**Genome Annotation**
aceA	1.039	1.698E-07	isocitrate lyase
aceK	0.527	4.180E-03	bifunctional isocitrate dehydrogenase kinase/phosphatase protein
acs	0.505	3.935E-03	acetyl-CoA synthetase
agaZ	-0.786	9.286E-03	tagatose 6-phosphate kinase
ahpC	0.604	1.439E-03	alkyl hydroperoxide reductase
apt	-1.163	2.762E-05	adenine phosphoribosyltransferase
aroL	-0.703	1.390E-03	shikimate kinase II
atpD	0.562	2.084E-03	ATP synthase F0F1 subunit beta
bioF	-0.962	2.930E-02	8-amino-7-oxononanoate synthase
btuC	0.940	9.710E-05	vtamin B12-transporter permease
btuD	1.491	1.040E-08	vitamin B12-transporter ATPase
cafA	0.504	1.861E-02	ribonuclease G
clpP	0.941	6.145E-05	ATP-dependent Clp protease proteolytic subunit
cls	-1.077	1.771E-08	cardiolipin synthetase
creA	0.584	2.217E-03	hypothetical protein YPO0457
cyaB	0.762	8.966E-05	adenylate cyclase
cydA	0.666	3.753E-04	cytochrome D ubiquinol oxidase subunit I
cydB	0.438	4.782E-02	cytochrome D ubiquinol oxidase subunit II
cyoC	0.496	4.250E-03	cytochrome o ubiquinol oxidase subunit III
cysK	-0.502	5.519E-03	cysteine synthase A
cysM	-0.649	3.036E-03	cysteine synthase B
cysN	-0.585	9.623E-02	sulfate adenylyltransferase subunit 1
cysT	-0.841	6.566E-04	sulfate/thiosulfate transporter subunit
cysW	-0.994	1.811E-04	sulfate/thiosulfate transporter permease
dadA	-1.291	8.502E-15	D-amino acid dehydrogenase small subunit
dapF	-1.145	1.024E-05	diaminopimelate epimerase
dcrB	0.820	1.027E-04	hypothetical protein YPO3823
ddhD	0.905	1.035E-02	CDP-6-deoxy-delta-3,4-glucoseen reductase
deoC	-0.574	1.704E-02	deoxyribose-phosphate aldolase
dsbB	-1.182	2.790E-09	disulfide bond formation protein B
elaB	1.243	7.757E-05	hypothetical protein YPO2531
engA	0.376	4.836E-02	GTP-binding protein EngA
fadJ	0.538	1.017E-03	multifunctional fatty acid oxidation complex subunit alpha
flgJ	-0.814	4.296E-02	peptidoglycan hydrolase
fliH	-0.767	5.874E-02	flagellar assembly protein H
fliN	-0.829	9.382E-02	flagellar switch protein
frdB	0.721	2.489E-03	fumarate reductase iron-sulfur subunit
ftsW	0.557	1.366E-02	cell division protein FtsW
gcsH	0.540	4.493E-02	glycine cleavage system protein H
gdhA	-0.441	3.749E-02	glutamate dehydrogenase
glnB	0.404	5.938E-02	nitrogen regulatory protein P-II 1
glnH	0.295	9.752E-02	glutamine ABC transporter substrate-binding protein
glnP	1.683	2.126E-13	glutamine ABC transporter permease
glnQ	1.449	1.671E-12	glutamine ABC transporter ATP-binding protein
glyA	0.490	3.028E-02	serine hydroxymethyltransferase
gnd	0.418	1.219E-02	6-phosphogluconate dehydrogenase

"-" indicates down regulation of expression

Autoinducer-2 dysregulation			
Gene Symbol	**log fold change**	***padj***	**Genome Annotation**
gpmA	0.712	2.995E-05	phosphoglyceromutase
grxA	0.798	2.991E-06	glutaredoxin
gsrA	0.722	2.534E-05	serine endoprotease
guaA	0.681	1.353E-02	GMP synthase
hcaT	-0.973	1.249E-03	3-phenylpropionic acid transporter
hflB	0.622	1.103E-04	ATP-dependent metalloprotease
hflC	0.414	4.702E-02	FtsH protease regulator HflC
hisJ	0.416	1.598E-02	histidine-binding periplasmic protein
hmwA	-0.396	9.433E-02	adhesin
hofQ	-0.307	9.582E-02	porin
hpaX	-1.041	2.193E-04	4-hydroxyphenylacetate permease
hslR	-0.674	1.098E-02	heat shock protein 15
hupA	0.481	6.079E-02	transcriptional regulator HU subunit alpha
icdA	0.759	1.811E-04	isocitrate dehydrogenase
ihfB	1.114	2.313E-08	integration host factor subunit beta
infB	0.418	1.804E-02	translation initiation factor IF-2
infC	1.767	2.558E-12	translation initiation factor IF-3
irp1	-1.719	9.119E-07	yersiniabactin biosynthetic protein
irp2	-1.081	7.403E-04	yersiniabactin biosynthetic protein
irp3	-1.375	4.403E-03	yersiniabactin biosynthetic protein YbtU
irp4	-0.901	8.090E-02	yersiniabactin biosynthetic protein YbtT
irp5	-1.006	3.447E-02	yersiniabactin siderophore biosynthetic protein
irp6	-0.873	4.437E-02	lipoprotein inner membrane ABC transporter
irp7	-0.961	2.817E-02	ABC transporter permease
irp8	-1.564	2.299E-04	signal transducer
ispG	0.534	1.817E-02	4-hydroxy-3-methylbut-2-en-1-yl diphosphate synthase
katA	0.415	3.099E-02	catalase
ksgA	1.241	1.903E-05	dimethyladenosine transferase
lcrG	0.835	6.349E-09	low calcium response protein G (plasmid)
livG	-0.723	5.525E-02	leucine/isoleucine/valine transporter ATP-binding protein
livM	-0.630	7.328E-03	leucine/isoleucine/valine transporter permease
lplA	1.579	4.750E-24	lipoate-protein ligase A
lpxC	0.521	1.740E-03	UDP-3-O
mipB	-1.088	4.479E-04	fructose-6-phosphate aldolase
mobA	0.976	8.764E-07	molybdopterin-guanine dinucleotide biosynthesis protein MobA
mobB	0.773	9.873E-04	molybdopterin-guanine dinucleotide biosynthesis protein B
mscL	0.612	8.228E-04	large-conductance mechanosensitive channel
mtta1	0.641	6.114E-04	#N/A
murB	0.449	1.560E-02	UDP-N-acetylenolpyruvoylglucosamine reductase
nagE	1.109	4.581E-08	PTS system N-acetylglucosamine-specific transporter subunit IIABC
nhaB	-1.284	1.417E-11	sodium/proton antiporter
nlpC	0.718	5.298E-03	lipoprotein
nqrF	0.540	2.765E-02	Na(+)-translocating NADH-quinone reductase subunit F

"-" indicates down regulation of expression

Autoinducer-2 dysregulation			
Gene Symbol	**log fold change**	***padj***	**Genome Annotation**
nudG	-1.433	5.901E-05	pyrimidine (deoxy)nucleoside triphosphate pyrophosphohydrolase
ompR	0.409	2.888E-02	osmolarity response regulator
ompW	0.433	7.787E-02	outer membrane protein W
ompX	1.014	6.365E-09	outer membrane protein X
oppD	-0.802	5.012E-05	oligopeptide transporter ATP-binding component
oppF	-1.172	1.010E-06	oligopeptide transport ATP-binding protein
pabB	-0.624	1.598E-02	para-aminobenzoate synthase component I
pal	0.744	3.316E-04	peptidoglycan-associated outer membrane lipoprotein
pbpG	1.073	1.060E-04	D-alanyl-D-alanine endopeptidase
pepD	0.368	3.133E-02	aminoacyl-histidine dipeptidase
pfkA	1.046	3.269E-05	6-phosphofructokinase
pheS	0.805	3.318E-06	phenylalanyl-tRNA synthetase subunit alpha
phrB	-0.918	8.188E-04	deoxyribodipyrimidine photolyase
pla	0.579	5.297E-02	outer membrane protease (plasmid)
pmrF	1.517	8.834E-21	undecaprenyl phosphate 4-deoxy-4-formamido-L-arabinose transferase
pncA	-1.043	1.677E-05	nicotinamidase/pyrazinamidase
prc	0.550	6.102E-04	carboxy-terminal protease
psaC	-0.724	2.875E-03	outer membrane usher protein PsaC
pspF	-0.731	7.076E-04	phage shock protein operon transcriptional activator
pspG	-1.692	1.630E-05	phage shock protein G
pst	1.093	7.453E-03	pesticin (plasmid)
ptsI	0.952	2.219E-05	phosphoenolpyruvate-protein phosphotransferase
rhaA	-1.239	4.257E-03	L-rhamnose isomerase
ribE	0.600	8.188E-04	riboflavin synthase subunit alpha
ribH	0.429	1.892E-02	6,7-dimethyl-8-ribityllumazine synthase
rlpA	0.403	8.737E-02	rare lipoprotein A
rnk	0.783	5.062E-04	nucleoside diphosphate kinase regulator
rplS	1.211	5.847E-05	50S ribosomal protein L19
rplT	1.757	5.262E-05	50S ribosomal protein L20
rpoN	0.776	2.658E-05	RNA polymerase factor sigma-54
rpoZ	1.111	2.488E-04	DNA-directed RNA polymerase subunit omega
rpsD	0.856	2.154E-03	30S ribosomal protein S4
rth	-0.491	2.227E-02	undecaprenyl pyrophosphate synthase
rumB	-0.905	9.024E-03	23S rRNA methyluridine methyltransferase
selD	-1.626	1.057E-18	selenophosphate synthetase
sodB	0.914	7.837E-07	superoxide dismutase
spf	1.185	8.773E-03	#N/A
sppA	-0.571	1.981E-03	protease 4
ssuB	-0.733	7.285E-02	aliphatic sulfonates transporter ATP-binding protein
surA	0.427	3.363E-02	peptidyl-prolyl cis-trans isomerase SurA
tam	1.299	6.118E-08	trans-aconitate 2-methyltransferase
tatE	-0.487	7.032E-02	twin-arginine translocation protein TatA
tauC	-0.945	5.332E-02	taurine transporter subunit
tauD	-0.644	4.019E-02	taurine dioxygenase
thrS	1.075	1.749E-05	threonyl-tRNA synthetase
tonB	-1.690	9.903E-18	transport protein TonB
topB	-1.048	3.311E-11	DNA topoisomerase III

"-" indicates down regulation of expression

Autoinducer-2 dysregulation			
Gene Symbol	**log fold change**	***padj***	**Genome Annotation**
tpiA	1.390	4.471E-08	triosephosphate isomerase
tppB	-0.544	4.592E-03	tripeptide transporter permease
trkH	-0.523	7.234E-03	potassium transporter
trmB	0.487	6.682E-02	tRNA (guanine-N(7)-)-methyltransferase
ubiH	-0.656	5.077E-03	2-octaprenyl-6-methoxyphenyl hydroxylase
ubiX	-0.368	8.126E-02	3-octaprenyl-4-hydroxybenzoate carboxy-lyase
ugpC	-0.795	4.740E-03	glycerol-3-phosphate transporter ATP-binding protein
uvrB	-0.309	9.692E-02	excinuclease ABC subunit B
wbyH	0.943	5.736E-06	hypothetical protein YPO3111
wbyK	0.609	7.387E-02	mannosyltransferase
xthA	-1.281	1.490E-09	exonuclease III
yapC	-0.928	1.727E-04	autotransporter protein
ybeX	0.385	4.944E-02	hypothetical protein YPO2617
ybjR	0.441	4.360E-02	#N/A
ydeN	1.081	2.393E-11	sulfatase
yebY	0.576	1.313E-02	hypothetical protein YPO1786
yecS	-0.780	2.231E-03	amino-acid ABC transporter permease
yeiB	-0.568	2.220E-02	hypothetical protein YPO1506
yfeA	1.965	3.266E-40	substrate-binding protein
yfeB	1.915	8.948E-35	ATP-binding transport protein
yfeC	1.357	7.281E-10	chelated iron transport system membrane protein
yfeD	1.188	4.872E-10	chelated iron transport system membrane protein
yfeE	2.343	2.143E-42	yfeABCD locus regulator
ygeD	-0.995	1.944E-03	lysophospholipid transporter LplT
yhbG	0.597	1.731E-03	ABC transporter ATP-binding protein YhbG
yidE	-0.648	1.498E-02	hypothetical protein YPO4083
ylaC	0.819	9.805E-07	hypothetical protein YPO1652
ypeI	2.192	5.649E-23	N-acylhomoserine lactone synthase
ypeR	2.140	1.284E-24	quorum-sensing transcriptional activator YpeR
YPMT1.03c	-0.701	2.408E-02	tail fiber assembly protein G (plasmid)
YPMT1.11c	-1.623	3.547E-05	hypothetical protein YPMT1.11c (plasmid)
YPMT1.22c	-1.388	2.450E-03	hypothetical protein YPMT1.22c (plasmid)
YPMT1.32	-1.183	5.539E-04	putative lipoprotein (plasmid)
YPMT1.33	-1.170	1.490E-03	putative transcriptional regulator (plasmid)
YPMT1.35c	-1.517	3.050E-05	hypothetical protein YPMT1.35c (plasmid)
YPMT1.45c	1.201	1.329E-02	hypothetical protein YPMT1.45c (plasmid)
YPMT1.46c	0.874	7.318E-02	hypothetical protein YPMT1.46c (plasmid)
YPMT1.59c	-1.801	5.220E-05	putative DNA-binding protein (plasmid)
YPMT1.71	-1.005	1.118E-06	hypothetical protein YPMT1.71 (plasmid)
YPMT1.72c	-0.812	1.722E-04	hypothetical protein YPMT1.72c (plasmid)
YPMT1.75c	-1.164	1.168E-02	reverse transcriptase (plasmid)
YPO0007	0.619	8.306E-04	D-ribose pyranase
YPO0014	0.635	1.282E-03	serine/threonine protein kinase
YPO0027	0.527	1.181E-02	phosphatase
YPO0032	-0.837	1.710E-06	hypothetical protein YPO0032
YPO0034	-0.900	1.234E-02	membrane permease
YPO0128	-1.050	2.485E-03	gluconate periplasmic binding protein
YPO0147	-1.185	4.057E-04	hypothetical protein YPO0147
YPO0148	-1.459	5.842E-04	hypothetical protein YPO0148
YPO0196	0.757	3.686E-04	DNA-binding protein

"-" indicates down regulation of expression

Autoinducer-2 dysregulation			
Gene Symbol	**log fold change**	***padj***	**Genome Annotation**
YPO0199	0.890	1.630E-08	sulfur transfer complex subunit TusB
YPO0391	0.700	1.371E-03	modification methylase
YPO0392	1.050	3.453E-04	hypothetical protein YPO0392
YPO0397	-1.125	8.544E-04	hypothetical protein YPO0397
YPO0405	-0.950	1.296E-03	phosphoenolpyruvate-protein phosphotransferase
YPO0498	0.957	7.921E-07	hypothetical protein YPO0498
YPO0502	0.786	1.378E-02	hypothetical protein YPO0502
YPO0599	-0.565	3.669E-03	adhesin
YPO0651	0.673	1.539E-04	signal transduction protein
YPO0659	-0.677	7.753E-02	hypothetical protein YPO0659
YPO0806	1.044	9.481E-03	prepilin peptidase
YPO0820	-0.887	7.479E-02	hypothetical protein YPO0820
YPO0912	0.824	1.862E-05	Z-ring-associated protein
YPO0919	0.635	3.617E-03	hypothetical protein YPO0919
YPO1001	-0.813	3.373E-03	integral membrane efflux protein
YPO1052	0.468	1.981E-03	outer membrane protein assembly factor YaeT
YPO1064	0.881	2.246E-04	Rho-binding antiterminator
YPO1072	1.003	1.913E-04	DL-methionine transporter permease
YPO1091	-0.689	1.366E-02	prophage protein
YPO1179	0.767	1.488E-03	hypothetical protein YPO1179
YPO1201	-0.359	9.032E-02	amino acid decarboxylase
YPO1255	0.797	9.842E-05	hypothetical protein YPO1255
YPO1257	0.747	6.594E-03	hypothetical protein YPO1257
YPO1316	-0.628	3.200E-02	iron/ascorbate oxidoreductase family protein
YPO1318	-1.197	5.867E-04	ABC transporter ATP-binding protein
YPO1364	0.486	3.049E-02	macrolide transporter subunit MacA
YPO1401	0.701	3.186E-03	hypothetical protein YPO1401
YPO1450d	-0.522	6.181E-02	hypothetical protein YPO1450d
YPO1490	0.751	3.592E-03	hypothetical protein YPO1490
YPO1492	0.759	2.158E-02	hypothetical protein YPO1492
YPO1500	1.277	1.320E-04	hypothetical protein YPO1500
YPO1575	0.905	1.213E-05	hypothetical protein YPO1575
YPO1614	-0.779	7.901E-02	hypothetical protein YPO1614
YPO1643	0.731	8.014E-04	hypothetical protein YPO1643
YPO1693	0.414	5.957E-02	hypothetical protein YPO1693
YPO1718	1.039	8.337E-09	hypothetical protein YPO1718
YPO1736	1.603	2.242E-14	hypothetical protein YPO1736
YPO1887	1.124	2.068E-03	hypothetical protein YPO1887
YPO1918	-0.611	3.565E-02	pili assembly chaperone
YPO1925	0.761	8.775E-06	two-component response regulator
YPO1931	0.698	1.312E-02	hypothetical protein YPO1931
YPO1933	-0.606	4.856E-02	dicarboxylic acid hydrolase
YPO1989	0.527	2.042E-02	hypothetical protein YPO1989
YPO2039	0.942	1.775E-04	hypothetical protein YPO2039
YPO2055	0.695	4.619E-04	hypothetical protein YPO2055
YPO2068	-0.939	1.886E-03	hypothetical protein YPO2068
YPO2082	0.993	2.731E-04	hypothetical protein YPO2082
YPO2095	1.793	7.315E-07	hypothetical protein YPO2095
YPO2123	-0.884	5.715E-02	phage minor tail protein
YPO2126	0.352	8.025E-02	hypothetical protein YPO2126
YPO2127	0.412	9.893E-02	phage-like membrane protein
YPO2128	0.994	7.858E-04	phage-like lipoprotein

"-" indicates down regulation of expression

Autoinducer-2 dysregulation			
Gene Symbol	**log fold change**	***padj***	**Genome Annotation**
YPO2133	-0.639	2.959E-02	hypothetical protein YPO2133
YPO2138	-1.656	3.282E-05	aminotransferase
YPO2139	-1.793	1.201E-04	hypothetical protein YPO2139
YPO2140	-1.338	3.514E-12	hypothetical protein YPO2140
YPO2145	-0.968	2.787E-08	SpoVR family protein
YPO2149	-0.985	5.412E-09	hypothetical protein YPO2149
YPO2150	-0.546	9.405E-02	LysR family transcriptional regulator
YPO2151	-0.941	8.150E-05	hypothetical protein YPO2151
YPO2152	-1.018	1.354E-07	hypothetical protein YPO2152
YPO2155	-0.626	3.444E-04	hypothetical protein YPO2155
YPO2156	-0.871	6.446E-07	hypothetical protein YPO2156
YPO2163	-1.906	8.821E-15	hypothetical protein YPO2163
YPO2169	-2.744	3.420E-16	LysR family transcriptional regulator
YPO2171	-0.877	3.413E-07	formyltetrahydrofolate deformylase
YPO2172	-1.767	9.037E-17	hypothetical protein YPO2172
YPO2189	-0.700	3.047E-02	hypothetical protein YPO2189
YPO2192	-1.422	6.844E-08	hypothetical protein YPO2192
YPO2202	0.907	1.163E-05	lipoprotein
YPO2231	1.581	1.022E-04	hypothetical protein YPO2231
YPO2246	-0.863	1.045E-02	Na(+)-translocating NADH-quinone reductase subunit E
YPO2271	0.877	2.944E-04	hypothetical protein YPO2271
YPO2272	0.850	6.710E-04	hypothetical protein YPO2272
YPO2321	-0.538	6.245E-02	hypothetical protein YPO2321
YPO2398	1.406	9.116E-17	murein L,D-transpeptidase
YPO2399	0.816	3.659E-03	cysteine desufuration protein SufE
YPO2406	0.979	7.146E-06	hypothetical protein YPO2406
YPO2407	1.191	1.702E-10	hypothetical protein YPO2407
YPO2408	1.217	1.490E-09	hypothetical protein YPO2408
YPO2410	0.963	1.259E-05	hypothetical protein YPO2410
YPO2419	1.449	3.844E-15	hypothetical protein YPO2419
YPO2420	1.865	8.667E-32	bifunctional UDP-glucuronic acid decarboxylase/UDP-4-amino-4-deoxy-L-arabinose formyltransferase
YPO2422	1.270	4.132E-15	UDP-4-amino-4-deoxy-L-arabinose--oxoglutarate aminotransferase
YPO2426	1.728	4.474E-18	hypothetical protein YPO2426
YPO2444	0.986	2.341E-06	hypothetical protein YPO2444
YPO2446	1.382	3.325E-08	2-deoxyglucose-6-phosphatase
YPO2449	1.640	2.667E-30	LuxR family transcriptional regulator
YPO2451	1.017	2.790E-09	hypothetical protein YPO2451
YPO2452	0.643	1.952E-02	hypothetical protein YPO2452
YPO2455	1.222	6.262E-06	hypothetical protein YPO2455
YPO2458	1.003	3.033E-05	LysR family transcriptional regulator
YPO2459	1.022	3.078E-03	transporter protein
YPO2460	0.959	2.281E-02	hypothetical protein YPO2460
YPO2461	0.823	2.953E-04	oxidoreductase
YPO2462	1.731	2.195E-10	hypothetical protein YPO2462
YPO2463	0.940	3.147E-05	hypothetical protein YPO2463
YPO2464	0.990	1.513E-04	hypothetical protein YPO2464
YPO2467	1.222	3.567E-10	hypothetical protein YPO2467
YPO2468	0.616	1.070E-02	hypothetical protein YPO2468
YPO2470	0.773	4.334E-02	hypothetical protein YPO2470
YPO2471	1.165	8.950E-07	hypothetical protein YPO2471
YPO2473	1.184	8.685E-06	hypothetical protein YPO2473

"-" indicates down regulation of expression

Autoinducer-2 dysregulation			
Gene Symbol	**log fold change**	***padj***	**Genome Annotation**
YPO2476	1.714	1.524E-10	sugar ABC transporter permease
YPO2477	0.799	2.987E-03	solute-binding protein
YPO2482	1.629	3.242E-09	hypothetical protein YPO2482
YPO2484	2.004	7.837E-07	hypothetical protein YPO2484
YPO2485	1.235	6.900E-07	hypothetical protein YPO2485
YPO2494	1.234	1.869E-05	transporter
YPO2495	1.118	2.762E-04	hypothetical protein YPO2495
YPO2496	1.452	6.602E-09	tartrate dehydrogenase
YPO2497	0.686	2.292E-02	LysR family transcriptional regulator
YPO2503	1.041	1.664E-03	hypothetical protein YPO2503
YPO2504	2.001	1.354E-14	hypothetical protein YPO2504
YPO2505	1.135	6.577E-05	hypothetical protein YPO2505
YPO2515	1.269	7.673E-12	chemotactic transducer
YPO2542	1.092	3.696E-06	hypothetical protein YPO2542
YPO2606	0.467	1.804E-02	hypothetical protein YPO2606
YPO2611	0.740	6.221E-05	hypothetical protein YPO2611
YPO2675	1.283	4.061E-10	voltage-gated potassium channel
YPO2701	-1.174	7.586E-04	hypothetical protein YPO2701
YPO2705	0.979	1.349E-06	autonomous glycyl radical cofactor GrcA
YPO2745	1.703	1.996E-05	hypothetical protein YPO2745
YPO2761	-1.020	4.474E-03	hypothetical protein YPO2761
YPO2795	0.790	2.484E-03	hypothetical protein YPO2795
YPO2820	0.979	7.398E-05	hypothetical protein YPO2820
YPO2840	-0.930	1.057E-02	chaperone
YPO2950	-0.695	1.473E-02	fimbrial protein
YPO2954	0.878	9.698E-06	hypothetical protein YPO2954
YPO2963	0.812	8.397E-03	hypothetical protein YPO2963
YPO3121	1.187	1.626E-05	hypothetical protein YPO3121
YPO3136	1.129	4.155E-07	hypothetical protein YPO3136
YPO3149	-0.736	8.544E-04	hypothetical protein YPO3149
YPO3309	-0.524	4.835E-02	hypothetical protein YPO3309
YPO3414	0.364	6.399E-02	hypothetical protein YPO3414
YPO3528	0.733	2.515E-04	hypothetical protein YPO3528
YPO3548	-0.660	1.211E-03	hypothetical protein YPO3548
YPO3564	-0.821	1.053E-04	hypothetical protein YPO3564
YPO3580	0.555	8.188E-04	lipopolysaccharide transport periplasmic protein LptA
YPO3681	-2.505	2.323E-41	insecticial toxin
YPO3682	-2.900	7.471E-31	LysR family transcriptional regulator
YPO3694	0.873	2.354E-05	cytochrome
YPO3744	-1.503	5.886E-04	hypothetical protein YPO3744
YPO3791	-0.851	1.727E-02	hypothetical protein YPO3791
YPO3821	-1.469	1.316E-06	sulfur transfer protein SirA
YPO3874	1.261	1.527E-07	hypothetical protein YPO3874
YPO3880	-0.490	5.623E-02	hypothetical protein YPO3880
YPO3908	0.906	2.758E-05	periplasmic protein
YPO3944	-0.459	4.389E-03	invasin
YPO3948	1.259	8.579E-04	hypothetical protein YPO3948
YPO3991	0.610	1.176E-04	insulinase family protease
YPO4050	1.083	2.024E-04	hypothetical protein YPO4050
YPO4081	1.053	3.849E-02	hypothetical protein YPO4081
YPO4109	-0.726	3.669E-03	amino acid transport system permease
YPO4110	-1.310	3.702E-07	ABC transporter permease
YPPCP1.08c	0.684	5.809E-04	putative transcriptional regulator (plasmid)
YPt_02	-1.132	2.412E-02	#N/A

"-" indicates down regulation of expression

Autoinducer-2 dysregulation			
Gene Symbol	**log fold change**	***padj***	**Genome Annotation**
YPt_03	-0.790	4.205E-02	#N/A
YPt_29	-1.535	3.083E-07	#N/A
YPt_59	-1.535	2.147E-06	#N/A
YPt_63	-1.679	1.791E-06	#N/A
YPt_65	-0.986	9.853E-06	#N/A
YPt_70	-0.850	9.324E-02	#N/A
yspI	-0.769	1.476E-01	N-acylhomoserine lactone synthase

"-" indicates down regulation of expression

References

1. **Hinnebusch BJ.** 2012. Biofilm-dependent and biofilm-independent mechanisms of transmission of Yersinia pestis by fleas. Adv Exp Med Biol **954:**237-243.

2. **Shannon JG, Hasenkrug AM, Dorward DW, Nair V, Carmody AB, Hinnebusch BJ.** 2013. Yersinia pestis subverts the dermal neutrophil response in a mouse model of bubonic plague. MBio **4:**e00170-00113.

3. **Comer JE, Sturdevant DE, Carmody AB, Virtaneva K, Gardner D, Long D, Rosenke R, Porcella SF, Hinnebusch BJ.** 2010. Transcriptomic and innate immune responses to Yersinia pestis in the lymph node during bubonic plague. Infect Immun **78:**5086-5098.

4. **Guinet F, Avé P, Filali S, Huon C, Savin C, Huerre M, Fiette L, Carniel E.** 2015. Dissociation of Tissue Destruction and Bacterial Expansion during Bubonic Plague. PLoS Pathog **11:**e1005222.

5. **Margolis DA, Burns J, Reed SL, Ginsberg MM, O'Grady TC, Vinetz JM.** 2008. Septicemic plague in a community hospital in California. Am J Trop Med Hyg **78:**868-871.

6. **Gould LH, Pape J, Ettestad P, Griffith KS, Mead PS.** 2008. Dog-associated risk factors for human plague. Zoonoses Public Health **55:**448-454.

7. **Anonymous.** 2016. Maps and Statistics | Plague | CDC. http://www.cdc.gov/plague/maps/index.html. Accessed

8. **Wong D, Wild MA, Walburger MA, Higgins CL, Callahan M, Czarnecki LA, Lawaczeck EW, Levy CE, Patterson JG, Sunenshine R, Adem P, Paddock CD, Zaki SR, Petersen JM, Schriefer ME, Eisen RJ, Gage KL, Griffith KS, Weber IB, Spraker TR, Mead PS.** 2009. Primary pneumonic plague contracted from a mountain lion carcass. Clin Infect Dis **49:**e33-38.

9. **Anonymous.** 2016-02-11 11:13:14 2016. WHO | Plague, *on* World Health Organization. http://www.who.int/entity/mediacentre/factsheets/fs267/en/index.html. Accessed

10. **Hinnebusch BJ, Chouikha I, Sun YC.** 2016. Ecological Opportunity, Evolution, and the Emergence of Flea-Borne Plague. Infect Immun **84:**1932-1940.

11. **Perdikogianni C, Galanakis E, Michalakis M, Giannoussi E, Maraki S, Tselentis Y, Charissis G.** 2006. Yersinia enterocolitica infection mimicking surgical conditions. Pediatr Surg Int **22:**589-592.

12. **Guinet F, Carniel E, Leclercq A.** 2011. Transfusion-transmitted Yersinia enterocolitica sepsis. Clin Infect Dis **53:**583-591.

13. **Guiyoule A, Grimont F, Iteman I, Grimont PA, Lefèvre M, Carniel E.** 1994. Plague pandemics investigated by ribotyping of Yersinia pestis strains. J Clin Microbiol **32:**634-641.

14. **Tran TN, Signoli M, Fozzati L, Aboudharam G, Raoult D, Drancourt M.** 2011. High throughput, multiplexed pathogen detection authenticates plague waves in medieval Venice, Italy. PLoS One **6:**e16735.

15. **Schuenemann VJ, Bos K, DeWitte S, Schmedes S, Jamieson J, Mittnik A, Forrest S, Coombes BK, Wood JW, Earn DJ, White W, Krause J, Poinar HN.** 2011. Targeted enrichment of ancient pathogens yielding the pPCP1 plasmid of Yersinia pestis from victims of the Black Death. Proc Natl Acad Sci U S A **108:**E746-752.

16. **Stenseth NC, Atshabar BB, Begon M, Belmain SR, Bertherat E, Carniel E, Gage KL, Leirs H, Rahalison L.** 2008. Plague: past, present, and future. PLoS Med **5:**e3.

17. **Drancourt M, Aboudharam G, Signoli M, Dutour O, Raoult D.** 1998. Detection of 400-year-old Yersinia pestis DNA in human dental pulp: an approach to the diagnosis of ancient septicemia. Proc Natl Acad Sci U S A **95:**12637-12640.

18. **Walsh M, Haseeb MA.** 2015. Modeling the ecologic niche of plague in sylvan and domestic animal hosts to delineate sources of human exposure in the western United States. PeerJ **3:**e1493.

19. **Duplantier JM, Duchemin JB, Chanteau S, Carniel E.** 2005. From the recent lessons of the Malagasy foci towards a global understanding of the factors involved in plague reemergence. Vet Res **36:**437-453.

20. **Anonymous.** 2016. Weekly epidemiological report. World Health Organization,

21. **Kwit N, Nelson C, Kugeler K, Petersen J, Plante L, Yaglom H, Kramer V, Schwartz B, House J, Colton L, Feldpausch A, Drenzek C, Baumbach J, DiMenna M, Fisher E, Debess E, Buttke D, Weinburke M, Percy C, Schriefer M, Gage K, Mead P.** 2015. Human Plague - United States, 2015. MMWR Morb Mortal Wkly Rep **64:**918-919.

22. **Adams DA, Jajosky RA, Ajani U, Kriseman J, Sharp P, Onwen DH, Schley AW, Anderson WJ, Grigoryan A, Aranas AE, Wodajo MS, Abellera JP, (CDC) CfDCaP.** 2014. Summary of notifiable diseases--United States, 2012. MMWR Morb Mortal Wkly Rep **61:**1-121.

23. **Kugeler KJ, Staples JE, Hinckley AF, Gage KL, Mead PS.** 2015. Epidemiology of human plague in the United States, 1900-2012. Emerg Infect Dis **21:**16-22.

24. **Runfola JK, House J, Miller L, Colton L, Hite D, Hawley A, Mead P, Schriefer M, Petersen J, Casaceli C, Erlandson KM, Foster C, Pabilonia KL, Mason G, Douglas JM, (CDC) CfDCaP.** 2015. Outbreak of Human Pneumonic Plague with Dog-to-Human and Possible Human-to-Human Transmission--Colorado, June-July 2014. MMWR Morb Mortal Wkly Rep **64:**429-434.

25. **Foster CL, Mould K, Reynolds P, Simonian PL, Erlandson KM.** 2015. Clinical problem-solving. Sick as a dog. N Engl J Med **372:**1845-1850.

26. **Hinckley AF, Biggerstaff BJ, Griffith KS, Mead PS.** 2012. Transmission dynamics of primary pneumonic plague in the USA. Epidemiol Infect **140:**554-560.

27. **Barras V, Greub G.** 2014. History of biological warfare and bioterrorism. Clin Microbiol Infect **20:**497-502.

28. **Derbes VJ.** 1966. De Mussis and the great plague of 1348. A forgotten episode of bacteriological warfare. JAMA **196:**59-62.

29. **Wheelis M.** 2002. Biological warfare at the 1346 siege of Caffa. Emerg Infect Dis **8:**971-975.

30. **Noah DL, Huebner KD, Darling RG, Waeckerle JF.** 2002. The history and threat of biological warfare and terrorism. Emerg Med Clin North Am **20:**255-271.

31. **Parkhill J, Wren BW, Thomson NR, Titball RW, Holden MT, Prentice MB, Sebaihia M, James KD, Churcher C, Mungall KL, Baker S, Basham D, Bentley SD, Brooks K, Cerdeño-Tárraga AM, Chillingworth T, Cronin A, Davies RM, Davis P, Dougan G, Feltwell T, Hamlin N, Holroyd S, Jagels K, Karlyshev AV, Leather S, Moule S, Oyston PC, Quail M, Rutherford K, Simmonds M, Skelton J, Stevens K, Whitehead S, Barrell BG.** 2001. Genome sequence of Yersinia pestis, the causative agent of plague. Nature **413:**523-527.

32. **Arbaji A, Kharabsheh S, Al-Azab S, Al-Kayed M, Amr ZS, Abu Baker M, Chu MC.** 2005. A 12-case outbreak of pharyngeal plague following the consumption of camel meat, in north-eastern Jordan. Ann Trop Med Parasitol **99:**789-793.

33. **Gage KL, Kosoy MY.** 2005. Natural history of plague: perspectives from more than a century of research. Annu Rev Entomol **50:**505-528.

34. **St Romain K, Tripp DW, Salkeld DJ, Antolin MF.** 2013. Duration of plague (Yersinia pestis) outbreaks in black-tailed prairie dog (Cynomys ludovicianus) colonies of northern Colorado. Ecohealth **10:**241-245.

35. **Erickson DL, Jarrett CO, Wren BW, Hinnebusch BJ.** 2006. Serotype differences and lack of biofilm formation characterize Yersinia

pseudotuberculosis infection of the Xenopsylla cheopis flea vector of Yersinia pestis. J Bacteriol **188:**1113-1119.

36. **Sun YC, Jarrett CO, Bosio CF, Hinnebusch BJ.** 2014. Retracing the evolutionary path that led to flea-borne transmission of Yersinia pestis. Cell Host Microbe **15:**578-586.

37. **Chouikha I, Hinnebusch BJ.** 2014. Silencing urease: a key evolutionary step that facilitated the adaptation of Yersinia pestis to the flea-borne transmission route. Proc Natl Acad Sci U S A **111:**18709-18714.

38. **Sun YC, Hinnebusch BJ, Darby C.** 2008. Experimental evidence for negative selection in the evolution of a Yersinia pestis pseudogene. Proc Natl Acad Sci U S A **105:**8097-8101.

39. **Fang N, Yang H, Fang H, Liu L, Zhang Y, Wang L, Han Y, Zhou D, Yang R.** 2015. RcsAB is a major repressor of Yersinia biofilm development through directly acting on hmsCDE, hmsT, and hmsHFRS. Sci Rep **5:**9566.

40. **Boyd CD, O'Toole GA.** 2012. Second messenger regulation of biofilm formation: breakthroughs in understanding c-di-GMP effector systems. Annu Rev Cell Dev Biol **28:**439-462.

41. **Gonzalez RJ, Lane MC, Wagner NJ, Weening EH, Miller VL.** 2015. Dissemination of a highly virulent pathogen: tracking the early events that define infection. PLoS Pathog **11:**e1004587.

42. **Fetherston JD, Schuetze P, Perry RD.** 1992. Loss of the pigmentation phenotype in Yersinia pestis is due to the spontaneous deletion of 102 kb of chromosomal DNA which is flanked by a repetitive element. Mol Microbiol **6:**2693-2704.

43. **Buchrieser C, Prentice M, Carniel E.** 1998. The 102-kilobase unstable region of Yersinia pestis comprises a high-pathogenicity island linked to a pigmentation segment which undergoes internal rearrangement. J Bacteriol **180:**2321-2329.

44. **Buchrieser C, Rusniok C, Frangeul L, Couve E, Billault A, Kunst F, Carniel E, Glaser P.** 1999. The 102-kilobase pgm locus of Yersinia pestis: sequence analysis and comparison of selected regions among different Yersinia pestis and Yersinia pseudotuberculosis strains. Infect Immun **67:**4851-4861.

45. **Welkos S, Pitt ML, Martinez M, Friedlander A, Vogel P, Tammariello R.** 2002. Determination of the virulence of the pigmentation-deficient and pigmentation-/plasminogen activator-deficient strains of Yersinia pestis in non-human primate and mouse models of pneumonic plague. Vaccine **20:**2206-2214.

46. **Hinnebusch BJ, Perry RD, Schwan TG.** 1996. Role of the Yersinia pestis hemin storage (hms) locus in the transmission of plague by fleas. Science **273:**367-370.

47. **Kutyrev VV, Filippov AA, Oparina OS, Protsenko OA.** 1992. Analysis of Yersinia pestis chromosomal determinants Pgm+ and Psts associated with virulence. Microb Pathog **12:**177-186.

48. **(CDC) CfDCaP.** 2011. Fatal laboratory-acquired infection with an attenuated Yersinia pestis Strain--Chicago, Illinois, 2009. MMWR Morb Mortal Wkly Rep **60:**201-205.

49. **Quenee LE, Hermanas TM, Ciletti N, Louvel H, Miller NC, Elli D, Blaylock B, Mitchell A, Schroeder J, Krausz T, Kanabrocki J, Schneewind O.** 2012. Hereditary hemochromatosis restores the virulence of plague vaccine strains. J Infect Dis **206:**1050-1058.

50. **Zhou D, Han Y, Dai E, Song Y, Pei D, Zhai J, Du Z, Wang J, Guo Z, Yang R.** 2004. Defining the genome content of live plague vaccines by use of whole-genome DNA microarray. Vaccine **22:**3367-3374.

51. **Perry RD, Craig SK, Abney J, Bobrov AG, Kirillina O, Mier I, Truszczynska H, Fetherston JD.** 2012. Manganese transporters Yfe and MntH are Fur-regulated and important for the virulence of Yersinia pestis. Microbiology **158:**804-815.

52. **Bearden SW, Perry RD.** 1999. The Yfe system of Yersinia pestis transports iron and manganese and is required for full virulence of plague. Mol Microbiol **32:**403-414.

53. **Cui Y, Yang X, Xiao X, Anisimov AP, Li D, Yan Y, Zhou D, Rajerison M, Carniel E, Achtman M, Yang R, Song Y.** 2014. Genetic variations of live attenuated plague vaccine strains (Yersinia pestis EV76 lineage) during laboratory passages in different countries. Infect Genet Evol **26:**172-179.

54. **Shen X, Wang Q, Xia L, Zhu X, Zhang Z, Liang Y, Cai H, Zhang E, Wei J, Chen C, Song Z, Zhang H, Yu D, Hai R.** 2010. Complete genome sequences of Yersinia pestis from natural foci in China. J Bacteriol **192:**3551-3552.

55. **Andrews GP, Heath DG, Anderson GW, Welkos SL, Friedlander AM.** 1996. Fraction 1 capsular antigen (F1) purification from Yersinia pestis CO92 and from an Escherichia coli recombinant strain and efficacy against lethal plague challenge. Infect Immun **64:**2180-2187.

56. **Meyer KF, Hightower JA, McCrumb FR.** 1974. Plague immunization. VI. Vaccination with the fraction I antigen of Yersinia pestis. J Infect Dis **129:**Suppl:S41-45.

57. **Simpson WJ, Thomas RE, Schwan TG.** 1990. Recombinant capsular antigen (fraction 1) from Yersinia pestis induces a protective antibody response in BALB/c mice. Am J Trop Med Hyg **43:**389-396.

58. **Chen TH, Elberg SS.** 1977. Scanning electron microscopic study of virulent Yersinia pestis and Yersinia pseudotuberculosis type 1. Infect Immun **15:**972-977.

59. **Du Y, Rosqvist R, Forsberg A.** 2002. Role of fraction 1 antigen of Yersinia pestis in inhibition of phagocytosis. Infect Immun **70:**1453-1460.

60. **Sha J, Endsley JJ, Kirtley ML, Foltz SM, Huante MB, Erova TE, Kozlova EV, Popov VL, Yeager LA, Zudina IV, Motin VL, Peterson JW, DeBord KL, Chopra AK.** 2011. Characterization of an F1 deletion mutant of Yersinia pestis CO92, pathogenic role of F1 antigen in bubonic and pneumonic plague, and evaluation of sensitivity and specificity of F1 antigen capture-based dipsticks. J Clin Microbiol **49:**1708-1715.

61. **Quenee LE, Cornelius CA, Ciletti NA, Elli D, Schneewind O.** 2008. Yersinia pestis caf1 variants and the limits of plague vaccine protection. Infect Immun **76:**2025-2036.

62. **Meka-Mechenko TV.** 2003. F1-negative natural Y. pestis strains. Adv Exp Med Biol **529:**379-381.

63. **Perry RD, Fetherston JD.** 1997. Yersinia pestis--etiologic agent of plague. Clin Microbiol Rev **10:**35-66.

64. **Lathem WW, Price PA, Miller VL, Goldman WE.** 2007. A plasminogen-activating protease specifically controls the development of primary pneumonic plague. Science **315:**509-513.

65. **Sodeinde OA, Goguen JD.** 1989. Nucleotide sequence of the plasminogen activator gene of Yersinia pestis: relationship to ompT of Escherichia coli and gene E of Salmonella typhimurium. Infect Immun **57:**1517-1523.

66. **McDonough KA, Falkow S.** 1989. A Yersinia pestis-specific DNA fragment encodes temperature-dependent coagulase and fibrinolysin-associated phenotypes. Mol Microbiol **3:**767-775.

67. **Welkos SL, Friedlander AM, Davis KJ.** 1997. Studies on the role of plasminogen activator in systemic infection by virulent Yersinia pestis strain C092. Microb Pathog **23:**211-223.

68. **Sodeinde OA, Subrahmanyam YV, Stark K, Quan T, Bao Y, Goguen JD.** 1992. A surface protease and the invasive character of plague. Science **258:**1004-1007.

69. **van Lier CJ, Sha J, Kirtley ML, Cao A, Tiner BL, Erova TE, Cong Y, Kozlova EV, Popov VL, Baze WB, Chopra AK.** 2014. Deletion of Braun lipoprotein and plasminogen activating protease-encoding genes attenuates Yersinia pestis in mouse models of bubonic and pneumonic plague. Infect Immun.

70. **van Lier CJ, Tiner BL, Chauhan S, Motin VL, Fitts EC, Huante MB, Endsley JJ, Ponnusamy D, Sha J, Chopra AK.** 2015. Further characterization of a highly attenuated Yersinia pestis CO92 mutant deleted for the genes encoding Braun lipoprotein and plasminogen activator protease in murine alveolar and primary human macrophages. Microb Pathog **80:**27-38.

71. **Erova TE, Rosenzweig JA, Sha J, Suarez G, Sierra JC, Kirtley ML, van Lier CJ, Telepnev MV, Motin VL, Chopra AK.** 2013. Evaluation of protective potential of Yersinia pestis outer membrane protein antigens as possible candidates for a new-generation recombinant plague vaccine. Clin Vaccine Immunol **20:**227-238.

72. **Miller VL, Bliska JB, Falkow S.** 1990. Nucleotide sequence of the Yersinia enterocolitica ail gene and characterization of the Ail protein product. J Bacteriol **172:**1062-1069.

73. **Miller VL, Falkow S.** 1988. Evidence for two genetic loci in Yersinia enterocolitica that can promote invasion of epithelial cells. Infect Immun **56:**1242-1248.

74. **Bartra SS, Ding Y, Fujimoto LM, Ring JG, Jain V, Ram S, Marassi FM, Plano GV.** 2015. Yersinia pestis uses the Ail outer membrane protein to recruit vitronectin. Microbiology **161:**2174-2183.

75. **Yamashita S, Lukacik P, Barnard TJ, Noinaj N, Felek S, Tsang TM, Krukonis ES, Hinnebusch BJ, Buchanan SK.** 2011. Structural insights into Ail-mediated adhesion in Yersinia pestis. Structure **19:**1672-1682.

76. **Tiner BL, Sha J, Kirtley ML, Erova TE, Popov VL, Baze WB, van Lier CJ, Ponnusamy D, Andersson JA, Motin VL, Chauhan S, Chopra AK.** 2015. Combinational deletion of three membrane protein-encoding genes highly attenuates yersinia pestis while retaining immunogenicity in a mouse model of pneumonic plague. Infect Immun **83:**1318-1338.

77. **Tsang TM, Felek S, Krukonis ES.** 2010. Ail binding to fibronectin facilitates Yersinia pestis binding to host cells and Yop delivery. Infect Immun **78:**3358-3368.

78. **Felek S, Krukonis ES.** 2009. The Yersinia pestis Ail protein mediates binding and Yop delivery to host cells required for plague virulence. Infect Immun **77:**825-836.

79. **Kolodziejek AM, Sinclair DJ, Seo KS, Schnider DR, Deobald CF, Rohde HN, Viall AK, Minnich SS, Hovde CJ, Minnich SA, Bohach GA.** 2007. Phenotypic characterization of OmpX, an Ail homologue of Yersinia pestis KIM. Microbiology **153:**2941-2951.

80. **Pierson DE, Falkow S.** 1993. The ail gene of Yersinia enterocolitica has a role in the ability of the organism to survive serum killing. Infect Immun **61:**1846-1852.

81. **Sha J, Kirtley ML, van Lier CJ, Wang S, Erova TE, Kozlova EV, Cao A, Cong Y, Fitts EC, Rosenzweig JA, Chopra AK.** 2013. Deletion of the Braun lipoprotein-encoding gene and altering the function of lipopolysaccharide attenuate the plague bacterium. Infect Immun **81:**815-828.

82. **Tiner BL, Sha J, Ponnusamy D, Baze WB, Fitts EC, Popov VL, van Lier CJ, Erova TE, Chopra AK.** 2015. Intramuscular Immunization of Mice with a Live-Attenuated Triple Mutant of Yersinia pestis CO92 Induces Robust Humoral and Cell-Mediated Immunity To Completely Protect Animals against Pneumonic Plague. Clin Vaccine Immunol **22:**1255-1268.

83. **Braun V, Hantke K.** 1974. Biochemistry of bacterial cell envelopes. Annu Rev Biochem **43:**89-121.

84. **Glauser MP, Zanetti G, Baumgartner JD, Cohen J.** 1991. Septic shock: pathogenesis. Lancet **338:**732-736.

85. **Pérez-Gutiérrez C, Llobet E, Llompart CM, Reinés M, Bengoechea JA.** 2010. Role of lipid A acylation in Yersinia enterocolitica virulence. Infect Immun **78:**2768-2781.

86. **Rebeil R, Ernst RK, Jarrett CO, Adams KN, Miller SI, Hinnebusch BJ.** 2006. Characterization of late acyltransferase genes of Yersinia pestis and their role in temperature-dependent lipid A variation. J Bacteriol **188:**1381-1388.

87. **Anisimov AP, Shaikhutdinova RZ, Pan'kina LN, Feodorova VA, Savostina EP, Bystrova OV, Lindner B, Mokrievich AN, Bakhteeva IV, Titareva GM, Dentovskaya SV, Kocharova NA, Senchenkova SN, Holst O, Devdariani ZL, Popov YA, Pier GB, Knirel YA.** 2007. Effect of deletion of the lpxM gene on virulence and vaccine potential of Yersinia pestis in mice. J Med Microbiol **56:**443-453.

88. **Plano GV, Schesser K.** 2013. The Yersinia pestis type III secretion system: expression, assembly and role in the evasion of host defenses. Immunol Res **57:**237-245.

89. **Schwiesow L, Lam H, Dersch P, Auerbuch V.** 2016. Yersinia Type III Secretion System Master Regulator LcrF. J Bacteriol **198:**604-614.

90. **Williams AW, Straley SC.** 1998. YopD of Yersinia pestis plays a role in negative regulation of the low-calcium response in addition to its role in translocation of Yops. J Bacteriol **180:**350-358.

91. **Ratner D, Orning MP, Starheim KK, Marty-Roix R, Proulx MK, Goguen JD, Lien E.** 2016. Manipulation of Interleukin-1β and Interleukin-18 Production by Yersinia pestis Effectors YopJ and YopM and Redundant Impact on Virulence. J Biol Chem **291:**9894-9905.

92. **Evdokimov AG, Tropea JE, Routzahn KM, Waugh DS.** 2002. Crystal structure of the Yersinia pestis GTPase activator YopE. Protein Sci **11:**401-408.

93. **Bliska JB, Guan KL, Dixon JE, Falkow S.** 1991. Tyrosine phosphate hydrolysis of host proteins by an essential Yersinia virulence determinant. Proc Natl Acad Sci U S A **88:**1187-1191.

94. **Guan KL, Dixon JE.** 1990. Protein tyrosine phosphatase activity of an essential virulence determinant in Yersinia. Science **249:**553-556.

95. **Cornelis GR.** 2002. The Yersinia Ysc-Yop virulence apparatus. Int J Med Microbiol **291:**455-462.

96. **Cornelis GR.** 1998. The Yersinia Yop virulon, a bacterial system to subvert cells of the primary host defense. Folia Microbiol (Praha) **43:**253-261.

97. **Stainier I, Cornelis GR.** 1998. The Yop virulon of Yersinia: a bacterial weapon to kill host cells. Clin Microbiol Infect **4:**673-676.

98. **Elvin SJ, Eyles JE, Howard KA, Ravichandran E, Somavarappu S, Alpar HO, Williamson ED.** 2006. Protection against bubonic and pneumonic plague with a single dose microencapsulated sub-unit vaccine. Vaccine **24:**4433-4439.

99. **Dewoody RS, Merritt PM, Marketon MM.** 2013. Regulation of the Yersinia type III secretion system: traffic control. Front Cell Infect Microbiol **3:**4.

100. **Yen YT, Bhattacharya M, Stathopoulos C.** 2008. Genome-wide in silico mapping of the secretome in pathogenic Yersinia pestis KIM. FEMS Microbiol Lett **279:**56-63.

101. **Mougous JD, Cuff ME, Raunser S, Shen A, Zhou M, Gifford CA, Goodman AL, Joachimiak G, Ordoñez CL, Lory S, Walz T, Joachimiak A, Mekalanos JJ.** 2006. A virulence locus of Pseudomonas aeruginosa encodes a protein secretion apparatus. Science **312:**1526-1530.

102. **Pukatzki S, Ma AT, Sturtevant D, Krastins B, Sarracino D, Nelson WC, Heidelberg JF, Mekalanos JJ.** 2006. Identification of a conserved bacterial protein secretion system in Vibrio cholerae using the Dictyostelium host model system. Proc Natl Acad Sci U S A **103:**1528-1533.

103. **Robinson JB, Telepnev MV, Zudina IV, Bouyer D, Montenieri JA, Bearden SW, Gage KL, Agar SL, Foltz SM, Chauhan S, Chopra AK, Motin VL.** 2009. Evaluation of a Yersinia pestis mutant impaired in a thermoregulated type VI-like secretion system in flea, macrophage and murine models. Microb Pathog **47:**243-251.

104. **Ponnusamy D, Fitts EC, Sha J, Erova TE, Kozlova EV, Kirtley ML, Tiner BL, Andersson JA, Chopra AK.** 2015. High-throughput signature-tagged mutagenic approach to identify novel virulence factors of Yersinia pestis CO92 in a mouse model of infection. Infect Immun.

105. **Cianfanelli FR, Monlezun L, Coulthurst SJ.** 2016. Aim, Load, Fire: The Type VI Secretion System, a Bacterial Nanoweapon. Trends Microbiol **24:**51-62.

106. **Smiley ST.** 2008. Current challenges in the development of vaccines for pneumonic plague. Expert Rev Vaccines **7:**209-221.

107. **Titball RW, Williamson ED.** 2004. Yersinia pestis (plague) vaccines. Expert Opin Biol Ther **4:**965-973.

108. **Green M, Rogers D, Russell P, Stagg AJ, Bell DL, Eley SM, Titball RW, Williamson ED.** 1999. The SCID/Beige mouse as a model to investigate protection against Yersinia pestis. FEMS Immunol Med Microbiol **23:**107-113.

109. **Bashaw J, Norris S, Weeks S, Trevino S, Adamovicz JJ, Welkos S.** 2007. Development of in vitro correlate assays of immunity to infection with Yersinia pestis. Clin Vaccine Immunol **14:**605-616.

110. **Smiley ST.** 2007. Cell-mediated defense against Yersinia pestis infection. Adv Exp Med Biol **603:**376-386.

111. **Parent MA, Berggren KN, Kummer LW, Wilhelm LB, Szaba FM, Mullarky IK, Smiley ST.** 2005. Cell-mediated protection against pulmonary Yersinia pestis infection. Infect Immun **73:**7304-7310.

112. **Parent MA, Wilhelm LB, Kummer LW, Szaba FM, Mullarky IK, Smiley ST.** 2006. Gamma interferon, tumor necrosis factor alpha, and nitric oxide synthase 2, key elements of cellular immunity, perform critical protective functions during humoral defense against lethal pulmonary Yersinia pestis infection. Infect Immun **74:**3381-3386.

113. **Meyer KF, Cavanaugh DC, Bartelloni PJ, Marshall JD.** 1974. Plague immunization. I. Past and present trends. J Infect Dis **129:**Suppl:S13-18.

114. **Cavanaugh DC, Elisberg BL, Llewellyn CH, Marshall JD, Rust JH, Williams JE, Meyer KF.** 1974. Plague immunization. V. Indirect evidence for the efficacy of plague vaccine. J Infect Dis **129:**Suppl:S37-40.

115. **Cohen RJ, Stockard JL.** 1967. Pneumonic plague in an untreated plague-vaccinated individual. JAMA **202:**365-366.

116. **Chu K, Hu J, Meng F, Li J, Luo L, Xu J, Yuan Z, Li Z, Chen W, Jiao L, Chang Y, Wang B, Hu Y.** 2016. Immunogenicity and safety of subunit plague vaccine: A randomized phase 2a clinical trial. Hum Vaccin Immunother**:**1-7.

117. **Kingston R, Burke F, Robinson JH, Bedford PA, Jones SM, Knight SC, Williamson ED.** 2007. The fraction 1 and V protein antigens of Yersinia pestis activate dendritic cells to induce primary T cell responses. Clin Exp Immunol **149:**561-569.

118. **Huang XZ, Lindler LE.** 2004. The pH 6 antigen is an antiphagocytic factor produced by Yersinia pestis independent of Yersinia outer proteins and capsule antigen. Infect Immun **72:**7212-7219.

119. **Galván EM, Nair MK, Chen H, Del Piero F, Schifferli DM.** 2010. Biosafety level 2 model of pneumonic plague and protection studies with F1 and Psa. Infect Immun **78:**3443-3453.

120. **Torres-Escobar A, Juárez-Rodríguez MD, Branger CG, Curtiss R.** 2010. Evaluation of the humoral immune response in mice orally vaccinated with live recombinant attenuated Salmonella enterica delivering a secreted form of Yersinia pestis PsaA. Vaccine **28:**5810-5816.

121. **Murphy BS, Wulff CR, Garvy BA, Straley SC.** 2007. Yersinia pestis YadC: a novel vaccine candidate against plague. Adv Exp Med Biol **603:**400-414.

122. **Sun W, Olinzock J, Wang S, Sanapala S, Curtiss R.** 2014. Evaluation of YadC protein delivered by live attenuated Salmonella as a vaccine against plague. Pathog Dis **70:**119-131.

123. **Sha J, Kirtley ML, Klages C, Erova TE, Telepnev M, Ponnusamy D, Fitts EC, Baze WB, Sivasubramani SK, Lawrence WS, Patrikeev I, Peel JE, Andersson JA, Kozlova EV, Tiner BL, Peterson JW, McWilliams D, Patel S, Rothe E, Motin VL, Chopra AK.** 2016. A Replication-Defective Human Type 5 Adenovirus-Based Trivalent Vaccine Confers Complete Protection against Plague in Mice and Nonhuman Primates. Clin Vaccine Immunol **23:**586-600.

124. **Tao P, Mahalingam M, Kirtley ML, van Lier CJ, Sha J, Yeager LA, Chopra AK, Rao VB.** 2013. Mutated and bacteriophage T4 nanoparticle arrayed F1-V immunogens from Yersinia pestis as next generation plague vaccines. PLoS Pathog **9:**e1003495.

125. **Feodorova VA, Sayapina LV, Motin VL.** 2016. Assessment of Live Plague Vaccine Candidates. Methods Mol Biol **1403:**487-498.

126. **Bubeck SS, Dube PH.** 2007. Yersinia pestis CO92 delta yopH is a potent live, attenuated plague vaccine. Clin Vaccine Immunol **14:**1235-1238.

127. **Deng W, Burland V, Plunkett G, 3rd, Boutin A, Mayhew GF, Liss P, Perna NT, Rose DJ, Mau B, Zhou S, Schwartz DC, Fetherston JD, Lindler LE, Brubaker RR, Plano GV, Straley SC, McDonough KA, Nilles ML, Matson JS, Blattner FR, Perry RD.** 2002. Genome sequence of Yersinia pestis KIM. J Bacteriol **184:**4601-4611.

128. **Parkhill J, Wren BW, Thomson NR, Titball RW, Holden MT, Prentice MB, Sebaihia M, James KD, Churcher C, Mungall KL, Baker S, Basham D, Bentley SD, Brooks K, Cerdeno-Tarraga AM, Chillingworth T, Cronin A, Davies RM, Davis P, Dougan G, Feltwell T, Hamlin N, Holroyd S, Jagels K, Karlyshev AV, Leather S, Moule S, Oyston PC, Quail M, Rutherford K, Simmonds M, Skelton J, Stevens K, Whitehead S, Barrell BG.** 2001. Genome sequence of Yersinia pestis, the causative agent of plague. Nature **413:**523-527.

129. **Cornelis GR.** 2002. Yersinia type III secretion: send in the effectors. J Cell Biol **158:**401-408.

130. **Sing A, Rost D, Tvardovskaia N, Roggenkamp A, Wiedemann A, Kirschning CJ, Aepfelbacher M, Heesemann J.** 2002. Yersinia V-antigen exploits toll-like receptor 2 and CD14 for interleukin 10-mediated immunosuppression. J Exp Med **196:**1017-1024.

131. **van Lier CJ, Sha J, Kirtley ML, Cao A, Tiner BL, Erova TE, Cong Y, Kozlova EV, Popov VL, Baze WB, Chopra AK.** Deletion of Braun lipoprotein and plasminogen-activating protease-encoding genes attenuates Yersinia pestis in mouse models of bubonic and pneumonic plague. Infect Immun **82:**2485-2503.

132. **Sha J, Kirtley ML, van Lier CJ, Wang S, Erova TE, Kozlova EV, Cao A, Cong Y, Fitts EC, Rosenzweig JA, Chopra AK.** Deletion of the Braun lipoprotein-encoding gene and altering the function of lipopolysaccharide attenuate the plague bacterium. Infect Immun **81:**815-828.

133. **Sha J, Agar SL, Baze WB, Olano JP, Fadl AA, Erova TE, Wang S, Foltz SM, Suarez G, Motin VL, Chauhan S, Klimpel GR, Peterson JW, Chopra AK.** 2008. Braun lipoprotein (Lpp) contributes to virulence of yersiniae: potential role of Lpp in inducing bubonic and pneumonic plague. Infect Immun **76:**1390-1409.

134. **Bartra SS, Styer KL, O'Bryant DM, Nilles ML, Hinnebusch BJ, Aballay A, Plano GV.** 2008. Resistance of Yersinia pestis to complement-dependent killing is mediated by the Ail outer membrane protein. Infect Immun **76:**612-622.

135. **Li B, Yang R.** 2008. Interaction between Yersinia pestis and the host immune system. Infect Immun **76:**1804-1811.

136. **Sebbane F, Lemaitre N, Sturdevant DE, Rebeil R, Virtaneva K, Porcella SF, Hinnebusch BJ.** 2006. Adaptive response of Yersinia pestis to extracellular effectors of innate immunity during bubonic plague. Proc Natl Acad Sci U S A **103:**11766-11771.

137. **Vadyvaloo V, Jarrett C, Sturdevant DE, Sebbane F, Hinnebusch BJ.** Transit through the flea vector induces a pretransmission innate immunity resistance phenotype in Yersinia pestis. PLoS Pathog **6:**e1000783.

138. **Chauvaux S, Rosso ML, Frangeul L, Lacroix C, Labarre L, Schiavo A, Marceau M, Dillies MA, Foulon J, Coppee JY, Medigue C, Simonet M, Carniel E.** 2007. Transcriptome analysis of Yersinia pestis in human plasma: an approach for discovering bacterial genes involved in septicaemic plague. Microbiology **153:**3112-3124.

139. **Lathem WW, Crosby SD, Miller VL, Goldman WE.** 2005. Progression of primary pneumonic plague: a mouse model of infection, pathology, and bacterial transcriptional activity. Proc Natl Acad Sci U S A **102:**17786-17791.

140. **Yang R, Du Z, Han Y, Zhou L, Song Y, Zhou D, Cui Y.** Omics strategies for revealing Yersinia pestis virulence. Front Cell Infect Microbiol **2:**157.

141. **Mazurkiewicz P, Tang CM, Boone C, Holden DW.** 2006. Signature-tagged mutagenesis: barcoding mutants for genome-wide screens. Nat Rev Genet **7:**929-939.

142. **Palace SG, Proulx MK, Lu S, Baker RE, Goguen JD.** Genome-wide mutant fitness profiling identifies nutritional requirements for optimal growth of Yersinia pestis in deep tissue. MBio **5**.

143. **Darwin AJ, Miller VL.** 1999. Identification of Yersinia enterocolitica genes affecting survival in an animal host using signature-tagged transposon mutagenesis. Mol Microbiol **32:**51-62.

144. **Karlyshev AV, Oyston PC, Williams K, Clark GC, Titball RW, Winzeler EA, Wren BW.** 2001. Application of high-density array-based signature-tagged mutagenesis to discover novel Yersinia virulence-associated genes. Infect Immun **69:**7810-7819.

145. **Mecsas J, Bilis I, Falkow S.** 2001. Identification of attenuated Yersinia pseudotuberculosis strains and characterization of an orogastric infection in BALB/c mice on day 5 postinfection by signature-tagged mutagenesis. Infect Immun **69:**2779-2787.

146. **Grim CJ, Kozlova EV, Ponnusamy D, Fitts EC, Sha J, Kirtley ML, van Lier CJ, Tiner BL, Erova TE, Joseph SJ, Read TD, Shak JR, Joseph SW, Singletary E, Felland T, Baze WB, Horneman AJ, Chopra AK.** 2014.

Functional genomic characterization of virulence factors from necrotizing fasciitis-causing strains of Aeromonas hydrophila. Appl Environ Microbiol.

147. **Hensel M, Shea JE, Gleeson C, Jones MD, Dalton E, Holden DW.** 1995. Simultaneous identification of bacterial virulence genes by negative selection. Science **269:**400-403.

148. **Silver AC, Rabinowitz NM, Kuffer S, Graf J.** 2007. Identification of Aeromonas veronii genes required for colonization of the medicinal leech, Hirudo verbana. J Bacteriol **189:**6763-6772.

149. **Silver AC, Kikuchi Y, Fadl AA, Sha J, Chopra AK, Graf J.** 2007. Interaction between innate immune cells and a bacterial type III secretion system in mutualistic and pathogenic associations. Proc Natl Acad Sci U S A **104:**9481-9486.

150. **Datsenko KA, Wanner BL.** 2000. One-step inactivation of chromosomal genes in Escherichia coli K-12 using PCR products. Proc Natl Acad Sci U S A **97:**6640-6645.

151. **Sha J, Endsley JJ, Kirtley ML, Foltz SM, Huante MB, Erova TE, Kozlova EV, Popov VL, Yeager LA, Zudina IV, Motin VL, Peterson JW, DeBord KL, Chopra AK.** Characterization of an F1 deletion mutant of Yersinia pestis CO92, pathogenic role of F1 antigen in bubonic and pneumonic plague, and evaluation of sensitivity and specificity of F1 antigen capture-based dipsticks. J Clin Microbiol **49:**1708-1715.

152. **Sha J, Rosenzweig JA, Kirtley ML, van Lier CJ, Fitts EC, Kozlova EV, Erova TE, Tiner BL, Chopra AK.** A non-invasive in vivo imaging system to study dissemination of bioluminescent Yersinia pestis CO92 in a mouse model of pneumonic plague. Microb Pathog **55:**39-50.

153. **Grim CJ, Kozlova EV, Ponnusamy D, Fitts EC, Sha J, Kirtley ML, van Lier CJ, Tiner BL, Erova TE, Joseph SJ, Read TD, Shak JR, Joseph SW, Singletary E, Felland T, Baze WB, Horneman AJ, Chopra AK.** 2014. Functional genomic characterization of virulence factors from necrotizing fasciitis-causing strains of Aeromonas hydrophila. Appl Environ Microbiol **80:**4162-4183.

154. **G S, JC S, ML K, AK. C.** 2010. Role of Hcp, a type 6 secretion system effector, of Aeromonas hydrophila in modulating activation of host immune cells, vol 156, p 3678–3688. Microbiology.

155. **Suarez G, Sierra JC, Sha J, Wang S, Erova TE, Fadl AA, Foltz SM, Horneman AJ, Chopra AK.** 2008. Molecular characterization of a functional type VI secretion system from a clinical isolate of Aeromonas hydrophila. Microb Pathog **44:**344-361.

156. **Barroga CF, Zhang H, Wajih N, Bouyer JH, Hermodson MA.** 1996. The proteins encoded by the rbs operon of Escherichia coli: I. Overproduction, purification, characterization, and functional analysis of RbsA. Protein Sci **5:**1093-1099.

157. **Zaitseva J, Zhang H, Binnie RA, Hermodson M.** 1996. The proteins encoded by the rbs operon of Escherichia coli: II. Use of chimeric protein constructs to isolate and characterize RbsC. Protein Sci **5:**1100-1107.

158. **Agar SL, Sha J, Baze WB, Erova TE, Foltz SM, Suarez G, Wang S, Chopra AK.** 2009. Deletion of Braun lipoprotein gene (lpp) and curing of plasmid pPCP1 dramatically alter the virulence of Yersinia pestis CO92 in a mouse model of pneumonic plague. Microbiology **155:**3247-3259.

159. **Williams SG, Varcoe LT, Attridge SR, Manning PA.** 1996. Vibrio cholerae Hcp, a secreted protein coregulated with HlyA. Infect Immun **64:**283-289.

160. **Karow M, Georgopoulos C.** 1992. Isolation and characterization of the Escherichia coli msbB gene, a multicopy suppressor of null mutations in the high-temperature requirement gene htrB. J Bacteriol **174:**702-710.

161. **Williamson EDP, P.J.Waters, E.L.Simpson, A.J.Dyer, D.Hartings, J.Twenhafel, N.** 2011. Recombinant (F1 + V) vaccine protects cynomolgus macaques against pneumonic plague, vol 29, p 4771–4777.

162. **Mei JM, Nourbakhsh F, Ford CW, Holden DW.** 1997. Identification of Staphylococcus aureus virulence genes in a murine model of bacteraemia using signature-tagged mutagenesis. Mol Microbiol **26:**399-407.

163. **Agar SL, Sha J, Foltz SM, Erova TE, Walberg KG, Parham TE, Baze WB, Suarez G, Peterson JW, Chopra AK.** 2008. Characterization of a mouse model of plague after aerosolization of Yersinia pestis CO92. Microbiology **154:**1939-1948.

164. **Flashner Y, Mamroud E, Tidhar A, Ber R, Aftalion M, Gur D, Lazar S, Zvi A, Bino T, Ariel N, Velan B, Shafferman A, Cohen S.** 2004. Generation of Yersinia pestis attenuated strains by signature-tagged mutagenesis in search of novel vaccine candidates. Infect Immun **72:**908-915.

165. **Bonacorsi SP, Scavizzi MR, Guiyoule A, Amouroux JH, Carniel E.** 1994. Assessment of a fluoroquinolone, three beta-lactams, two aminoglycosides, and a cycline in treatment of murine Yersinia pestis infection. Antimicrob Agents Chemother **38:**481-486.

166. **Walker DL, Foster LE, Chen TH, Larson A, Meyer KF.** 1953. Studies on immunization against plague. V. Multiplication and persistence of virulent and avirulent Pasteurella pestis in mice and guinea pigs. J Immunol **70:**245-252.

167. **Zhao H, Li X, Johnson DE, Mobley HL.** 1999. Identification of protease and rpoN-associated genes of uropathogenic Proteus mirabilis by negative selection in a mouse model of ascending urinary tract infection. Microbiology **145 (Pt 1):**185-195.

168. **Leigh SA, Forman S, Perry RD, Straley SC.** 2005. Unexpected results from the application of signature-tagged mutagenesis to identify Yersinia pestis genes required for adherence and invasion. Microb Pathog **38:**259-266.

169. **Ben-Gurion R, Hertman I.** 1958. Bacteriocin-like material produced by Pasteurella pestis. J Gen Microbiol **19:**289-297.

170. **Boyer F, Fichant G, Berthod J, Vandenbrouck Y, Attree I.** 2009. Dissecting the bacterial type VI secretion system by a genome wide in silico analysis: what can be learned from available microbial genomic resources? BMC Genomics **10:**104.

171. **Pukatzki S, McAuley SB, Miyata ST.** 2009. The type VI secretion system: translocation of effectors and effector-domains. Curr Opin Microbiol **12:**11-17.

172. **Horazdovsky BF, Hogg RW.** 1987. High-affinity L-arabinose transport operon. Gene product expression and mRNAs. J Mol Biol **197:**27-35.

173. **Park Y, Cho YJ, Ahn T, Park C.** 1999. Molecular interactions in ribose transport: the binding protein module symmetrically associates with the homodimeric membrane transporter. Embo J **18:**4149-4156.

174. **Park Y, Park C.** 1999. Topology of RbsC, a membrane component of the ribose transporter, belonging to the AraH superfamily. J Bacteriol **181:**1039-1042.

175. **Bladergroen MR, Badelt K, Spaink HP.** 2003. Infection-blocking genes of a symbiotic Rhizobium leguminosarum strain that are involved in temperature-dependent protein secretion. Mol Plant Microbe Interact **16:**53-64.

176. **Davidson AL, Dassa E, Orelle C, Chen J.** 2008. Structure, function, and evolution of bacterial ATP-binding cassette systems. Microbiol Mol Biol Rev **72:**317-364, table of contents.

177. **Kovacs-Simon A, Titball RW, Michell SL.** Lipoproteins of bacterial pathogens. Infect Immun **79:**548-561.

178. **Liu T, Agar SL, Sha J, Chopra AK.** Deletion of Braun lipoprotein gene (lpp) attenuates Yersinia pestis KIM/D27 strain: role of Lpp in modulating host immune response, NF-kappaB activation and cell death. Microb Pathog **48:**42-52.

179. **Nakajima R, Brubaker RR.** 1993. Association between virulence of Yersinia pestis and suppression of gamma interferon and tumor necrosis factor alpha. Infect Immun **61:**23-31.

180. **Ponnusamy D, Fitts EC, Sha J, Erova TE, Kozlova EV, Kirtley ML, Tiner BL, Andersson JA, Chopra AK.** 2015. High-throughput, signature-tagged mutagenic approach to identify novel virulence factors of Yersinia pestis CO92 in a mouse model of infection. Infect Immun **83:**2065-2081.

181. **Liu T, Agar SL, Sha J, Chopra AK.** 2010. Deletion of Braun lipoprotein gene (lpp) attenuates Yersinia pestis KIM/D27 strain: role of Lpp in modulating host immune response, NF-kappaB activation and cell death. Microb Pathog **48:**42-52.

182. **Armbruster CE, Pang B, Murrah K, Juneau RA, Perez AC, Weimer KE, Swords WE.** 2011. RbsB (NTHI_0632) mediates quorum signal uptake in nontypeable Haemophilus influenzae strain 86-028NP. Mol Microbiol **82:**836-850.

183. **Shao H, James D, Lamont RJ, Demuth DR.** 2007. Differential interaction of Aggregatibacter (Actinobacillus) actinomycetemcomitans LsrB and RbsB proteins with autoinducer 2. J Bacteriol **189:**5559-5565.

184. **Pereira CS, de Regt AK, Brito PH, Miller ST, Xavier KB.** 2009. Identification of functional LsrB-like autoinducer-2 receptors. J Bacteriol **191:**6975-6987.

185. **Henke JM, Bassler BL.** 2004. Three parallel quorum-sensing systems regulate gene expression in Vibrio harveyi. J Bacteriol **186:**6902-6914.

186. **Lenz DH, Mok KC, Lilley BN, Kulkarni RV, Wingreen NS, Bassler BL.** 2004. The small RNA chaperone Hfq and multiple small RNAs control quorum sensing in Vibrio harveyi and Vibrio cholerae. Cell **118:**69-82.

187. **Bejerano-Sagie M, Xavier KB.** 2007. The role of small RNAs in quorum sensing. Curr Opin Microbiol **10:**189-198.

188. **Bansal T, Jesudhasan P, Pillai S, Wood TK, Jayaraman A.** 2008. Temporal regulation of enterohemorrhagic Escherichia coli virulence mediated by autoinducer-2. Appl Microbiol Biotechnol **78:**811-819.

189. **Duan K, Dammel C, Stein J, Rabin H, Surette MG.** 2003. Modulation of Pseudomonas aeruginosa gene expression by host microflora through interspecies communication. Mol Microbiol **50:**1477-1491.

190. **Choi J, Shin D, Ryu S.** 2007. Implication of quorum sensing in Salmonella enterica serovar typhimurium virulence: the luxS gene is necessary for expression of genes in pathogenicity island 1. Infect Immun **75:**4885-4890.

191. **Miller ST, Xavier KB, Campagna SR, Taga ME, Semmelhack MF, Bassler BL, Hughson FM.** 2004. Salmonella typhimurium recognizes a chemically distinct form of the bacterial quorum-sensing signal AI-2. Mol Cell **15:**677-687.

192. **Taga ME, Semmelhack JL, Bassler BL.** 2001. The LuxS-dependent autoinducer AI-2 controls the expression of an ABC transporter that functions in AI-2 uptake in Salmonella typhimurium. Mol Microbiol **42:**777-793.

193. **Yu J, Madsen ML, Carruthers MD, Phillips GJ, Kavanaugh JS, Boyd JM, Horswill AR, Minion FC.** 2013. Analysis of autoinducer-2 quorum sensing in Yersinia pestis. Infect Immun **81:**4053-4062.

194. **Taga ME, Miller ST, Bassler BL.** 2003. Lsr-mediated transport and processing of AI-2 in Salmonella typhimurium. Mol Microbiol **50:**1411-1427.

195. **Pereira CS, Thompson JA, Xavier KB.** 2013. AI-2-mediated signalling in bacteria. FEMS Microbiol Rev **37:**156-181.

196. **Mitra A, Herren CD, Patel IR, Coleman A, Mukhopadhyay S.** 2016. Integration of AI-2 Based Cell-Cell Signaling with Metabolic Cues in Escherichia coli. PLoS One **11:**e0157532.

197. **Xavier KB, Bassler BL.** 2005. Regulation of uptake and processing of the quorum-sensing autoinducer AI-2 in Escherichia coli. J Bacteriol **187:**238-248.

198. **Choi J, Shin D, Kim M, Park J, Lim S, Ryu S.** 2012. LsrR-mediated quorum sensing controls invasiveness of Salmonella typhimurium by regulating SPI-1 and flagella genes. PLoS One **7:**e37059.

199. **Wang L, Li J, March JC, Valdes JJ, Bentley WE.** 2005. luxS-dependent gene regulation in Escherichia coli K-12 revealed by genomic expression profiling. J Bacteriol **187:**8350-8360.

200. **Pereira CS, Santos AJ, Bejerano-Sagie M, Correia PB, Marques JC, Xavier KB.** 2012. Phosphoenolpyruvate phosphotransferase system regulates detection and processing of the quorum sensing signal autoinducer-2. Mol Microbiol **84:**93-104.

201. **Taga ME, Xavier KB.** 2011. Methods for analysis of bacterial autoinducer-2 production. Curr Protoc Microbiol **Chapter 1:**Unit1C.1.

202. **Choi KH, Gaynor JB, White KG, Lopez C, Bosio CM, Karkhoff-Schweizer RR, Schweizer HP.** 2005. A Tn7-based broad-range bacterial cloning and expression system. Nat Methods **2:**443-448.

203. **Andersson JA, Fitts EC, Kirtley ML, Ponnusamy D, Peniche AG, Dann SM, Motin VL, Chauhan S, Rosenzweig JA, Sha J, Chopra AK.** 2016. New Role for FDA-Approved Drugs in Combating Antibiotic-Resistant Bacteria. Antimicrob Agents Chemother **60:**3717-3729.

204. **Lawrence M, Huber W, Pagès H, Aboyoun P, Carlson M, Gentleman R, Morgan MT, Carey VJ.** 2013. Software for computing and annotating genomic ranges. PLoS Comput Biol **9:**e1003118.

205. **Love MI, Huber W, Anders S.** 2014. Moderated estimation of fold change and dispersion for RNA-seq data with DESeq2. Genome Biol **15:**550.

206. **Witten DM.** 2011. Classification and clustering of sequencing data using a Poisson model.2493-2518.

207. **Agarkov A, Chauhan S, Lory PJ, Gilbertson SR, Motin VL.** 2008. Substrate specificity and screening of the integral membrane protease Pla. Bioorg Med Chem Lett **18:**427-431.

208. **Galindo CL, Sha J, Moen ST, Agar SL, Kirtley ML, Foltz SM, McIver LJ, Kozlova EV, Garner HR, Chopra AK.** 2010. Comparative Global Gene Expression Profiles of Wild-Type Yersinia pestis CO92 and Its Braun Lipoprotein Mutant at Flea and Human Body Temperatures. Comp Funct Genomics**:**342168.

209. **Perrett CA, Karavolos MH, Humphrey S, Mastroeni P, Martinez-Argudo I, Spencer H, Bulmer D, Winzer K, McGhie E, Koronakis V, Williams P, Khan CM, Jepson MA.** 2009. LuxS-based quorum sensing does not affect the ability of Salmonella enterica serovar Typhimurium to express the SPI-1 type 3 secretion system, induce membrane ruffles, or invade epithelial cells. J Bacteriol **191:**7253-7259.

210. **Vendeville A, Winzer K, Heurlier K, Tang CM, Hardie KR.** 2005. Making 'sense' of metabolism: autoinducer-2, LuxS and pathogenic bacteria. Nat Rev Microbiol **3:**383-396.

211. **Kozlova EV, Popov VL, Sha J, Foltz SM, Erova TE, Agar SL, Horneman AJ, Chopra AK.** 2008. Mutation in the S-ribosylhomocysteinase (luxS) gene involved in quorum sensing affects biofilm formation and virulence in a clinical isolate of Aeromonas hydrophila. Microb Pathog **45:**343-354.

212. **Guo M, Gamby S, Zheng Y, Sintim HO.** 2013. Small molecule inhibitors of AI-2 signaling in bacteria: state-of-the-art and future perspectives for anti-quorum sensing agents. Int J Mol Sci **14:**17694-17728.

Vita

Eric Charles Fitts was born to Dana and Linda Fitts in Minnetonka, MN on April 03, 1989. He grew up in Excelsior, MN with one older brother, Andrew Fitts. He attended St. John the Baptist Elementary School for K-5 and then Minnetonka Middle School West for grades 6-8. He graduated from Minnetonka High School in 2007 before attending Gustavus Adolphus College. During summers between undergraduate work, Eric taught swimming lessons at Foss Swim School. In the midst of undergraduate work, Eric was employed by the chemistry and biology departments as a tutor and as a laboratory teaching assistant. After graduating in December 2010 with a BA in biology and chemistry from Gustavus Adolphus College, Eric tutored at Huntington Learning Center, teaching students aged 5-17 math, reading and writing as well as tutoring for standardized testing. Eric then attended the University of Texas Medical Branch at Galveston in the MD/PhD combined degree program with graduate work in the Microbiology and Immunology graduate program.

Education

B.A. *cum laude*, December 2010, Gustavus Adolphus College, Saint Peter, MN

Publications

1. Ponnusamy D***, Fitts EC*,** Sha J, Erova TE, Kozlova EV, Kirtley ML, Tiner BL, Andersson JA, Chopra AK. High-throughput signature-tagged mutagenic approach to identify novel virulence factors of Yersinia pestis CO92 in a mouse model of infection. Infect Immun. 2015. Epub 2015/03/11. doi: 10.1128/iai.02913-14. PubMed PMID: 25754198.

*** Equal Contribution**

2. Sha J, Kirtley ML, Klages C, Erova TE, Telepnev M, Ponnusamy D, **Fitts EC**, Baze WB, Sivasubramani SK, Lawrence WS, et al. A replication-defective human type-5 adenovirus-based trivalent vaccine confers complete protection against plague in mice and non-human primates. Clin Vaccine Immunol. 2016 May 11. pii: CVI.00150-16. [Epub ahead of print] PubMed PMID: 27170642.

3. Andersson JA**, Fitts EC**, Kirtley ML, Ponnusamy D, Peniche AG, Dann SM, Motin VL, Chauhan S, Rosenzweig JA, Sha J, et al. New role for FDA-approved drugs in combating antibiotic-resistant bacteria. Antimicrob Agents Chemother. 2016 Apr 11. pii: AAC.00326-16. [Epub ahead of print] PubMed PMID: 27067323.

4. Tiner BL, Sha J, Ponnusamy D, Baze WB, **Fitts EC**, Popov VL, van Lier CJ, Erova TE, Chopra AK. Intramuscular Immunization of Mice with a Live-Attenuated Triple Mutant of Yersinia pestis CO92 Induces Robust Humoral and Cell-Mediated Immunity To Completely Protect Animals against Pneumonic Plague. Clin Vaccine Immunol. 2015 Dec;22(12):1255-68. doi: 10.1128/CVI.00499-15. Epub 2015 Oct 7. PubMed PMID: 26446423; PubMed Central PMCID: PMC4658590.

5. Ponnusamy D, Kozlova EV, Sha J, Erova TE, Azar SR, **Fitts EC**, Kirtley ML, Tiner BL, Andersson JA, Grim CJ, Isom RP, Hasan NA, Colwell RR, Chopra AK. Cross-talk among flesh-eating Aeromonas hydrophila strains in mixed infection leading to necrotizing fasciitis. Proc Natl Acad Sci U S A. 2016 Jan 5. pii: 201523817. [Epub ahead of print] PubMed PMID: 26733683.

6. Grim CJ, Kozlova EV, Sha J, **Fitts EC**, van Lier CJ, Kirtley ML, Joseph SJ, Read TD, Burd EM, Tall BD, Joseph SW, Horneman AJ, Chopra AK, Shak JR. Characterization of Aeromonas hydrophila wound pathotypes by comparative genomic and functional analyses of virulence genes. MBio. 2013;4(2):e00064-13. doi: 10.1128/mBio.00064-13. PubMed PMID: 23611906; PMCID: PMC3638308.

7. Grim CJ, Kozlova EV, Ponnusamy D, **Fitts EC**, Sha J, Kirtley ML, van Lier CJ, Tiner BL, Erova TE, Joseph SJ, Read TD, Shak JR, Joseph SW, Singletary E, Felland T, Baze WB, Horneman AJ, Chopra AK. Functional genomic characterization of virulence factors from necrotizing fasciitis-causing strains of Aeromonas hydrophila. Appl Environ Microbiol. 2014. doi: 10.1128/AEM.00486-14. PubMed PMID: 24795370.

8. Sha J, Kirtley ML, van Lier CJ, Wang S, Erova TE, Kozlova EV, Cao A, Cong Y, **Fitts EC**, Rosenzweig JA, Chopra AK. Deletion of the Braun lipoprotein-encoding gene and altering the function of lipopolysaccharide attenuate the plague bacterium. Infect Immun. 2013;81(3):815-28. doi: 10.1128/IAI.01067-12. PubMed PMID: 23275092; PMCID: PMC3584885.

9. Sha J, Rosenzweig JA, Kirtley ML, van Lier CJ, **Fitts EC**, Kozlova EV, Erova TE, Tiner BL, Chopra AK. A non-invasive in vivo imaging system to study dissemination of bioluminescent Yersinia pestis CO92 in a mouse model of pneumonic plague. Microb Pathog. 2013;55:39-50. Epub 2012/10/16. doi: 10.1016/j.micpath.2012.09.011. PubMed PMID: 23063826; PMCID: Pmc3552012.

10. van Lier CJ, Tiner BL, Chauhan S, Motin VL, **Fitts EC**, Huante MB, Endsley JJ, Ponnusamy D, Sha J, Chopra AK. Further characterization of a highly attenuated Yersinia pestis CO92 mutant deleted for the genes encoding Braun lipoprotein and plasminogen activator protease in murine alveolar and primary human macrophages. Microb Pathog. 2015;80:27-38. Epub 2015/02/24. doi: 10.1016/j.micpath.2015.02.005. PubMed PMID: 25697665; PMCID: PMC4363157.

In Revisions

1. Tzipora C. Falik Zaccai MD[1,2], David Savitzki MD[3]*, Yifat Zivony-Elboum PhD[1]*, Thierry Vilboux PhD[4,5*], **Eric C. Fitts** [6]*, Yishay Shoval PhD[1], Limor Kalfon PhD[1], Nadra Samra MD[1], Zohar Keren PhD[1], Bella Gross MD[2,7], Natalia Chesnik MD[1], Rachel Straussberg MD[8,9], James C Mullikin PhD[10,11], Jamie K. Teer PhD[12], Dan Geiger PhD[13], Daniel Kornitzer PhD[14] Ora Bitterman-Deutsch MD[2,15], Tatiana Freidman MD[16], Abraham O. Samson PhD[2], Maki Wakamiya PhD[17], Johnny W. Peterson PhD[6], William A Gahl MD PhD[4], Robert Kleta MD PhD[18], Yair Anikster MD PhD[9,19] Ashok K. Chopra PhD[6]. Sequence variant in Phospholipase A2 Activating Protein and Leukoencephalopathy**.** Brain.

Under Review

1. **Eric C. Fitts[a]**, Jourdan A. Andersson[a], Michelle L. Kirtley[a], Jian Sha[a], Tatiana E. Erova[a], Sadhana Chauhan[a], Vladimir Motin[a,b], and Ashok K. Chopra[a#]. New Paradigm in Autoinducer-2 Signaling: Potent *in vivo* Bacterial Virulence Regulator. mSphere.

Summary of Dissertation

Identification of new virulence factors in *Yersinia pestis*, the causative agent of plague, and understanding their molecular mechanisms during an infection process are necessary in designing a better vaccine or to formulate an appropriate therapeutic intervention. By using a high-throughput, signature-tagged mutagenic approach, we screened 5,088 mutants of *Y. pestis* CO92. From this screen, 118 clones showing impairment in disseminating to spleen were obtained. In a subsequent screen, 20/118 mutants exhibited attenuation when tested individually in a mouse model of bubonic plague, with 10/20 aforementioned mutants providing 40% or higher survival rates at an infectious dose of 40 LD_{50}. Upon sequencing, six of the attenuated mutants carried interruptions in genes encoding hypothetical proteins or proteins with putative functions. In-frame deletion mutation of two of the genes identified from the screen were also found to exhibit some attenuation at 11-12 LD_{50} in a mouse model of pneumonic plague. Likewise, among the remaining 18 signature-tagged mutants, 9 were also attenuated (40-100%) at 12 LD_{50} in a pneumonic plague mouse model. Combinatorial deletions including the newly identified genes, *rbsA* and *vasK*, were significantly attenuated in pneumonic plague models. Interestingly, *rbsA* gene products have been associated with a highly conserved inter-bacterial signaling system mediated by autoinducer-2 (AI-2) quorum-sensing molecule. Deletion of the gene encoding the synthetic enzyme for AI-2 substrate, *luxS*, leads to either no change or, paradoxically, an increase in *in vivo* bacterial virulence. Deletion of *rbsA* and *lsrA* genes, ABC transport components interacting with AI-2, synergistically disrupted AI-2 signaling patterns and resulted in an over 50-fold decrease in *Y. pestis* CO92 virulence in a mouse model. Deletion of *luxS* from the Δ*rbsA*Δ*lsrA* strain reverted the virulence phenotype similar to wild-type CO92. Administration of AI-2 in mice infected with the Δ*rbsA*Δ*lsrA*Δ*luxS* mutant strain attenuated this triple mutant. Role of AI-2 signaling genes that modulated bacterial virulence was determined by RNAseq. Characterization of AI-2 signaling in *Y. pestis*

should lead to re-examination of AI-2 systems in other pathogens and may represent a broad-spectrum therapeutic target to combat antibiotic-resistant bacteria.

This dissertation was typed by Eric Fitts